

ABSTRACT

Title of Document:

ACTIVE VIBRATION ATTENUATING SEAT
SUSPENSION FOR AN ARMORED
HELICOPTER CREW SEAT

Pablo Sztein, Master of Science, 2013

Directed By:

Professor Norman M. Wereley, Department of
Aerospace Engineering

An Active Vibration Attenuating Seat Suspension (AVASS) for an MH-60S helicopter crew seat is designed to protect the occupants from harmful whole-body vibration (WBV). Magnetorheological (MR) suspension units are designed, fabricated and installed in a helicopter crew seat. These MR isolators are built to work in series with existing Variable Load Energy Absorbers (VLEAs), have minimal increase in weight, and maintain crashworthiness for the seat system. Refinements are discussed, based on testing, to minimize friction observed in the system. These refinements include the addition of roller bearings to replace friction bearings in the existing seat. Additionally, semi-active control of the MR dampers is achieved using special purpose built custom electronics integrated into the seat system. Experimental testing shows that an MH-60S retrofitted with AVASS provides up to 70.65% more vibration attenuation than the existing seat configuration as well as up to 81.1% reduction in vibration from the floor.

ACTIVE VIBRATION ATTENUATING SEAT SUSPENSION FOR AN
ARMORED HELICOPTER CREW SEAT

By

Pablo Javier Sztein

Thesis submitted to the Faculty of the Graduate School of the
University of Maryland, College Park, in partial fulfillment
of the requirements for the degree of
Master of Science
2013

Advisory Committee:

Professor Norman M. Wereley, Chair
Professor Amr Baz
Professor Inderjit Chopra

© Copyright by
Pablo Javier Sztein
2013

Acknowledgements

I would like to thank my advisor, and committee chair, Dr. Norman Wereley for his support throughout my Master's studies. Witnessing the continual advancement of a collective body of work and continuing career has been inspirational. I am grateful for the time he has given to assuring that my experience was productive and worthwhile. I would also like to thank my committee members, Dr. Amr Baz and Dr. Inder Chopra, for their time and dedication to teaching in a manner which challenges and inspires a student's best work.

I owe this opportunity, of assisting in the development of this important technology, to a still ongoing Navy BAA project which applied a Semi-Active Magnetorheological Seat Suspension (SAMSS) to an unarmored MH-60R helicopter crew seat. Mr. William Glass of NAVAIR at Patuxent River NAS is the project sponsor for both SAMSS and now AVASS. I would like to take this opportunity to thank him for his faith in allowing students to help develop technology for the Navy. I owe a debt of gratitude to Dr. Gregory Hiemenz for allowing me to continue his line of work. Dr. Hiemenz, as my supervisor at Techno Sciences Inc., has fully supported my studies and collegiate development. I can't thank him enough.

In addition, I would like to thank Dr. Wei Hu and all those who assisted throughout the development and testing of the AVASS system. There is no doubt that they deserve a lot of credit for this Thesis and the developments that stem from it.

Table of Contents

Acknowledgements.....	ii
Table of Contents.....	iii
List of Tables	vi
List of Figures	vii
CHAPTER 1: INTRODUCTION AND PURPOSE.....	1
Introduction.....	1
Helicopter Crew Seat Systems.....	3
Viscous Dampers as part of a Vibration Isolating Technology	7
Magnetorheological Fluid Technology in Viscous Dampers	9
Previous Work	14
SAMSS Performance and Lessons Learned	15
AVASS Goals	18
CHAPTER 2: APPLICATION OF VIBRATION ISOLATION THEORY	19
Single Degree of Freedom Base Excitation	19
Spring and Damper Characterization for AVASS	22
Skyhook Algorithm for Semi-Active Vibration Control	27
CHAPTER 3: CREW SEAT INTEGRATION CONCEPTS	33
SAMSS versus AVASS Design Review.....	33
Disassembly of OEM Seat for Ease of Retrofit Study.....	38
AVASS Retrofit Design Concept	39

Damper Mounting Design Ideas	40
Electronics Mounting Design Ideas	41
CHAPTER 4: MR DAMPER DESIGN.....	45
MR Dampers – Damper Design Reality/Practical Approach	45
AVASS MR Damper Piston and Magnetic Circuit Design	52
Initial Damper Body, Seal and Stepped Rod Design	58
MR Damper Design Version 2.0 Changes.....	64
MR Damper Mounting Tube	65
Spring Design.....	67
Rod Seal & Bushing Holder	72
Damper Body	73
Damper Accumulator.....	74
MR Isolator Fabrication & Assembly Notes	76
MR Isolator Testing	80
Study of the Effects of Varying Diaphragm Pressure on Damper Friction	85
Further Changes for Future AVASS Systems	91
CHAPTER 5: ROLLER BEARING DESIGN	95
AVASS Bearing Bracket- Roller Bearing Design	95
Design and Installation of Roller Bearing Brackets	100
Moving Forward After Successful Roller Bearing Tests.....	104
Documentation of Roller Bearing V 2.0 Assembly	119
AVASS Roller Bearing V 2.0 Performance Verification Testing	132
CHAPTER 6: TESTING METHODOLOGY	135

Vibration Testing of the MH-60S Seat System	135
Smart BART Test Ballast	138
CHAPTER 7: AVASS REPORTED RESULTS	145
OEM MH-60S Test Results	145
AVASS Preliminary Vibration Stand Testing Plan	150
AVASS Preliminary Testing Results	152
Vibration Testing with Roller Bearings and Sand Bag Mass	157
AVASS Tests of MR Controller Performance.....	160
Final AVASS Modifications	167
CHAPTER 8: FINAL TESTING RESULTS AND CONCLUSIONS	181
Final Configuration for Testing	181
Final Vibration Testing Results for Characterization of AVASS.....	184
Conclusions and Future Work	196
APPENDIX I: MRF-132DG Magneto-Rheological Fluid	200
Bibliography	202

List of Tables

Table 1: Properties of MRF-132DG Magneto-Rheological Fluid as listed on the LORD Corporation website	12
Table 2: Sample Output from MR Damper Design Analysis Software.....	54
Table 3: Loads and Constraints On Aluminum Spring and Bearing Holder	66
Table 4: Weight Trade Study for Spring Selection.....	69
Table 5: Spring Options for the AVASS System.....	71
Table 6: Table of Star Bart Component Weight Composition.....	142
Table 7: AVASS Percent Reduction in Vibration from OEM SH-60S measured at the Seat Pan	185
Table 8: AVASS Percent Reduction in Vibration from Floor measured at the Seat Pan	185
Table 9: OEM MH-60S Percent Reduction in Vibration from Floor measured at the Seat Pan..	185
Table 10: AVASS Percent Reduction in Vibration from OEM MH-60S measured at the Seat Cushion	188
Table 11: AVASS Percent Reduction in Vibration from Floor measured at the Seat Cushion...	188
Table 12: OEM MH-60S Percent Reduction in Vibration from Floor measured at the Seat Cushion	188

List of Figures

Figure 1: Armored Wall Mounted, Unarmored Freestanding, Armored Freestanding Crew Seats.	4
Figure 2: Bingham Plastic Model Representation of MR fluid effect	13
Figure 3: SAMSS Rear Seat Pan Vertical Transmissibility for 50th Percentile Male, 0.2 g Excitation [3]	16
Figure 4: Single Degree of Freedom Spring-Mass Base Excitation	19
Figure 5: Single Degree of Freedom Spring-Mass-Damper Base Excitation	21
Figure 6: Effects of Damping on the Transmissibility of a Single Degree of Freedom System with Base Excitation	22
Figure 7: Damping Ratio as a Function of Spring Rate to Achieve 90% Attenuation of 4/rev Vibrations.....	24
Figure 8: System Natural Frequency as a Function of Spring Rate	24
Figure 9: Off-State Damping Vs. Spring Rate to Achieve 90% Attenuation of 4/rev Vibrations .	24
Figure 10: On-State Yield Force Required to Suppress Resonance While Achieving 90% Attenuation of 4/rev Vibrations Vs. Spring Rate: Assuming 0.7 g Amplitude Input	24
Figure 11: Required Controllable Range (On State Yield Force / Off-State Damping) As a Function of Spring Rate to Achieve 90% Attenuation of 17.2 Hz Blade Passing Vibrations	26
Figure 12: Static Deflection as a Function of Spring Rate and Occupant	26
Figure 13: Total Stroke Required for the Range of Occupants Vs. Spring Rate, Assuming 0.7 g Amplitude Input	26
Figure 14: Semi-active Vibration Control Goal Using Single Degree of Freedom Transmissibility	27
Figure 15: Skyhook Model	28
Figure 16: Transmissibility of the Skyhook Model	29
Figure 17: Skyhook Control Logic	30
Figure 18: AVASS Damper Characterization Equations for Use with Skyhook Control Logic ...	31
Figure 19: SAMSS Vibration Isolation System Integrated into MH-60R Crew Seat.....	33
Figure 20: MH-60S Seat for AVASS program Integration	34
Figure 21: Seat Bracket Clearance when Raising Crossbar.....	35
Figure 22: Loosely Fitted Guide Tube Bearings.....	37
Figure 23: Flanged MR Damper Mounting Tube	40
Figure 24: MR Damper Mounting with Lower Tension Wire Support	41
Figure 25: Electronics Seat Bracket Design	42
Figure 26: Accelerometer Box and VLEA Wire Containment Tube Concept	43
Figure 27: Magnetic Field Lines Around a Magnetic Coil	46
Figure 28: MRF-132 Magnetic Properties [18]	47
Figure 29: Representative 1018 Steel B-H Plot.....	48
Figure 30: Basic Magnetic Circuit [27]	48
Figure 31: Magnetic Coil Typical Design Process [27].....	49

Figure 32: MR Piston configurations.....	53
Figure 33: Piston Design with Wire Seal Design and Plastic Wear Ring.....	57
Figure 34: First Damper Body Design Concept.....	58
Figure 35: All Steel Damper Body Design	59
Figure 36: First Design of Bushing and U-Cup Insertion Method.....	60
Figure 37: Flanged Mounting Tube with Stepped Shaft, Spring, Spring Retainer and Linear Bearing.....	62
Figure 38: Three Piece Stepped Shaft Design with Spring Retainer	63
Figure 39: Lip Design Change.....	65
Figure 40: FEA Analysis of MR Damper Mounting Tubes.....	66
Figure 41: Effect of Spring Options on Damper Integration Design	68
Figure 42: Rod Seal Assembly & Damper Body	73
Figure 43: Diaphragm Test Setup	75
Figure 44: Assembly of Piston Rod to Piston	77
Figure 45: Damper Body	78
Figure 46: Spring and Bearing Holder/ Mounting Tube.....	78
Figure 47: Diaphragm Cap.....	79
Figure 48: MTS Mounting Design CAD Model and set in MTS Machine.....	81
Figure 49: Damper 1 - 0.5 Hz	82
Figure 50: Damper 1 - 2 Hz	82
Figure 51: Damper 1 - 4.3 Hz	83
Figure 52: Damper 1 - 8 Hz	83
Figure 53: Damper 1 - 17.2 Hz Data; Dark Blue Indicates Bingham Plastic Model of Desired Characteristics.....	84
Figure 54: Damper Characterization Equations.....	85
Figure 55: Damper 2 - 4.3 Hz, 0 PSI (0 amps, 1 amp)	88
Figure 56: Damper 2 - 4.3 Hz, 40 PSI (0 amps, 1 amp).....	88
Figure 57: Variation of Friction at 0 Amps and Raising Diaphragm Pressures.....	89
Figure 58: Friction vs Diaphragm Pressure	89
Figure 59: Required Yield Force at 0.2 g and 370 lb/in total spring force	90
Figure 60: Required Yield Force at 0.7 g and 370 lb/in total spring force	90
Figure 61: MH-60R (left) and MH-60S (right) both with AVASS dampers installed	93
Figure 62: BAE Proposed Bearing Design	96
Figure 63: FBD of Seat System	97
Figure 64: Calculated Forces on Bearings	97
Figure 65: CAD Models of Top (left) and Bottom (right) OEM Guide Tube Bearing Brackets...	98
Figure 66: CAD Model of Roller with Bearings.....	98
Figure 67: Top Bracket Roller Bearing Design Concept.....	99
Figure 68: Bottom Bracket Roller Bearing Design Concept	99
Figure 69: Top Bearing Bracket Design	101
Figure 70: Roller Bearing Bracket on Upper guide Tube Bearing Bracket.....	101
Figure 71: Roller Bearing Bracket on Lower Guide Tube Bearing Bracket.....	102
Figure 72: AVASS Before Roller Bearings.....	105

Figure 73: AVASS with Roller Bearing Brackets V1.0	105
Figure 74: First Iteration Roller Bearing Bracket Design Methodology	106
Figure 75: AVASS Seat At 2nd From the Top Position	109
Figure 76: Second Iteration Roller Bearing Design for Top Brackets, Rear View (Adjustment Screws Easy to Reach).....	110
Figure 77: AVASS Roller Bearing Design for Top Brackets V2.0 Top Angle View	112
Figure 78: AVASS Roller Bearing Design for Top Brackets V2.0 Bottom Angle View.....	112
Figure 79: Problems with Clearance in 1st Iteration for.....	113
Figure 80: Problems with Clearance in 1st Iteration for.....	114
Figure 81: Problems with Clearance in 1st Iteration for.....	114
Figure 82: Geometric Constraints on the AVASS Roller Bearing Lower Brackets	115
Figure 83: Design of Second iteration of AVASS Roller Bearing Bracket for Lower Brackets with additional Geometric Constraints	116
Figure 84: AVASS Roller Bearing Design for Lower Brackets V2.0 Top Angle View	117
Figure 85: Larger Roller in AVASS Roller Bearing Design for Top Brackets V2.0 Top Angle	118
Figure 86: AVASS Roller Bearing Design V2.0 Fully Installed.....	119
Figure 87: Lower Assembly - Bottom Brackets	120
Figure 88: Lower Assembly - Top Brackets.....	120
Figure 89: Lower Assembly - Bearing Holders	121
Figure 90: Lower Assembly - Axle Covers	121
Figure 91: Lower Assemblies - Angled View	122
Figure 92: Lower Assemblies - Top View.....	122
Figure 93: Lower Assembly - Comparison to SH-60B OEM Roller Bracket	123
Figure 94: Upper Assembly - Bottom Brackets.....	123
Figure 95: Upper Assembly - Top Brackets	124
Figure 96: Upper Assembly - Bearing Holders	124
Figure 97: Upper Assemblies - Top View	125
Figure 98: Upper Assemblies - Alternate View.....	125
Figure 99: Left Side Upper Assembly - Installed On Seat - Top View	126
Figure 100: Left Side Upper Assembly - Second From Top OEM Position Clearance	126
Figure 101: Right Side Lower Bracket - Installed On Seat	127
Figure 102: Upper Bracket - Armor Side - Spring Clearance Issue on Crash Stroke.....	129
Figure 103: Upper Bracket - Armor Side - Armor Spring Bracket Clearance Issue	130
Figure 104: Proposed Armor Spring Bracket Modification.....	130
Figure 105: The Proposed Modified Armor Spring Bracket Over the Original bracket.....	131
Figure 106: Lower Bracket - Right Side (From the back) - X-bar Clearance Issue	131
Figure 107: Lower Brackets Clearance on Full Down During Crash Stroke.....	132
Figure 108: Comparison of V 1.0 and V 2.0 Roller Bearing Performance.....	133
Figure 109: Sensor Mounting Positions for Testing.....	135
Figure 110: University of Maryland Smart Structures Laboratory Vibration Test Stand.....	136
Figure 111: AVASS Performance with Different Mass Distribution	139
Figure 112: Star Bart with Arms.....	140
Figure 113: Photo of Star Bart Taken Apart.....	141

Figure 114: Relative weight and length of body segments for adult men and women	143
Figure 115: Anthropomorphic data versus Star Bart measured data	144
Figure 116: Frequency Response of MH-60S Seat in Baseline OEM Configuration for 5th Percentile Female with Seat at Highest Position	146
Figure 117: Frequency Response of MH-60S Seat in Baseline OEM Configuration for 50th Percentile Male with Seat at Middle Position.....	146
Figure 118: Frequency Response of MH-60S Seat in Baseline OEM Configuration for 95th Percentile Male with Seat at Lowest Position.....	147
Figure 119: Vertical Vibration Data at the Cockpit Floor from UH-60 for a 30 Degree Bank at 130 Kias Flight Condition.....	148
Figure 120: Reproducing the Representative Flight Vibrations in Shock and Vibration Test Stand	149
Figure 121: OEM Guide Tube Bearing Design	151
Figure 122: Expected Field-Off AVASS Performance.....	152
Figure 123: Initial Testing Results at 0.2 g	153
Figure 124: Low Friction Tape Application	154
Figure 125: Low Friction Tape Modification Comparison.....	155
Figure 126: 50th Male Performance Comparison.....	156
Figure 127: Transmissibility of System with Bearing Brackets versus Single Degree of Freedom Theory	157
Figure 128: AVASS Control Gain Testing Results	160
Figure 129: AVASS Sine Sweep using 50 th male Star BART Ballast.....	163
Figure 130: OEM Transient Testing	164
Figure 131: OEM Transient Testing PSD.....	164
Figure 132: AVASS with MRF-132 Transient Testing	165
Figure 133: AVASS with MRF-132 Transient Testing PSD.....	165
Figure 134: AVASS with MRF-126 Transient Testing	166
Figure 135: AVASS with MRF-126 Transient Testing PSD.....	166
Figure 136: AVASS SH-60S Transmissibility from Floor Acceleration at Different Locations	168
Figure 137: Accelerometer Positions.....	169
Figure 138: Seat Pan to Seat Cushion Transmissibility	170
Figure 139: Effect of Changing Cushions at the Seat Pan.....	172
Figure 140: Effect of Changing Cushions at the Seat Cushion.....	172
Figure 141: Cushion Dynamics for Tested Seat Cushion Options	173
Figure 142: Photo of Clevis Screw Change.....	175
Figure 143: Clevis Screw Length Change Effect.....	176
Figure 144: Large Clearance Clevis and Samples of Tubing from Testing.....	177
Figure 145: New Clevis with Freedom of Motion Results at the Seat Pan from 5 to 20 Hz.....	177
Figure 146: New Clevis with Freedom of Motion Results at the Seat Pan from 16.5 to 17.5 Hz	178
Figure 147: New Clevis with Freedom of Motion Results at the Seat Cushion from 5 to 20 Hz	178
Figure 148: New Clevis with Freedom of Motion Results at the Seat Cushion from 16.5 to 17.5 Hz.....	179
Figure 149: Final Configuration of MH-60S with AVASS.....	181

Figure 150: AVASS Damper V2.0	182
Figure 151: TSi MR Controller Electronics v4.0 for use with AVASS.....	183
Figure 152: AVASS Sine Sweep Data for 5th Female Mass at the Seat Pan Accelerometer.....	186
Figure 153: AVASS Sine Sweep Data for 50th Male Mass at the Seat Pan Accelerometer	186
Figure 154: AVASS Sine Sweep Data for 95th Male Mass at the Seat Pan Accelerometer	187
Figure 155: AVASS Sine Sweep Data for 5th Female Mass at the Seat Cushion Accelerometer	189
Figure 156: AVASS Sine Sweep Data for 50th Male Mass at the Seat Cushion Accelerometer	189
Figure 157: AVASS Sine Sweep Data for 95th Male Mass at the Seat Cushion Accelerometer	190
Figure 158: Effect of Seat Height Position on the 50th Male Mass at the Seat Pan Accelerometer	192
Figure 159: Effect of Seat Height Position on the 50th Male Mass at the Seat Cushion Accelerometer	193
Figure 160: AVASS Sine Sweep Data for 50th Male Mass at the Seat Pan at 0.2 g and 0.4 g ...	194
Figure 161: AVASS Sine Sweep Data for 50th Male Mass at the Seat Cushion at 0.2 g and 0.4 g	194
Figure 162: OEM MH-60S Transmissibility for all Occupants at the Seat Pan and at the Seat Cushion	195

CHAPTER 1: INTRODUCTION AND PURPOSE

Introduction

This thesis will discuss the development of an Active Vibration Attenuating Seat Suspension (AVASS) for an MH-60S helicopter crew seat. The BAE/Simula UH-60M is an armored bucket crashworthy helicopter crew seat fielded by the Navy on the MH-60S Seahawk variant often called the Knighthawk. The project seeks to design a vibration isolation kit that can be applied as a retrofit to existing helicopter crew seats. AVASS successfully applies the lessons learned from past projects and is currently leveraging the experience gained to generate a product which the Navy can be proud to procure for its fleet of crew seats.

Vibration reduction technology has allowed rotorcraft to fly faster, quieter and more efficiently than ever before. Unfortunately, the human factors problems within the cockpit of these aircraft have not been fully addressed. The retirement of young officers and life-long pain in veteran helicopter pilots is a current hot topic throughout the military [1]. The consensus is that the damage is caused by a combination of pilot posture and whole body vibration due to rotor forces carried into the cabin [2]. Applying vibration isolation technology to existing crew seats may help to reduce early retirement and medical expenses, as well as extend the flight time capabilities of helicopter pilots.

Helicopter vibrations are known to be largely due to the rotor dynamics passed to the fuselage of the aircraft. The Seahawk helicopter rotor's rotational frequency is constant at 258 rpm (or 1/rev) during flight, creating lift by varying the pitch of its blades. It is expected that the four blades ($N=4$) would generate vibrations at the 4/rev frequency and further harmonics ($(N-1)/\text{rev}$, N/rev , $(N+1)/\text{rev}$) with lower frequencies due to transient loading in the rotor blades. In fact, the FFT of on board accelerometer data, in hover, clearly shows that vibrations occur primarily at blade passing frequency of 17.2 Hz (4/rev) with a smaller amount of energy at 4.3 Hz (1/rev). Recently analyzed accelerometer data, acquired during SAMSS flight testing, indicate that the 2/rev, 3/rev and 8/rev frequencies are readily apparent in high lift flight maneuvers [3]. This puts an emphasis on studying the reduction of transmissibility to the occupant for frequencies ranging from 4 Hz to 40 Hz. Vibrations measured at the cockpit range in amplitude from 0.1 g to 0.7 g with an RMS value of approximately 0.2 g to 0.3 g.

Whole Body Vibration (WBV) has been studied at length by those in the field of Human Factors and Ergonomics [4]. The effects of vibration on the body can vary depending on the frequency and amplitude, but it is known that it can hasten the onset of fatigue and cause circulatory disorders [4]. The International Organization for Standardization (ISO) document 2631-1 specifies that WBV monitoring is important from 0.5 Hz to 80 Hz [5]. In the U.S.A., standards offer suggested exposure values and offer guidance, but do not provide a regulatory limit [4]. Additionally, measurements of transmissibility through the spine of the human body have shown a resonant effect in the range of 4 Hz to 8 Hz to the thoracic region and possibly a wider range higher up the spine, towards the neck [6].

There is clear indication that reducing vibration to the helicopter occupant would be a positive step towards achieving a more aware and efficient piloting atmosphere.

Complaints from Helicopter Pilots about lower back pain and loss of feeling in the extremities have spurred various medical studies on the effects of seated vibration [1] [2] [6] [7]. More to the point, a 2005 Navy internal study concludes that “Since the average flight during a deployment or mission could last up to 8 hours, the current exposure places the pilots at an unacceptable risk of injury, lack of mission readiness, and possible equipment damage“ [8]. Hazard reports note that pilots begin to feel pain in the lumbar region and lack of sensation in the legs at the two to four hour mark of a typical flight [8]. Also, pilots who are constantly shifting in their seats to get comfortable have shown a decrease in situational awareness [8]. Many of those being treated for pain issues are on military pensions and have to be provided health care and assistance [8]. Exact numbers of those who have been affected are not readily available, although it is obvious that this is an expansive issue.

Helicopter Crew Seat Systems

A modern helicopter crew seat can be decomposed into three parts: a frame, a seat bucket and a crash attenuation system. The most important feature for most modern fielded helicopter seats is an energy absorption (EA) system to increase crash safety [9] [10]. Very few creature comforts are afforded to military helicopter crew seats. The design parameters are heavily dictated by MIL-STD-58095A [11]. This standard was created to

assure the quality of equipment will be consistent for all occupants and that the design will be tested for reliability issues before procurement [11]. This section will not cover the full extent of the standard, but will highlight a few important points for the project under discussion.



Figure 1: Armored Wall Mounted, Unarmored Freestanding, Armored Freestanding Crew Seats

The size and total loaded weight, with equipment, of occupants can vary drastically. The occupant anthropomorphic masses discussed most often are the 5th percentile female (~120 lbs.), the 50th percentile male (~180 lbs.) and the 95th percentile male (~220 lbs.) [12]. MIL-STD-58095A asks that the seat design “cover an occupant weight range from 140 to 250 pounds (64 to 114 kg)” [11]. The design of the suspension system to be designed must readily accept this range while maintaining a minimum in static seat height change, maintaining the originally designed line of sight for the occupant.

In general, MIL-STD-58095A dictates mechanical and ergonomic functions that must be maintained as well as restrictions on materials and fastening of assembly components. It is imperative that any engineer tasked with modifying a helicopter crew seat be readily familiar with this document. The standard calls for specific standardized qualification testing to survive large inertial loads. Static loading is tested to show a minimum of deformation in the seat before EA stroke. Dynamic tests measure loads on the occupant during a crash event and the effectiveness of the EA [11]. All components designed must meet a 20-20-10 analysis. The components must pass yielding calculations to 20 *g* (occupant inertia) in downward, longitudinal and lateral directions as well as 10 *g* in upward direction [13]. It is important that the load path be properly analyzed and that original designs are well understood. There are components, clearances and attachments which have been designed specifically to withstand loading in a specific direction. A misunderstanding of the desired load path could lead to a reduction in the quality of the final design.

The frame of a modern helicopter crew seat is designed to allow the EA to stroke as designed. The typical design has circular tubes used as vertical guides for the seat stroke. Required stroke length is a key factor in the overall height of the structure. Additionally, these tubes usually have an incline from vertical which is the first way to reduce the vertical load on the occupant. In the case of the MH-60S, this angle is approximately 4 degrees [9]. The seat bucket is usually cantilevered so that the frame actually sits in front and ahead of the guide tubes. This design puts large bending loads on the guide tubes. The system has a rocking mode resonance which has been found to be within the range of

helicopter rotor vibrations [3]. Mounted to the floor of the helicopter is a rail system that allows for fore-aft adjustment. The space directly below the seat bucket must be kept clear to allow the seat bucket to stroke as much as possible. In fact, there is often a well in the helicopter floor to allow the bottom of the seat bucket to dip below the floor line [9].

The seat bucket of a modern helicopter crew seat is designed to securely hold a large range of occupants. “Seat and restraint dimensions shall be based on the anthropometric data of MIL-STD-1472 to fit a 5th to 95th percentile male aviator with allowances for clothing and equipment” [11]. This requirement, as well as the requirements on restraint harness mounting points, leads to a fairly consistent seat bucket shape and size. The variation between seat systems is between armored and un-armored versions of the seat bucket. The mass of the seat bucket can triple when armor is required. This added weight has the effect of requiring a more resilient (heavier) frame construction to manage structural integrity under large inertial loads.

The frame and seat bucket of a modern helicopter crew seat form a system that allows for vertical motion to allow energy from the floor to be passed through a sophisticated energy absorber (EA) before the load is passed to the occupant. EA technology has evolved from a fixed load system tuned for the 50th male mass, to a variable load system, which can be tuned by the occupant for his or her body mass. In many energy absorber technologies there is some form of plastic deformation or cutting of material. The two most common of these technologies are inversion tube and wire bending designs, but

different companies have developed proprietary technologies. An in depth discussion of EA technologies can be found in a paper by Desjardins [9]. To reiterate, it is imperative that retrofit designs allow the EA to function as it did in original qualification tests. A review of original manufacturer test data, and notes from qualification tests, is helpful in understanding potential pitfalls. Understanding the variety of potential helicopter seat system EA designs may also help in designing a product that may become applicable to a greater range of helicopter crew seat models [9].

The successful application of retrofitting a suspension to a modern helicopter crew seat must have the following goals. First, the final retrofit design must allow for a minimum deviation from the original fore-aft and seat height adjustment range. Next, the seat system must essentially revert to its solid mode and stroke the EA in a high g crash event. Finally, the system must be kept simple, light and effective to merit adaptation past the prototype stage.

Viscous Dampers as part of a Vibration Isolating Technology

First, a general overview of damping technology and development will help to convince the reader that a linear damper was a good choice for the AVASS project. A review of vibration isolation theory is covered in chapter 2. The basic vibration isolation system requires a “soft” spring for vibration isolation and damping to control the resonant frequencies. The project team has developed a linear stroke magnetorheological (MR) damper which has been developed for use specifically for the MH-60S seat system.

Linear viscous dampers work by moving a piston through a tube to apply pressure to an incompressible fluid, forcing the fluid to pass through an orifice in the piston. The fluid dynamics involved in passing the fluid through the orifice cause a large pressure difference and in turn a force on the piston. In most cases, the orifice is designed so that fluid is passed from one side of the piston to the other, therefore allowing the forces from piston motion to be bidirectional and repeatable. The design of linear MR dampers will be discussed further in chapter 4. Linear viscous dampers have been in use for almost 100 years. Their development process is well documented and straight forward [14]. The current state of mathematical representative models allows for the capability to design for very precise desired damping forces.

In designing any vibration isolation system the stroke required depends on the frequency and amplitude of vibration as well as the stroking mass. The system may have to handle a changing mass and react appropriately. Occupants of different weight will settle at different static displacements. This requires designing in available stroke for variable spring static compression, sometimes finding this stroke is difficult. The motion of the suspended mass will be at its greatest at the system's resonant frequency. Reducing this resonance effect is important to manage the required stroke and the forces passed to the occupant from potentially bottoming out. In a passive damper, the force required to reduce the stroke at resonance to an acceptable level should be balanced with the corresponding reduction in vibration isolation performance. Fortunately, AVASS is able to minimize resonance and work well in high frequencies by utilizing

Magnetorheological (MR) fluid technology. MR fluids can turn linear dampers from a passive energy absorbing system to what is referred to as a semi-active system.

Semi-active vibration control uses dampers which have a controllable damping force.

Although the project acronym includes the word “Active”, this may be a misnomer due to the fact that what is actively changing is not an actuator force and is instead changing how much energy the system can absorb [15]. Traditional viscous dampers use oils to provide a fluid with a consistent, predictable viscosity. MR fluid dampers utilize the advantages of a controllable apparent viscosity. The very important advantage of a semi-active system is that the failsafe mode is to turn into a passive damper; reverting to an inherently stable system and maintaining most operational characteristics. The next section will discuss some of the particulars of MR technology.

Magnetorheological Fluid Technology in Viscous Dampers

Magnetorheological (MR) fluid demonstrates a measurable change in apparent viscosity when exposed to a magnetic field [16]. The history of MR fluid is relatively long in the world of modern engineering, but only recently have reliable fluids been patented, characterized and sold as a product [17]. The advancements in producing a repeatable effect have allowed engineers to create highly specialized dampers for both shock and vibration absorption [18]. Modeling the effect of changing magnetic fields in an MR fluid flow has been achieved using various methods which have furthered the advancement of closed loop control of the damping forces on a system [19].

Early documentation of MR fluid can be found from the 1950's. In 1956, Jacob Rabinow patented a “magnetic particle clutch” design using a “fine powder of magnetically susceptible material.” Early fluids showed many problems, such as abrasiveness, chemical instability and rapid deterioration of properties [16]. The general idea persisted and the magnetic particle in a suspension recipe has been refined and re-patented many times. Today, LORD Corporation owns most of these patents and sells the MR fluid from their website [18]. MR fluids continue to have limitations due to variation in properties due to temperature and high shear rates, but these effects can be compensated for in mathematical models.

The concept of MR fluid is quite simple. Changes to the suspension fluid and percent content of magnetic particles tend to change the zero field viscosity and maximum yield force respectively. No magnetic field means that there is little to no interaction between the magnetic particles. When a shear stress is applied to MR fluid with no field, the viscosity reduces to levels close to the viscosity of the suspension fluid alone. When placed within range of a magnetic field, the particles of magnetic material start to polarize and are attracted to each other. The particles form chains in the direction of the magnetic field lines. If these chains are formed perpendicular to the shear direction, the chains must be broken before large shear strains can occur. The stress required to break the chains is often described as the yield stress. Since the viscosity of a fluid is defined as the variation of shear stress with shear strain rate, the apparent viscosity is then increased greatly in the presence of a magnetic field. If the number of magnetic particles is increased as a percentage of fluid volume the distance between particles is decreased. The

decrease in distance increases the magnetic attraction between the particles. The yield stress is limited by the permittivity of the magnetic particles and the associated magnetic attraction between them [19].

LORD Corporation sells many different types of MR fluid, the company also provides reference material describing their uses [18]. The main difference between these is the volume percentage (vol%) which is made up of magnetic particles. For instance, MRF-122EG is 22 vol% magnetic particles by volume. It provides the lowest passive viscosity but may have particle settling issues. MRF-140CG is 40 vol% magnetic particles. Unfortunately MRF-140CG is very heavy and feels more like a greasy paste than a fluid. AVASS has been designed to use MRF-132DG. This fluid is recommended by LORD Corporation as the least likely to have particle settling issues with a large dynamic range. Its properties are listed in Table 1 for reference. Magnetic properties are available on technical data sheets also available on the website and in Appendix 1 [18].

Table 1: Properties of MRF-132DG Magneto-Rheological Fluid as listed on the LORD Corporation website

Appearance	Dark Gray Liquid
Viscosity, Pa-s @ 40°C (104°F) Calculated as slope 500-800 sec⁻¹	0.112 ± 0.02
Density, g/cm³ (lb/gal)	2.95-3.15 (24.6-26.3)
Solids Content by Weight, %	80.98
Flash Point, °C (°F)	>150 (>302)
Operating Temperature, °C (°F)	-40 to +130 (-40 to +266)

Shear strains can be induced in the MR fluid by various modes, and each has been studied separately. Today, the most common terms are flow mode, shear mode and squeeze mode [16]. When the fluid is pressurized through a rectangular passage, or gap, it is called flow mode. Flow mode shear is caused by the pressure gradient across the fluid and stagnation points at each surface of the passage. The fluid is in shear mode when the forces are due to direct shear. The fluid is sheared due to the surfaces of the gap moving relative to each other while maintaining the same gap width. Squeeze mode is due to compression of the gap and bulging of the fluid [16]. In all cases the gap in discussion is small, usually no larger than 0.1". In a linear viscous damper, the forces are almost completely due to flow mode.

Modern mathematical representations of MR fluid mechanics allow for very high fidelity models of damping systems [19]. The simplest and most common representation of the

MR effect is called the Bingham Plastic model. A constitutive damper model based on a Bingham plastic yield stress adds a representative constant yield stress opposing the motion of the piston. The system acts as a solid until the yield force threshold is reached. A representative shear stress vs. shear strain graph is shown in Figure 2 to demonstrate how the system behavior can be simulated by the Bingham Plastic model. The shape of the hysteresis can vary due to many variables unaccounted for in this simple model. Fluid magnetic properties, damper accumulator effects, fluid compressibility and fluid cavitation are just some examples of variables that can affect the performance of a damper [16]. Although mathematical models approaching the experimental shape are available, they are often unnecessary for good system performance and controllability. For the AVASS program, the Bingham Plastic representation has been used to assess whether the dampers in testing match the desired characteristics.

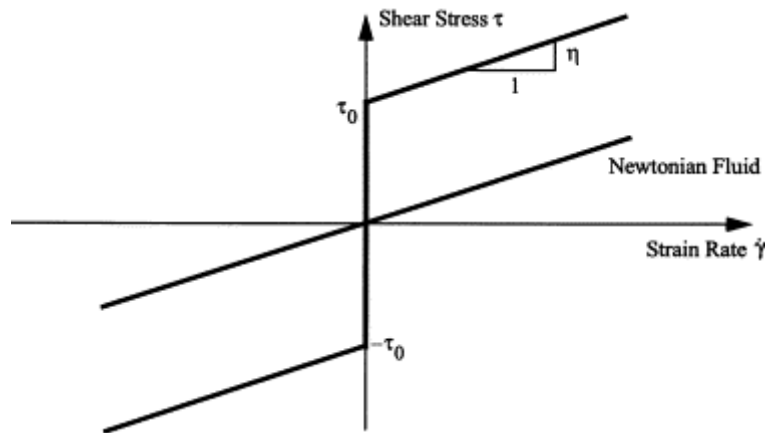


Figure 2: Bingham Plastic Model Representation of MR fluid effect

The AVASS system uses the electronic controllers and software from the SAMSS system for applying an appropriate magnetic field to the fluid. The limitation of the implemented microcontroller, specifically the required sampling rate for controllability, is the main reason why a high fidelity model is not used for these systems. The system, discussed in brief in this thesis, uses polynomial models for current applied to a coil versus yield force. The model is quite accurate to these specific dampers because it is created through empirical testing results.

Previous Work

Magnetorheological (MR) dampers for use in seat suspensions have been in research papers since the late 1990's [20]. MR dampers for use in helicopter crew seats were first studied at the University of Maryland in the early 2000's [21]. The concept was originally analyzed for shock mitigation and later adapted for vibration isolation [22].

The Semi-Active Magnetorheological Seat Suspension (SAMSS) project started in 2006 as an effort to study the possibility of utilizing MR dampers in a dual use shock mitigation and vibration isolation system [22]. The design of a dual use damper was found to be too bulky and heavy for use in existing helicopter crew seat designs [22]. By 2008, the project team developed a vibration isolation system for an MH-60R which maintained functionality of the FLEA system for crash events [23]. The AVASS project, started in 2011, serves to study the possibility of adding a technology with similar performance gains as SAMSS to an armored helicopter crew seat. AVASS maintains

personnel from the SAMSS project and hopes to refine the design of the components using their experience and knowledge.

SAMSS Performance and Lessons Learned

SAMSS experience provided the AVASS team realistic goals and a method which would lead the project away from any time consuming pitfalls. SAMSS results are well documented. Conference and Journal papers have been published describing the test methodology and results from SAMSS design [3] [23] [24]. Matching SAMSS performance means achieving 90% reduction in vibration from the floor at 17.2 Hz (Figure 3). This result was achieved through refinements of the design over three years [24]. Below is a review of the key principles which played a part in the success of SAMSS.

Reducing friction is of key importance when designing for vibration isolation. The lesson was learned that friction at any point in the motion of the seat bucket reduces the possibility of vibration isolation performance. Specifically, if the vibration amplitude is not large enough to overcome friction, the system may not stroke. The vibrational amplitude for SAMSS and AVASS may be similar as both will work in variants of the Seahawk helicopter. As an anecdotal example, assume vibration amplitudes are on the order of 0.2 g. If the suspended mass is 100 lbs, then the peak vibration force is on the range of 20 lbs. If the system must overcome 10 lbs of friction force, the vibration isolation technology can only reduce vibration transmission by a maximum of 50%.

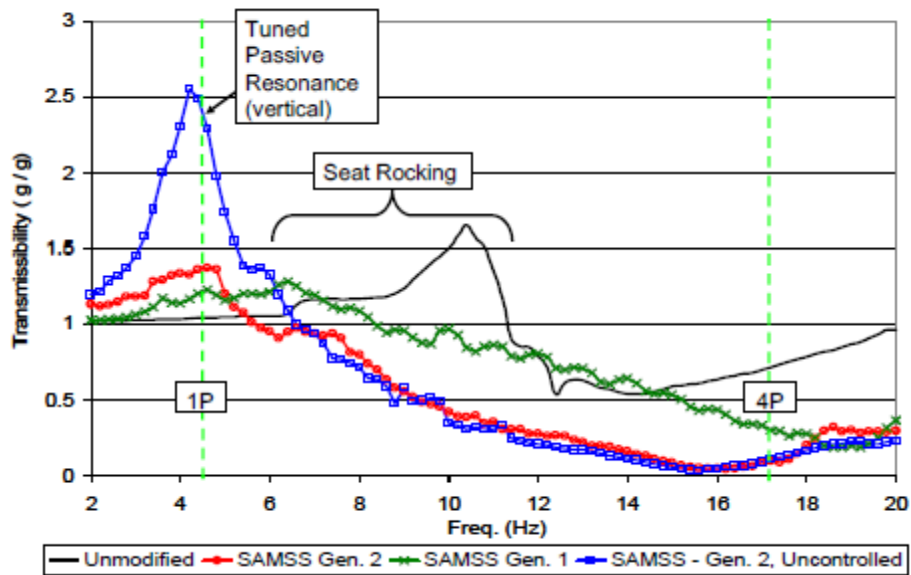


Figure 3: SAMSS Rear Seat Pan Vertical Transmissibility for 50th Percentile Male, 0.2 g Excitation

[3]

SAMSS had early friction issues due to bending loads on the damper rod and rubbing on the guide tube (Figure 3). The first version of the SAMSS damper had friction due to the piston ring seal and the rod seal. Refinements were able to reduce friction directly at the damper dramatically. Unfortunately, the moment generated by the static seat loads created further friction problems. The original design of the MH-60R does not have a crossbar joining the two guide tubes. The seat bucket is attached to the seat frame through FLEAs attached at the top of each of the crossbars. The FLEAs are angled in towards the center of the seat bucket and produce a large lateral force component. The FLEA forces pulling on the damper attachment point were reduced by adding a crossbar. A crossbar to react lateral forces is necessary for the dual damper in guide tube design.

For the MH-60S seat, the development focused on reducing friction in the damper as well as in the connection point to the crossbar, and in the overall system. Fortunately, a crossbar was part of the OEM design for the MH-60S. Unfortunately, the project team found that the MH-60S does not have the roller bearings at the guide tubes that the MH-60R has. The effect of this high friction bearing surface, and the corresponding design of replacement roller bearing brackets, is documented in chapter 5.

Finally, the design of the system was reassessed for ease of manufacturability, assembly and maintenance. The AVASS team members who worked on SAMSS believe that making the system easier to work on can make the system more appealing to the Navy. SAMSS required removing the guide tubes from the MH-60R to add mounting holes for the dampers, increasing the time required for retrofit. This is an example of why modifications to the OEM seat system, as part of the retrofit design, were kept to a minimum. Assembly of the individual components was judged just as important as assembling the components onto the MH-60S frame. The project team hopes that good design practices will make this a product which could be quickly mass produced and adopted to existing seats. Along the same line, although pleasing aesthetics was not at the top of the list of requirements, the project team has tried to make the system look as close as possible to OEM construction. The AVASS seat system is an evolutionary step on SAMSS, and as such should be cleaner and more refined. The rest of this thesis will document the development of this latest technology in helicopter crew seat occupant vibration isolation, its final design and expected performance.

AVASS Goals

The goals of the AVASS project have been loosely discussed throughout this introduction. The clear objective of this effort is to design a suspension utilizing magnetorheological dampers, to suspend the seat bucket of the MH-60S helicopter crew seat, which can be analyzed in a single degree of freedom to remove the rocking mode effect and greatly reduce the transmission of vibrations to the occupant. The underlying goals are to maintain the crashworthy functionality of the seat system and to limit any added weight to a minimum. Throughout the project the team is attempting to reduce friction in the suspension and identify the potential cause of deviations from the single degree of freedom model. Solutions are either implemented or discussed for future work.

CHAPTER 2: APPLICATION OF VIBRATION ISOLATION THEORY

Single Degree of Freedom Base Excitation

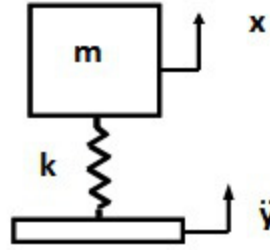


Figure 4: Single Degree of Freedom Spring-Mass Base Excitation

The simplest case of vibration isolation is a suspended mass, with motion allowed in a single degree of freedom, subject to sinusoidal base excitation. Figure 4 shows this case as a mass (m) suspended on a spring (K) attached to a forced base. This is a fundamental topic found in almost any textbook on the analysis of vibration. Passive vibration isolation solutions suspend the mass which should be isolated from vibrations and allow it to “float” free from its base. The relationship between transmissibility and the system mass, spring rate and frequency input is used to analyze performance options.

If K is the spring rate, m is the suspended mass and ω is the frequency of motion, the transmissibility of an un-damped single degree of freedom system is given as:

$$T = \frac{1}{\text{abs}\left(1 - \frac{m\omega^2}{K}\right)} \quad (1)$$

It can be observed that there is an asymptote at the resonant frequency, ω_n , indicating a point of instability:

$$\text{Resonant frequency} = \omega_n = \sqrt{\frac{k}{M}} \quad (2)$$

Understanding the frequency dynamics of this relationship is important for tuning the system properly. If the base is vibrating, the spring will pass some of the force from vibration to the suspended mass. This force will vary based on frequency due to the properties of the spring mass system, specifically the resonant frequency of the system. It turns out that at very low frequencies the spring remains fairly solid compared to the inertial forces of the mass. The transmissibility from the base vibrations to the mass is close to 1. As the frequency increases, and we approach the resonant frequency, the mass will see an increase in vibration from the base. At the resonant frequency, this effect can multiply the vibration amplitude from the base to the mass many times over. At a frequency which is 1.401 times the resonant frequency, the vibration transmissibility is back to 1 and will continue to continue to fall after this. This reduction in transmissibility is what is generally referred to as vibration isolation. The goal of vibration isolation is to design a system so that the frequency response will produce transmissibility much lower than 1.

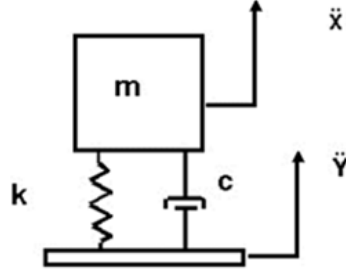


Figure 5: Single Degree of Freedom Spring-Mass-Damper Base Excitation

With the addition of a damper with damping force C to the system, the transmissibility can be written using a ratio of the excitation frequency to the resonant frequency, r , and the damping ratio, ζ :

$$T = \sqrt{\frac{(1+4\zeta^2r^2)}{(1-r^2)^2+4\zeta^2r^2}} \quad (3)$$

$$r = \frac{\omega}{\omega_n} \quad (4), \quad \omega_n = \sqrt{\frac{K}{M}} \quad (5), \quad \zeta = \frac{C}{2\sqrt{KM}} \quad (6)$$

In real life situations, when avoiding the resonant frequency completely is not always possible, damping can be added to reduce the problem of an unstable system. This damping can be described as a damping ratio, or the percent of critical damping, using equation (6).

Critical damping, $\zeta = 1$, allows for the fastest settling time of a system. Unfortunately, if this damping is constant at all frequencies, this also reduces the vibration isolation performance, as seen in Figure 6. The key, then, would be to apply forces to mitigate resonance only around the resonant frequency and to reduce the damping forces at high

frequencies. This is where the advancements in the technology of linear viscous dampers have been so important.

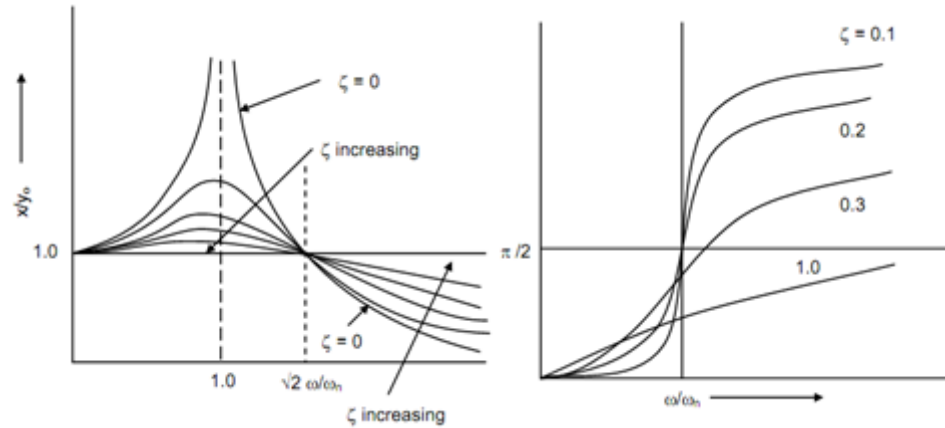


Figure 6: Effects of Damping on the Transmissibility of a Single Degree of Freedom System with Base Excitation

A hypothesis from the start of this project was that analysis of the seat system suspension we hope to implement can be simplified to a single degree of freedom system. The characterization of AVASS springs and dampers is conducted below with this assumption.

Spring and Damper Characterization for AVASS

The AVASS program set design goals based on past knowledge of Seahawk helicopter vibration. In the SAMSS program, it was found that a transmissibility of 10% (i.e., 90% reduction) was achievable for the primary cockpit excitation frequency of 17.2 Hz (4/rev blade passing frequency) at 0.2 g. As such, this 10% transmissibility was set as a goal and design constraint for this program. The program also legitimized the idea that a reduction of the model to a single degree of freedom is acceptable for the analysis of

these systems. The magnitude of the resonance will be used to calculate the desired Yield Force needed from the MR fluid effect.

An MR damper may be characterized by the Bingham-Plastic force model [16]:

$$F_{MR} = Cv + F_y \left(\frac{v}{|v|} \right) \quad (7)$$

where F_{MR} is the total MR force, C is the off-state viscous damping, v is the stroking velocity, and F_y is the controllable yield force. Further, the off-state damping may be represented using a damping ratio, ζ , which is a percent of critical viscous damping [14]:

$$C = 2\zeta\omega_n M = 2\zeta\sqrt{KM}, \quad (8)$$

where ω_n is the natural frequency of the system, M is the effective occupied seat mass, and K is the spring stiffness.

Using the stroking seat mass of 58 lbs. and the 80% rule for the range of occupants, a parametric study was conducted to aid in the design of the AVASS system. Using the

transmissibility equation $T = \sqrt{\frac{(1+4\zeta^2r^2)}{(1-r^2)^2+4\zeta^2r^2}}$ (3) for a damped SDOF system, the damping

ratio, ζ , to achieve 90% attenuation at $\omega=17.2$ Hz with 50th percentile mass can be

calculated as a function of the systems spring stiffness, K (Figure 7). This plot shows that

90% attenuation cannot be achieved with spring stiffness above 650 lb/in, which

corresponds to system natural frequencies below 5 Hz as shown in Figure 8. Further,

since it is not desirable to have the system resonant frequency match the main rotor

frequency (1/rev) of 4.3 Hz, the project team agreed the system should be designed with a

spring rate of lower than 400 lbs/in.

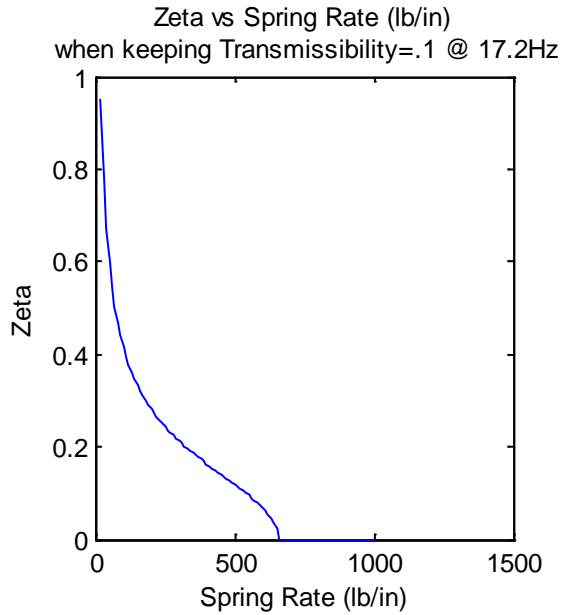


Figure 7: Damping Ratio as a Function of Spring Rate to Achieve 90% Attenuation of 4/rev Vibrations

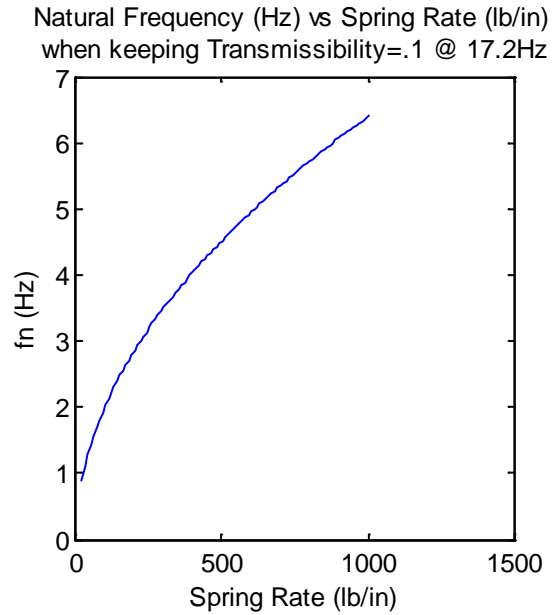


Figure 8: System Natural Frequency as a Function of Spring Rate

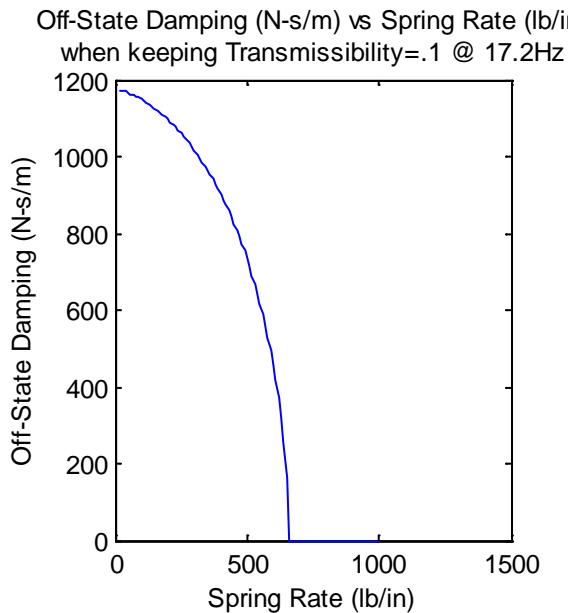


Figure 9: Off-State Damping Vs. Spring Rate to Achieve 90% Attenuation of 4/rev Vibrations

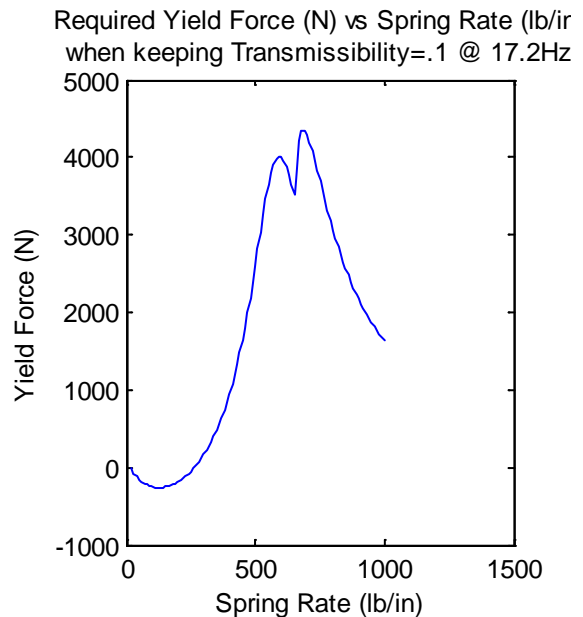


Figure 10: On-State Yield Force Required to Suppress Resonance While Achieving 90% Attenuation of 4/rev Vibrations Vs. Spring Rate: Assuming 0.7 g Amplitude Input

Figure 9 shows the resulting off-state damping to allow 90% attenuation of 4/rev vibration as a function of spring rate. Further, Figure 10 shows the on-state yield force required to suppress the resonance of a system which provides 90% attenuation of 4/rev vibration, assuming 0.7 g amplitude input. Figure 11 shows the resulting required controllable range (on-state yield force / off-state damping) to provide both resonance suppression and 90% attenuation of 4/rev vibrations as a function of spring rate, also assuming 0.7 g amplitude input. It can be seen that this controllable range rises sharply after approximately 500 lbs/in. Guidance from past experience states that a controllable range above 5 is likely unachievable with the geometric restrictions within the seat. Further, this plot shows that below 250 lbs/in, no controllable range is required – that is, a passive vibration isolator could suffice. This, however, comes with a penalty of unreasonably high static deflection as shown in Figure 7. From this parametric study thus far, the range of spring stiffness can be narrowed to 300-400 lbs/in, with the lower limits dictated by static deflection and the upper limits dictated by controllable range and avoiding resonance at the 1/rev frequency.

Finally, total stroke required for the range of occupants, including static deflection and assuming 0.7 g amplitude input, is shown in Figure 8. In this plot, it can be seen that in the 300-400 lbs/in range, the total required stroke for the MR dampers is around 1 inch. The project team will begin design of the MR dampers considering this range of spring stiffness, the corresponding yield force and viscous damping requirements, and the geometric limitations of the seat.

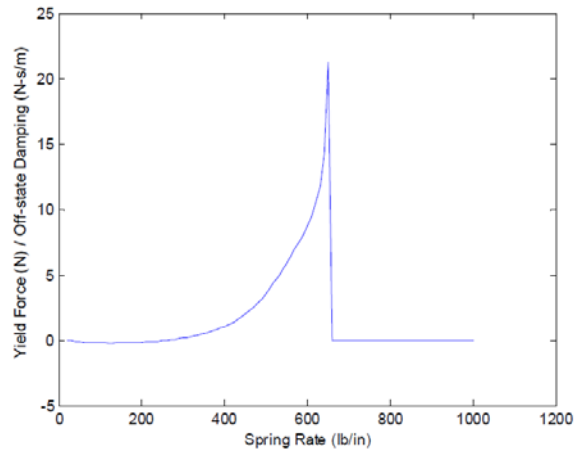


Figure 11: Required Controllable Range (On State Yield Force / Off-State Damping) As a Function of Spring Rate to Achieve 90% Attenuation of 17.2 Hz Blade Passing Vibrations

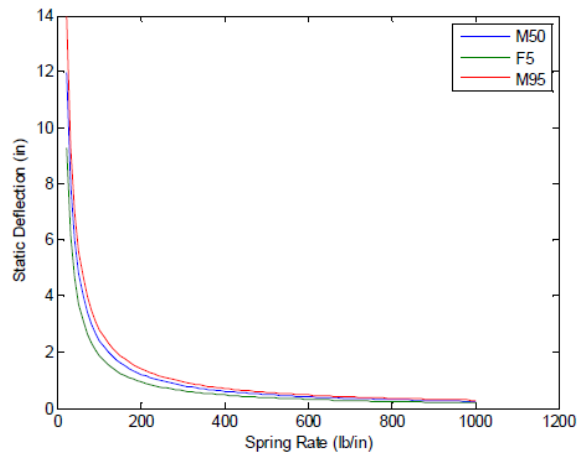


Figure 12: Static Deflection as a Function of Spring Rate and Occupant

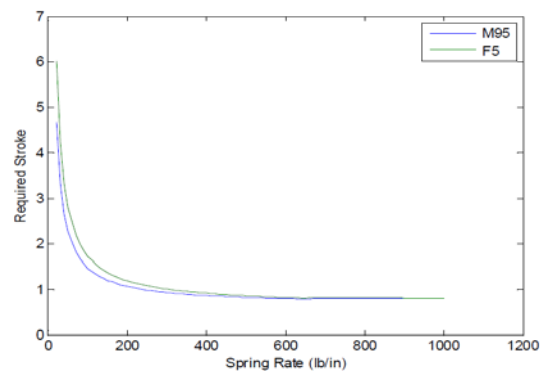


Figure 13: Total Stroke Required for the Range of Occupants Vs. Spring Rate, Assuming 0.7 g Amplitude Input

Following the analysis above, the preliminary design goals for the each of the two MR suspension points are:

- Spring stiffness: 150 lb/in
- Passive viscous damping: 508.5 N-s/m
- Maximum Yield Force: 500 N
- Stroke: 1 in.

Skyhook Algorithm for Semi-Active Vibration Control

The project team will use the Techno Sciences MR Controller electronics as part of the AVASS system. The SAMSS project helped to develop the software and hardware required for this effort although refinements are planned for the AVASS system. The controller uses a software defined algorithm based on the classic Skyhook control system to vary the current applied to the MR isolator. The concept of the algorithm is discussed below along with any changes that may be required due to the change in systems parameters.

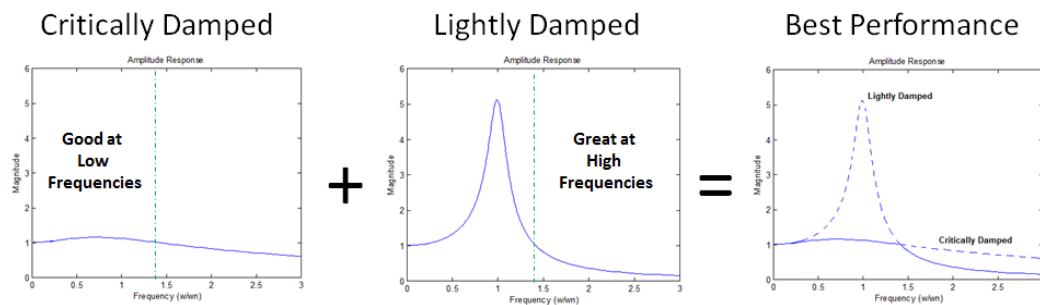


Figure 14: Semi-active Vibration Control Goal Using Single Degree of Freedom Transmissibility

Semi active control algorithms are designed to leverage the properties of the transmissibility of the single degree of freedom system [25]. In the introductory section to

this chapter, the discussion of the transmissibility of a single degree of freedom system showed the effects of varying damping. Figure 14 demonstrates how one system can be tuned to provide the theoretical best performance. Following the solid line in the “Best Performance” plot, the goal is to achieve a critically damped system for low frequencies and switch to the lowest possible damping setting at the intersection of the two plots.

Ideal Skyhook control system attempts to achieve optimal vibration reduction for a single degree of freedom system. The algorithm was first proposed in the 1970’s as the analysis of a system shown in Figure 15. The basic constituents are a spring-mass system under base excitation with a damper attached to a reference in the sky which is non-moving. The dissociation of the damper displacement from the motion of the base allows for the analysis of the system for ideal damping forces which could be applied to reduce transmissibility in the system [25] [26].

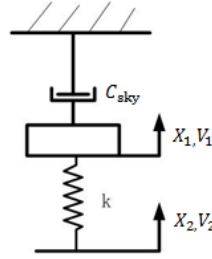


Figure 15: Skyhook Model

The transmissibility equation derived from this model is given by [20]:

$$T_{sky} = \frac{1}{1-r^2+j2\zeta_{sky}r} \quad (9)$$

Ideally, with the skyhook model, transmissibility values less than one are possible at very low frequencies (Figure 16). Unfortunately, this layout is physically impossible. Attempts at realizing this performance have led to the development of a simplified algorithm.

Using the ideas from this analysis, a relationship can be created to dictate the force levels required for optimal control [20].

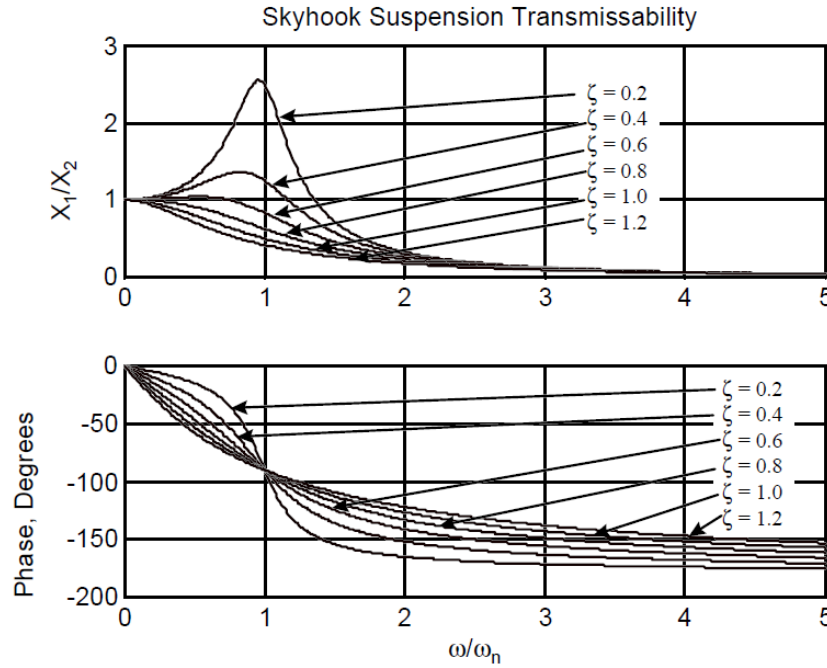


Figure 16: Transmissibility of the Skyhook Model

The modified Skyhook algorithm used for AVASS control uses the relative velocity of the suspended seat mass to the measured floor velocity as a method of proportionally varying the damping force required. If V_1 is the measured seat velocity and V_2 is the measured floor velocity then $V_{12} = V_1 - V_2$ is a measure of the relative velocity which is positive when they are separating. Using the Skyhook model, if V_1 is positive our damping force should be in the negative direction and be of magnitude

$$F_{\text{sky}} = -C_{\text{sky}}V_1 \quad (10)$$

Transferring this to the real scenario, the MR damper force can be written,

$$F_{\text{sky}} = F_{\text{Damper}} = -C_{\text{damper}}V_{12} \quad (11)$$

$$C_{\text{damper}} = C_{\text{sky}} \frac{V_1}{V_{12}} \quad (12)$$

Although this is the optimal situation, this force can only be applied by a viscous damper if the relative velocity, V_{12} , is in the same direction as V_1 . In fact if they are in opposite directions, the force required would only be possible using an actuated system. Using this logic, and the known limitations, a quick algorithm measuring the velocity of the seat and floor and calculating the relative velocity can use the following rule:

$$\begin{aligned} & \text{If } V_1V_{12} > 0 \\ & \text{Then } F_{\text{Damper}} = C_{\text{sky}}V_1 \end{aligned}$$

$$\begin{aligned} & \text{ElseIf } V_1V_{12} < 0 \\ & \text{Then } F_{\text{Damper}} = 0 \end{aligned}$$

Figure 17: Skyhook Control Logic

Accordingly, these statements determine when to apply a current to the damper proportional to the velocity, thereby increasing the damping when needed. The process does not give the full transmissibility of the Skyhook model, but it does approximate the “Best Performance” transmissibility graph quite well. More importantly, it can be used in transient signals where there may be more than one input frequency.

The MR controller software integrates the velocity of both the seat and the floor inputs from accelerometer measurements. The accelerometer signals are filtered and then integrated to calculate an instantaneous velocity of the seat and relative velocity of the seat to the damper. The current output is based on the F_{Damper} force, calculated above,

using a polynomial fit from damper characterization testing. A discussion of these equations is found in chapter 4.

$$\text{DampingForce}(i) = -0.1698i^2 + 0.522i + 0.4993$$

$$\text{YieldForce}(i) = -6.295i^2 + 183.7806i + 7.8251$$

$$F_{\text{Damper}} = \text{DampingForce}(i)V_{12} + \text{YieldForce}(i)\text{Sign}(V_{12})$$

Figure 18: AVASS Damper Characterization Equations for Use with Skyhook Control Logic

The adaptation of this algorithm for MR dampers is very effective due to the possibility of changing damping almost as fast as the data rate loop. Additionally, for testing purposes a single proportional gain is added to tune the system performance. This gain helps to quickly refine the forces applied to the system to assure that the resonance suppression is complete.

PAGE LEFT INTENTIONALLY BLANK

CHAPTER 3: CREW SEAT INTEGRATION CONCEPTS

SAMSS versus AVASS Design Review

There are a number of lessons learned from the SAMSS program for the MH-60R seat which have affected the integration design of the AVASS.



Figure 19: SAMSS Vibration Isolation System Integrated into MH-60R Crew Seat

For the purposes of retrofit, the primary difference between the MH-60R and the MH-60S seats is in the design of the crash load energy absorbers (EAs). The MH-60R seat uses an inversion-tube fixed load EA (FLEA) design and the MH-60S seat uses a wire bender variable load EA (VLEA) design [22]. Among the challenges faced by the original SAMSS program was the effect of the angled FLEAs (see Figure 19) creating side loads and moments on the damper piston rod. In order to maintain an even loading between the parallel dampers, react the moments/loads from the angled guide tubes, and mitigate the rocking mode of each guide tube evenly, a crossbar with a vertical guide was

introduced spanning the space between the two vertical guide tubes. The MH-60S seat design, however, already has a crossbar integrated into the design (see Figure 20). This crossbar is a support for the wire bending mechanism which will be in tension in case of a crash [3].

In order to isolate the seat using the MR dampers in the same manner as SAMSS, the crossbar will have to be decoupled from the tops of the guide tubes. A few issues arise when trying to raise the crossbar off of the guide tubes. The first is that the bottom bearing ring seat brackets will not allow for raising the seat 1 inch (to accommodate static deflection) when the seat is at its tallest position (see Figure 21). The second is that the wires that run through the VLEA are pinned down to the bottom crossbar and will need to be unpinned in order to allow vertical movement.

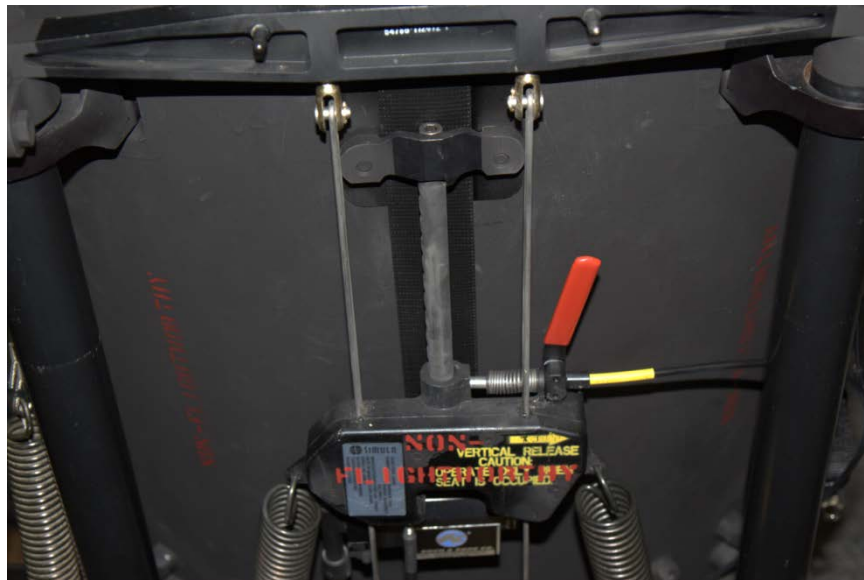


Figure 20: MH-60S Seat for AVASS program Integration

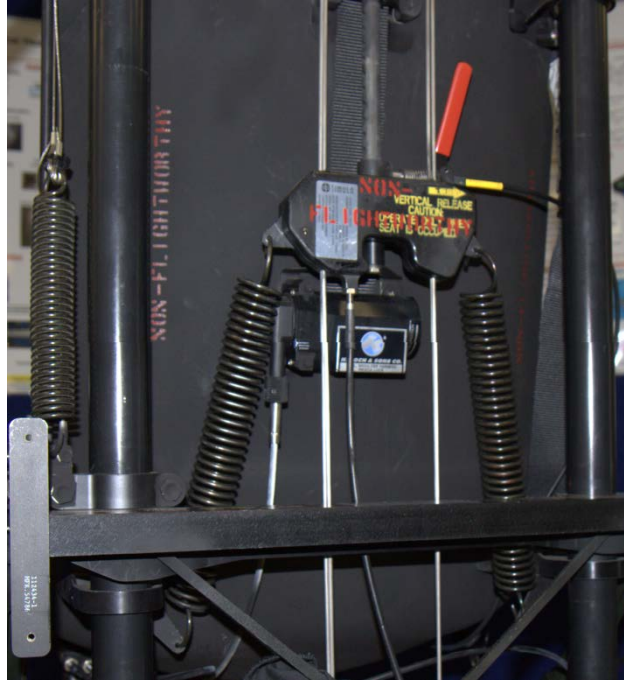


Figure 21: Seat Bracket Clearance when Raising Crossbar

The spring will be preloaded to hold the seat mass at the full 1 inch of deflection with no occupant and sit at halfway down the stroke with the 50th male mass. The relative position of the crossbar to the VLEA will need to change by 0.5 inches to maintain the OEM line of sight for the occupant.

At first glance, the VLEA wire connection to the bottom crossbeam of the seat support frame does not seem to be structural. The wire bender functions by running the wire through a series of offset bending rollers inside of the VLEA box. As the seat strokes in a crash, the length of wire below the unit are forced through these rollers and the energy from the crash is absorbed by the work done in bending the wires. The project team

initially intended to let these move freely in the vertical direction but keep them constrained in the lateral directions for safety [9].

It was later learned that this pinned system also assists in constraining the seat bucket motion in an inverted crash event. If the pin slipped, the next impact point would be the lower bearing brackets on the central cross member. Thus, the new design must maintain the vertical constraint at the top of the suspension stroke.

Also noted is much more fore/aft movement of the seat bucket relative to the frame in the MH-60S seat versus the MH-60R seat. This is a result of the difference in guide tube bearing design. On the MH-60R seat, rollers are used to prevent seat rocking. On the MH-60S seat the bearings are just loosely fitting rings which have a fibrous coating to reduce metal to metal contact (see Figure 22). This ring allows for noticeable movement perpendicular to the guide tube vertical axis. The seat is free to rock because the single point of contact to the main structure is the single adjustment pin for the VLEA. There is no moment reacted through the adjustment pin.



Figure 22: Loosely Fitted Guide Tube Bearings

Another issue with the MH-60S seat bearing rings is that they do not allow for the same clearance for MR damper mounting screws as the MH-60R seat. The MH-60R seat made use of the staggered rollers in the guide tube bearings, which allowed clearance for screw heads. Mounting options are limited by the fact that any protrusions along the guide tube may be contacted by the bearing rings and obstruct in its downward motion in a crash or even in vibration [3]. For this reason, a different MR damper mounting method is required with the requirement of no protrusions from the guide tube surface and a secondary goal of not needing to remove the guide tubes for installation (to ease retrofit and reduce cost).

Disassembly of OEM Seat for Ease of Retrofit Study

Physically going through the steps required to disassemble the seat made it clear what changes would make the retrofit effort more difficult. The process also gave a better idea of how the seat functions as a whole.

The following procedure was used to disassemble the seat. Disassembly was started by attempting to disconnect the crossbar from the seat. The Phillips head screws at the top of the guide tubes were removed. The nuts holding the clevis rod ends holding up the VLEA wires were also removed. At this point it was noticed that the entire seat was falling and was being suspended solely by the wires in buckling. The wires were very resilient to yielding in buckling, as they supported the seat. It was required that the seat back and bearings move down as far as possible in order to be able to drill out the rivets in the guide tube. At the time, the wires were still being held into the seat, and in order to do this the project team was forced to remove the seat height post from the seat. It was difficult to move the seat without the seat collapsing down at an angle. Potential future improvements to this process may be to support the seat may be with a floor jack to keep the seat vertical and be able to move it up and down.

Once the seat was out of the way, the rivets holding the threaded insert in the top of the guide tube had to be removed. The rivets were removed by first using a center punch to locate and remove the center of the rivet and then drilling with a slightly undersized drill bit until a punch could be used to remove the head of the rivet. For many of the rivets it was necessary to go back and make sure that enough material had been removed before

the inserts came out. The crossbar was used as leverage to persuade the inserts to leave the guide post.

The conceptual design at the time of disassembly called for switching out both the supports for the seat height adjustment on the seat so that the seat is lowered to keep the same line of sight as the OEM seat. On disassembly, it was noticed that it may be possible to lower the seat directly using the clevis rod ends directly. This solution, it was thought, would save time during the retrofit effort and lower the cost of the system compared to new seat bucket mounts. If the retrofit process first involved removing the pins holding the wires to the lower support bar of the seat, the seat could be lowered completely by just releasing the wires from the clevises. The crossbar could be replaced with a new “assembled” crossbar with dampers, harness and new clevises ready to be installed. The seat could then be picked back up and pinned to the new clevises.

AVASS Retrofit Design Concept

Conceptual ideas of how to design the components of the AVASS system are discussed below. It was envisioned that the retrofit kit would be made of two dampers and electronics, each with their required mounting hardware. The full development processes for these components are documented in chapters 4 and 5.

Damper Mounting Design Ideas

A lipped or flanged damper mounting tube that fits inside the guide tubes was envisioned to provide support against lateral loads as well the downward vertical loads. For upward vertical loads, it was envisioned that the dampers would be secured with wire or composite ropes fastened to a flanged mounting tube at the bottom end of the guide tube. In assembly, one would slide the attached wire rope down the tube before sliding the damper down and sitting it on the top side of the guide tube. From underneath, the wire rope would be secured and tightened to designed specifications. This mounting concept is shown in Figure 23 and Figure 24. This lipped damper design is still the basis for the design of the damper, but the restraining method was changed for the final version.

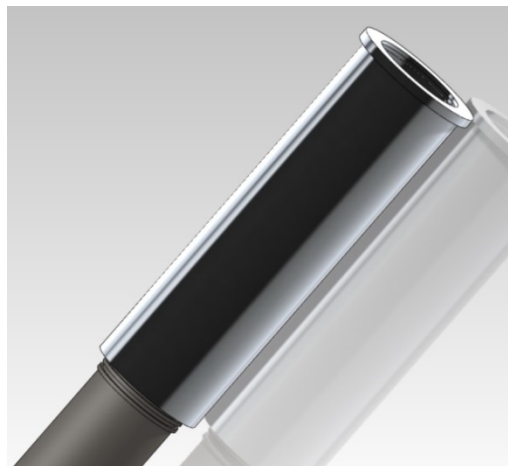


Figure 23: Flanged MR Damper Mounting Tube

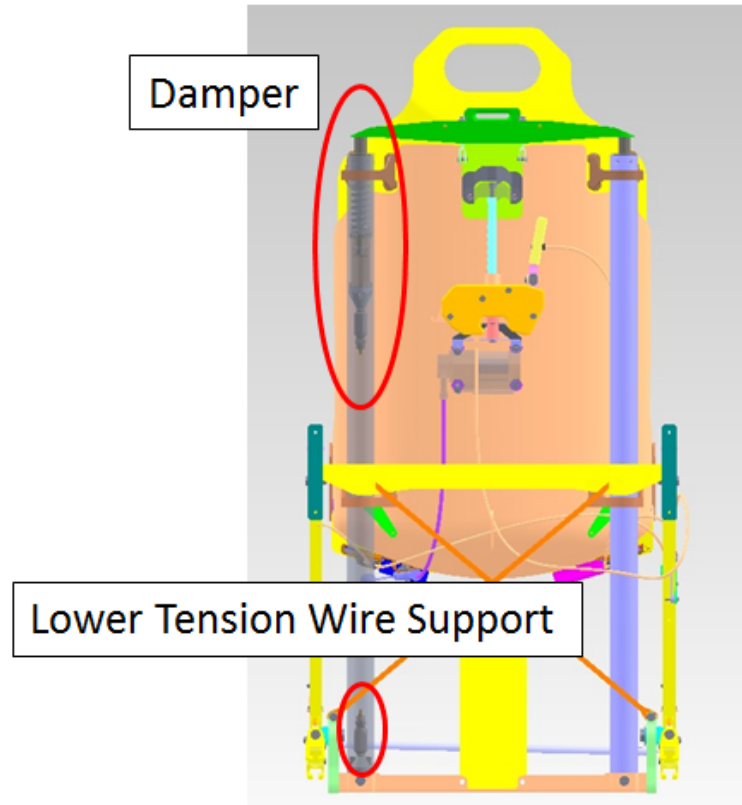


Figure 24: MR Damper Mounting with Lower Tension Wire Support

Electronics Mounting Design Ideas

The electronics mounting solution that is proposed, Figure 25, sits behind the seat belt locking mechanism. The design has clinched fasteners which allow for the quick attachment of the current electronics enclosure. The seat box mounting bracket has been designed to follow the contour of the seat. The assembly method is to remove the nuts holding the seat belt bracket mechanism and use a screw driver or pin to drive the long bolts out the front of the seat. The back seat pad will have to be removed in order to get at these bolts. Once these bolts are out, the installer can slip the bracket underneath the seat belt locking mechanism and start to slide the bolts back through the holes to fasten the

seat belt locking mechanism. There is enough thread to allow the tightening of the nut onto the bolt even after adding the 0.06” thick plate behind the seat belt locking mechanism, but it may be safe to provide replacement nuts and bolts in the final retrofit effort. A method of keeping the bracket from vibrating fore and aft was also implemented in later design revisions.

The secondary accelerometer board the project team plans on using is 20mm x 20mm. An aluminum enclosure can be designed which attaches this accelerometer directly to the seat using the threaded holes that originally held the wire pins in place on the bottom support beam of the seat system. The concept is visualized in Figure 26



Figure 25: Electronics Seat Bracket Design

The final attachments to the seat are constraining components for the VLEA wires. The original concept had two cups with threads at the bottom which will contain the VLEA wires. The parts are shown, as envisioned, in Figure 26. These would be attached to the bottom bracket of the seat using screws which are passed up through the holes that the VLEA wires originally were placed into to be pinned. This design was later changed to a channel design which allowed for the positive stop of the system in an inverted vertical crash event.

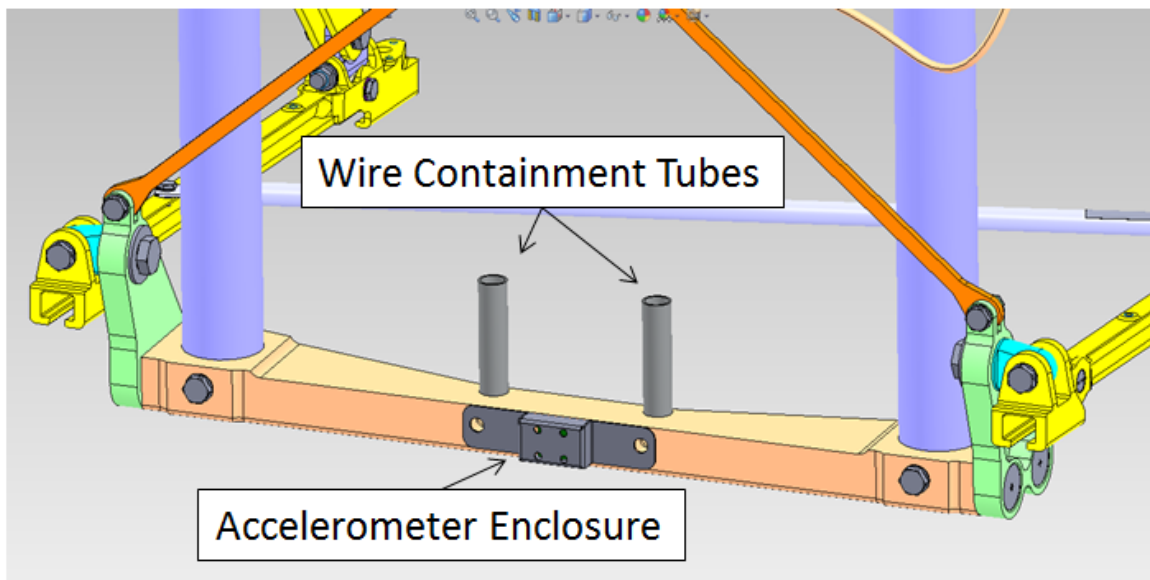


Figure 26: Accelerometer Box and VLEA Wire Containment Tube Concept

The procedure for implementing the retrofit redesign order of operations could be as follows:

- Put the seat on a raised platform with the back of the seat on the edge of the platform
- Support the seat with a floor jack
- Cut the guide wires 1.5” above the lower support bracket (where the wires are held to the seat).
- Remove the bolts, pins and wire ends that are left attached to the lower support bracket.
- Remove clevis pins and detach wires from upper crossbar.
- Lower seat as far as possible (will have to move the wires to the back side of the lower support bracket and off the edge of the platform)
- Remove the Phillips head screws from the crossbar and remove crossbar
- Drill out the rivets in the guide post
- Reattach crossbar and use rubber mallet and leverage to remove inserts
- Insert suspension system consisting of:
 - Crossbeam with dampers and new clevis parts attached
- The two dampers will go into the guide tubes and get riveted in.
- Remove the seat pad on the back rest.
- Remove the four bolts holding the seat belt locking mechanism in place (you will need a long rod or screw driver to push the bolts out the front of the seat)
- Slide the controller box assembly (box mounted on bracket) under the seat belt locking mechanism. Make sure that the controller box assembly sits between the seat belt locking mechanism and the lower seat height support bracket where the top two bolts come through.
- Use provided replacement bolts and nuts to re-fasten the seat belt locking mechanism, controller box assembly and lower seat height post bracket to the seat. These bolts are slightly longer to account for the thickness of the controller box plate.
- Apply black silicon caulking around the edge of the controller plate where the plate meets the seat.
- Raise the seat and pin the VLEA wires to the new clevis parts.
- Pass the VLEA wire containment tubes over the wires and attach to lower seat bracket.
- Connect the accelerometer box to the back side of the lower seat bracket using pin bolts.
- Connect the harness from the controller box to the crossbar.
- Connect power
- Test seat for correct performance

CHAPTER 4: MR DAMPER DESIGN

This chapter outlines the design methodology for MR dampers which was used for the AVASS system. Physical parameterization, trade-offs, and design iterations are discussed. The process by which the AVASS MR damper was designed is documented in detail.

MR Dampers – Damper Design Reality/Practical Approach

The linear telescoping MR dampers which are planned for AVASS are similar in structure to the design of the modern day passive viscous telescoping damper. The main distinction is the difference in design goals for the piston. Aside from the piston, the strength of the damper housings and accumulator design can be analyzed in a very similar fashion. Today's most sophisticated passive dampers use complicated tubes, shims and valves which require constant changing to vary the damping curve. MR fluid can simplify the system, and allows for continuous variation of damper characteristics by applying a current through an electromagnet [14].

Due to the importance of the functionality of the piston, the design process for an MR damper starts at the piston and works outwards. The piston must balance the fluid dynamics of a passive damper with the requirements of the built in magnetic circuit. The geometry of the piston is the most important factor for developing the magnetic properties for fluid control.

A piston with a wire coiled around its central axis will induce a magnetic field which runs down its central axis, curving around the outside of the coil passing up the outside of the coil reconnecting it to the top of the coil where the field line started (Figure 27). These magnetic field lines expand away from the coil radially creating loops of lower density with an increased distance from the coil itself. In this way, the field is most normal to the flow at the points closest to the top and bottom of the coil itself [27]. The parts of the piston closest to just above and below the coil can be designed into active valve areas for MR fluid dampers.

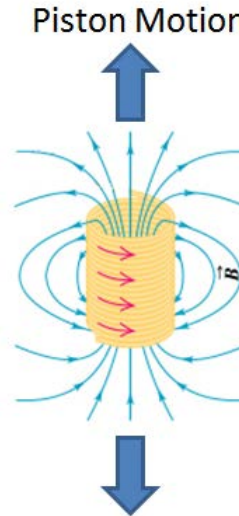


Figure 27: Magnetic Field Lines Around a Magnetic Coil

adapted from http://www.physics.sjsu.edu/becker/physics51/mag_field.htm

The piston of the telescoping damper will form a tubular magnetic circuit with flux lines which run within a material of high magnetic permeability. The design of the piston will allow fluid to pass through small orifices, serving as restrictive valve for the magnetic fluid to pass through. There is more discussion on how this is achieved in the next section.

The physical properties of the materials to be used are necessary for the design of the magnetic circuit. The fluid specifications posted from the vendor, LORD Corporation in our case are shown in Figure 28. Magnetic properties of steel alloys are available from manufacturers and distributors. A representative B-H plot for 1018 Steel is shown in Figure 29.

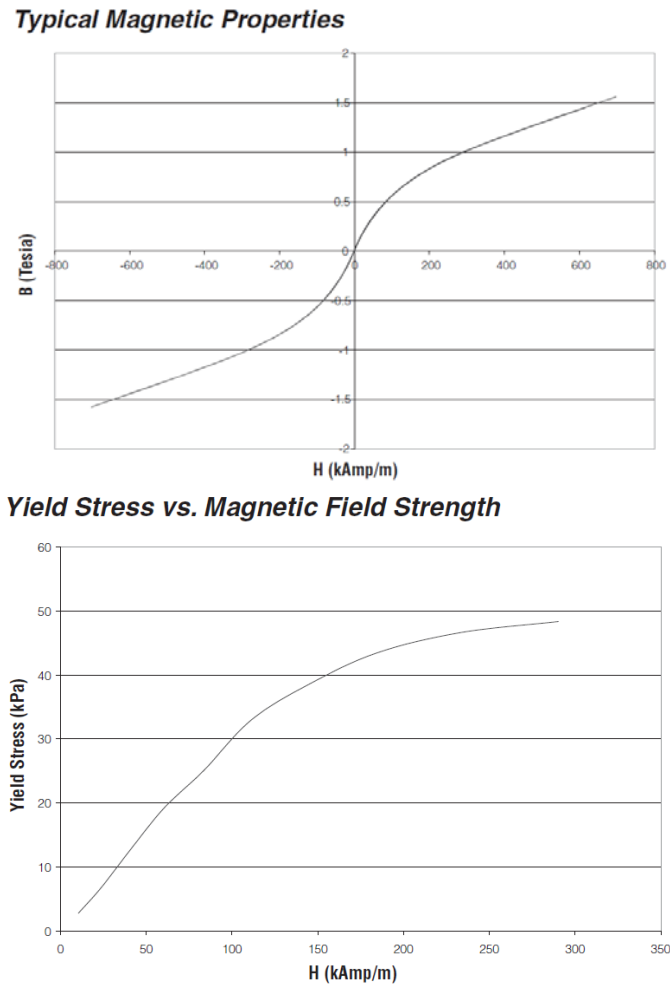


Figure 28: MRF-132 Magnetic Properties [18]

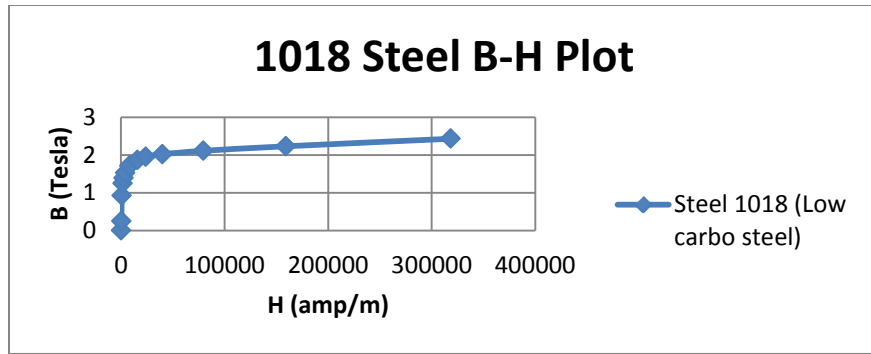


Figure 29: Representative 1018 Steel B-H Plot

A good overview of the typical design process for a Magnetic Circuit can be found in the support documents for MR products at the LORD Corporation website. The main section is replicated in Figure 31 [27].

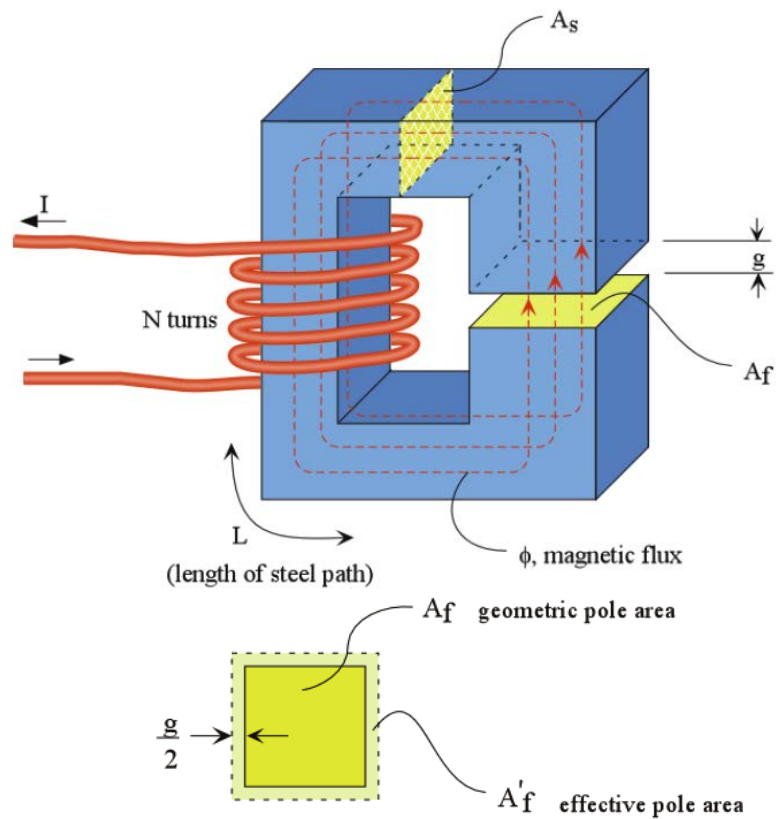


Figure 30: Basic Magnetic Circuit [27]

Typical Design Process:

1 . Select **operating point** (H_f , B_f) in **MR fluid** to give desired yield stress (τ).

- Total magnetic flux is given by $\Phi = B_f * A_f'$ where A_f' is the effective pole area due to fringing.

2 . Use principal of **Continuity of Magnetic Flux** to determine flux density B_s throughout flux conduit:

- $\Phi_{\text{fluid}} = \Phi_{\text{steel1}} = \Phi_{\text{steel2}} = \dots$

3 . Determine **operating point in steel**. (Note, this may not be the same at different places in the flux conduit if cross section varies.)

- $B_s = \Phi_{\text{steel}} / A_s = B_f * A_f' / A_s$

- Determine H_s from BH curve for steel.

4 . Use **Kirchoff's Law for Magnetic Circuits** to determine necessary amp-turns (NI):

- $NI = \oint H \cdot dl$

or

- $NI = \sum H_i * L_i$

or

- $NI = H_f * g + H_s * L$

Figure 31: Magnetic Coil Typical Design Process [27]

The above equations must be balanced with the parameters for the physical design of the damper and fluid dynamics for passive damper force based on vibration analysis. For AVASS, existing parameterization software was used to determine a possible damper design. A brief overview of what variables are used in code may help the reader understand what is involved in designing the damper [19].

Variables from Parameterization code:

- Initial Design Parameters
 - K : Spring Rate for the System
 - C_0 : Desired field off viscous damping
 - Operating frequencies, ω_4 and ω_1 for 4/rev and 1/rev
 - ζ : Desired damping ratio when max field is applied
 - ζ_0 : Desired damping ratio when no field is applied
 - g_i : Max expected g input
 - S : Max damper stroke
 - D_d : Max damper OD
- Material Parameters
 - μ : Kinematic viscosity of MR fluid
 - τ_y : Maximum Yield Stress of MR fluid with field on
 - ρ_{mr} : Density of MR fluid
 - B_{mr} : Flux Density for MR fluid
 - H_{mr} : Magnetic Field strength for MR fluid
 - B_{steel} : Flux Density for MR fluid
 - H_{steel} : Magnetic Field strength for MR fluid
- Iterated Parameters
 - D_{rod} : Damper rod diameter
 - D_p : Damper piston diameter
 - Re: Reynolds number
- Output
 - d : Gap thickness
 - l_a : Active valve length
 - D_a : Active valve diameter
 - D_m : Central flux diameter
 - D_o : Outer flux diameter
 - L_p : Piston Length
 - Coil: Total Number of Coils
 - N_h : Desired Coils levels in the radial direction
 - N_w : Desired Coils levels in the length direction
 - F_{max} : Maximum damper force
 - L_d : Expected dynamic range of MR damper

Equations of Interest from Parameterization Code [19]:

- Passive mode equivalent damping: $C_{eq} = \frac{12\mu L(\frac{A_p}{d})^2}{A_d}$ **(13)**
- Bingham number: $Bi = \frac{\tau_y g}{\mu} \frac{Ad}{Ap\nu}$ **(14)**
- Ratio of plug thickness to gap: $\bar{\delta} = 2\sqrt{1 + \frac{4}{Bi}} \cos(\frac{1}{3} \arccos(-\sqrt{\frac{Bi}{Bi+4}}))^3$ **(15)**
- Maximum expected yield force: $F_{y_{max}} = \frac{Bi}{6\bar{\delta}} C_{eq}\nu - C_{eq}\nu$ **(16)**

Using the iterated variables and equations above, the code defines only the locus of designs which are physically possible for reaching the design parameters. The area of the piston, defined by the iterated diameters, and Reynolds numbers are used to define a set of gap thickness numbers which will not cause compressibility issues. An active valve length set is defined by the desired max damper force using the gap thickness numbers. The ideal damper yield force is calculated using Bingham Plastic equations. The possible designs are then analyzed and fleshed out using the magnetic circuit process described above.

This set of variables is only one way in which a dimensional parameterization code can be defined. There are multiple papers on non-dimensional analysis of magnetorheological dampers defining equations which relate the geometry of the gap to the equivalent damping and yield forces [19].

AVASS MR Damper Piston and Magnetic Circuit Design

In Chapter 2, the design goals for the MR suspension were identified – the spring stiffness, the maximum required MR yield force, the off-state viscous damping, and the required stroke. These design goals were identified by using a single-degree-of-freedom (SDOF) model using both 4/rev (17.2 Hz) and 1/rev (4.3 Hz) excitations as inputs. The MR yield force and off-state damping were designed such that the system exhibits significant (90%) attenuation of the 4/rev vibrations while in the off-state, while the MR yield force is used to suppress the tuned resonance that may be excited by the 1/rev or other low frequency disturbances that may occur during flight. Below are the preliminary design goals for each the two MR suspension spring/damper devices:

- Spring stiffness: 150 lb/in
- Passive viscous damping: 508.5 N-s/m
- Maximum Yield Force: 500 N
- Stroke: 1 in

There are two standard configurations for MR pistons that have been evaluated. The simplest configuration (Figure 32a) is to size the piston diameter slightly smaller in diameter than the inner diameter of the damper body, thus creating a fluid flow gap between the two. In this case, the damper body acts as a flux return for the electromagnetic circuit and must be a ferrous material. In the second configuration (Figure 32b), a low friction (i.e., Teflon) piston ring is used to provide a seal between the damper body and the piston, forcing fluid to flow through an annular gap within the

piston. In this case, the entire electromagnetic circuit (including the flux return) resides within the piston and the cylinder can be non-ferrous (i.e., aluminum). The benefits to this second approach tends to be the reduced weight of the damper body, but the drawbacks are 1) more complex piston design, 2) added friction associated with the piston ring seal and 3) surface finish/coatings required on the inner diameter of the damper body to minimize friction [28]. Both piston configurations have been evaluated for this application.

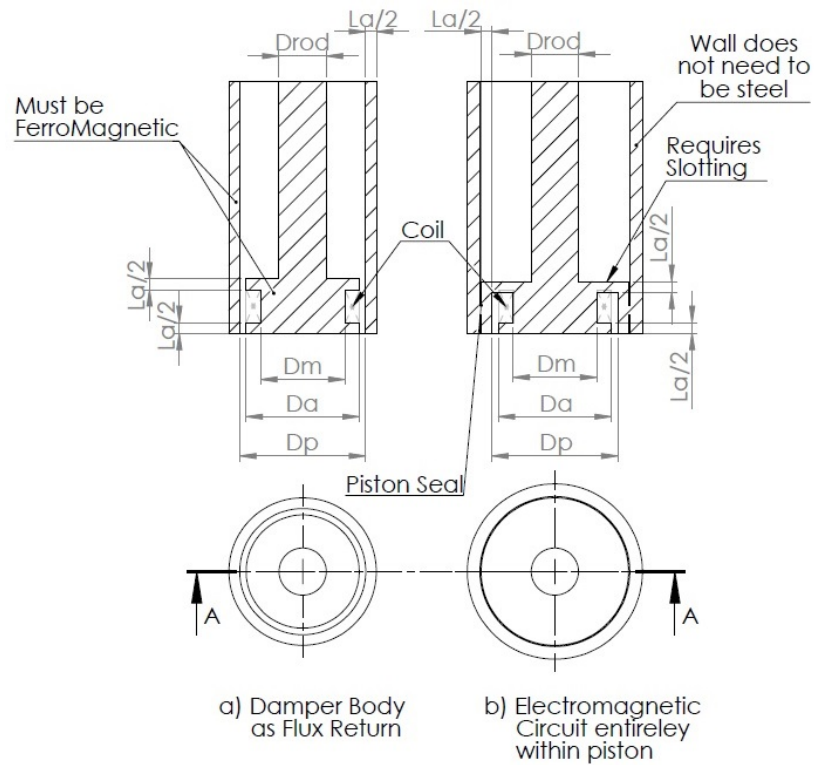


Figure 32: MR Piston configurations

The size of the fluid flow gap is an important parameter in the design as it affects both the off-state viscous damping and the controllable yield force. A small gap may increase the viscous damping too much, while making the gap too large will make it unrealistic to

generate the magnetic field required in the active valve area to create the required yield force.

The modified design analysis software uses the above relationship and parameterizes the geometry of the damper piston based upon the design goals/constraints and fluid properties. As described in the introductory section to this chapter, the program iterates through possible gap distance possibilities for a given passive force and will compute the amount of material area and coils needed to create the magnetic circuit for the desired MR force. This data can be used to design the piston and damper body in either of the previously discussed MR damper configurations. Table 2 shows a sample output for a 1” piston diameter with 3/8” piston rod is displayed below. Notice the variety of options which theoretically would produce the required passive damping force and field-on yield stress.

Table 2: Sample Output from MR Damper Design Analysis Software

Piston diameter(in)		Rod diameter(in)		Maximum velocity(m/s)											
1		0.375		0.23394956											
No.	Re	d(mm)	La(mm)	Da(in)	Dm(in)	Do(in)	Lp(in)	Coil No.	Nh	Nw	Fmax(N)	Control ratio	Damper weight		
1	44	0.353930669	4.371294318	0.996189515	0.668837646	1.11626105	0.413298201	1	6	10	549.1355257	4.620549172	0.343023648		
2	45	0.357930013	4.420689041	0.97405197	0.667187207	1.095269208	0.415242876	1	6	10	549.1355257	4.620549172	0.348466821		
3	44	0.353930669	4.371294318	0.996189515	0.590484461	1.071152105	0.509778201	2	8	7	549.1355257	4.620549172	0.376865392		
4	45	0.357930013	4.420689041	0.97405197	0.589550155	1.049783432	0.559962876	2	7	8	549.1355257	4.620549172	0.393825165		
5	44	0.353930669	4.371294318	0.996189515	0.561944184	1.055687548	0.606258201	3	9	6	549.1355257	4.620549172	0.403658947		
6	45	0.357930013	4.420689041	0.97405197	0.561289815	1.034177028	0.680562876	3	8	7	549.1355257	4.620549172	0.426396709		
7	44	0.353930669	4.371294318	0.996189515	0.547116029	1.047869688	0.750978201	4	9	6	549.1355257	4.620549172	0.440325186		
8	45	0.357930013	4.420689041	0.97405197	0.546612013	1.026284834	0.849402876	4	8	7	549.1355257	4.620549172	0.468860625		
9	44	0.353930669	4.371294318	0.996189515	0.53802301	1.043150849	0.895698201	5	9	6	549.1355257	4.620549172	0.476286606		
10	45	0.357930013	4.420689041	0.97405197	0.537613015	1.021520251	0.897642876	5	9	6	549.1355257	4.620549172	0.481540771		

This software was run through a range of piston and piston rod diameters, while the damper body outer diameter was limited to the inner diameter of the guide tubes of the

MH-60S seat. Through this process, some key decision making factors were observed. Increasing the piston diameter too far creates very small active valve lengths and the geometry of the valve on either side of the coils become too thin to be realistic designs. Further, the coils can either be wrapped to increase the diameter or to increase the length of the piston, and that a balance of the two would be optimal for weight and also for actually creating the coil without issues with manufacturing.

Based on these analyses, the project team has chosen to move forward with the MR damper piston configuration that uses the damper body as the magnetic flux return. There were three factors that led to this decision.

1. Weight: Typically, having a steel damper body results in a heavier device design. However, in this case, there is not a significant difference between the weights of the two configurations because of the short damper length (~2 inches).
2. Strength: The system must be structurally adequate for the static 20-20-10 requirements (20g vertical, 20g longitudinal, and 10g lateral) and it is expected that a majority of the vertical force will pass through the damper body.
3. Friction: The piston ring seal rubs on the damper wall and creates friction. Such parasitic friction (coulomb damping) can adversely affect vibration isolation performance.

The damper with the following geometric parameters (design option #1 in Table 2) was selected:

- Piston diameter: 1"
- Piston rod diameter: 3/8"
- Gap width: 0.3539mm
- Active length: 4.371mm

Figure 33 shows the resulting piston design with the piston rod attached. The piston rod is fastened to the piston with 3/8" -24 threads. The design of an MR damper piston must also include features to allow for coil wire integration, sealing and travel up the damper rod and out to the current supplying control box. The rod has a central bore for the electrical wires. At the piston side of the rod, there is a conical rubber seal with two holes which the wires pass through. This seal sits central to the rod and is compressed by the #2 screws used to hold the plastic wear ring in place. A wear ring is used to keep the piston centered in the damper and to avoid friction and damage to the damper body. The piston has grooves cut into it which are used to guide the wires to the inner diameter of the piston, wound around the coil area and finally back through the opposite groove and up through the piston rod.

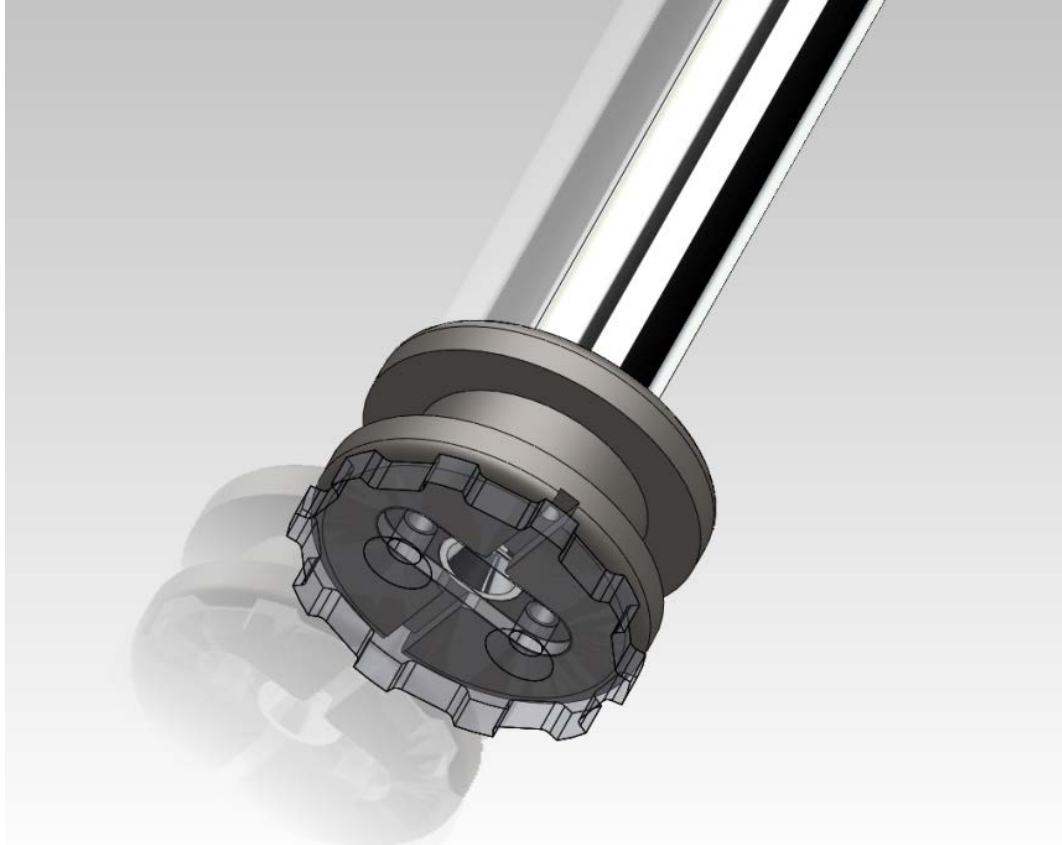


Figure 33: Piston Design with Wire Seal Design and Plastic Wear Ring

Initial Damper Body, Seal and Stepped Rod Design

In most aerospace design, weight is of upmost importance. As such, the designs are aimed at minimizing the amount of steel used in the design by limiting the damper body to as little steel as is needed for the magnetic circuit design. The design of damper seals, accumulator and a stepped damper rod are detailed.



Figure 34: First Damper Body Design Concept

The damper body design started with a tube that is long enough for the required stroke plus the length of the piston and wear ring and a little room to spare. Plastic spacers & aluminum caps to seal the damper were envisioned as shown in Figure 34. It became apparent that the amount of steel needed for the magnetic circuit design was more than

enough for structural adequacy and that the additional aluminum caps were unnecessary from a structural standpoint. It was found that it was more weight and cost efficient to add threads directly into the steel body (Figure 35), which also reduces the number of parts in the design.



Figure 35: All Steel Damper Body Design

Next the top of the damper body, where the piston exits, is addressed. A rod seal is required to make sure the fluid stays inside of the damper body while the rod freely slides. There are many commercial rod seals that are readily available for standard diameters. Based upon past experience, a low-friction Nitrile U-cup design from Allegheny-York was selected [29]. This design comes with specified groove parameters and is pre-compressed to allow for a 0 psi sealing capability. The U-Cups are easily broken and are much less risky to assemble if they are passed over the rod before installation. This method means that the groove must be accessible without having to deform or pinch the U-Cup to fit. It is also necessary to leave room in the design for a PTFE impregnated bronze bushing directly above or below the rod seal. This bushing

will be able to limit the deflections of the piston rod, helping to keep the piston centered and keep the seal from deforming.

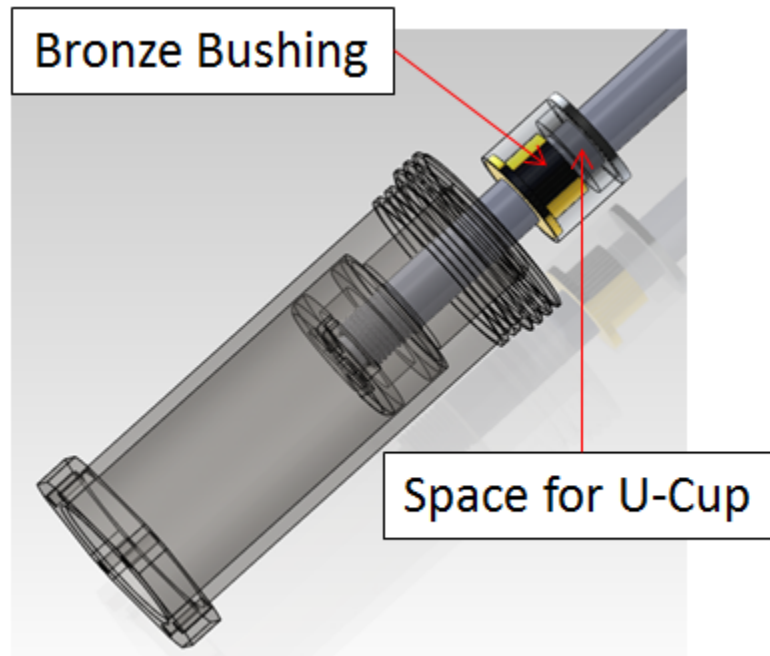


Figure 36: First Design of Bushing and U-Cup Insertion Method

An early design for assembly of the bushing and U-cup design is shown in Figure 36. The design calls for a simple aluminum bearing holder into which an off-the-shelf PTFE coated bronze bushing is pressed in from the bottom. This bearing holder is simply fit into a bore at the top of the damper body. The bottom surface of this bore has a flat gasket for sealing fluid. The lip of the bushing stops it from being forced up into the U-cup or down in to the damper in case of galling with the piston rod. The U-cup is then slid over the piston rod and lowered with the piston rod with the U shape opening towards the fluid side. Finally, a cap is passed over the rod and held down in place with an internal snap ring. The groove for this snap ring is a feature of the damper body.

The top flanged mounting tube is designed to house the coil spring and provide lateral support of the MR damper rods (and thus the seat) to prevent the seat from rocking. The SAMSS system for the MH-60R seat added a bracket for a linear bearing which was attached to the back of the seat. In an attempt to minimize changes to the seat itself, this design for the MH-60S seat integrates side load rated linear bearings within the flanged MR damper mounting tube as shown in Figure 37. Placing this bearing as close to the load point as possible creates a shorter moment arm. The bearing will be placed just inside the lip of the mounting tube. A larger diameter shaft will be able to handle bending moments with less material. Off-the-shelf bearings were found that fit into a 1.25" bore and is built to accept a $\frac{3}{4}$ " shaft. These bearings are rated for side loads of up to 1300 lbs. The 5/16" bolt which is currently fastening the seat crossbeam to the top of the guide tubes will be reused and threaded directly into this $\frac{3}{4}$ " shaft. The $\frac{3}{4}$ " shaft will then be stepped down to a $\frac{3}{8}$ " shaft which will be the MR damper piston rod. This step creates a perfect opportunity to place a spring retainer to compress the spring as in Figure 37.

The step for this shaft will be made with three pieces as shown in Figure 38. A single piece stepped shaft would require post machining case hardening and grinding/coating to rod seal and linear bearing shaft specifications. This process would be expensive. With a multi-pieced shaft, we can use off-the-shelf shafts with machine able ends. In the three piece shaft, the piston rod is threaded into a spring retainer ledge, which is, in turn, threaded into the linear bearing shaft.

This shaft configuration also gives the opportunity to solve a common issue with MR damper wire connection strength. The 26 gauge cable wire which is used to wind the coil is quite weak and prone to breakage. Many times, the coil wire is soldered to a multi strand insulated wire inside the damper, before it leaves the end of the piston rod. This connection is a point of concern when manufacturing and maintaining MR dampers. This intermediate step sitting inside of a larger shaft is a perfect place to design a connection block. Instead of the solder joint sitting loose inside of the damper, a strain relief screw connection is created. This will allow for manufacturing and maintaining the dampers, harnesses and electrical control boxes of this seat suspension as separate subsystems.

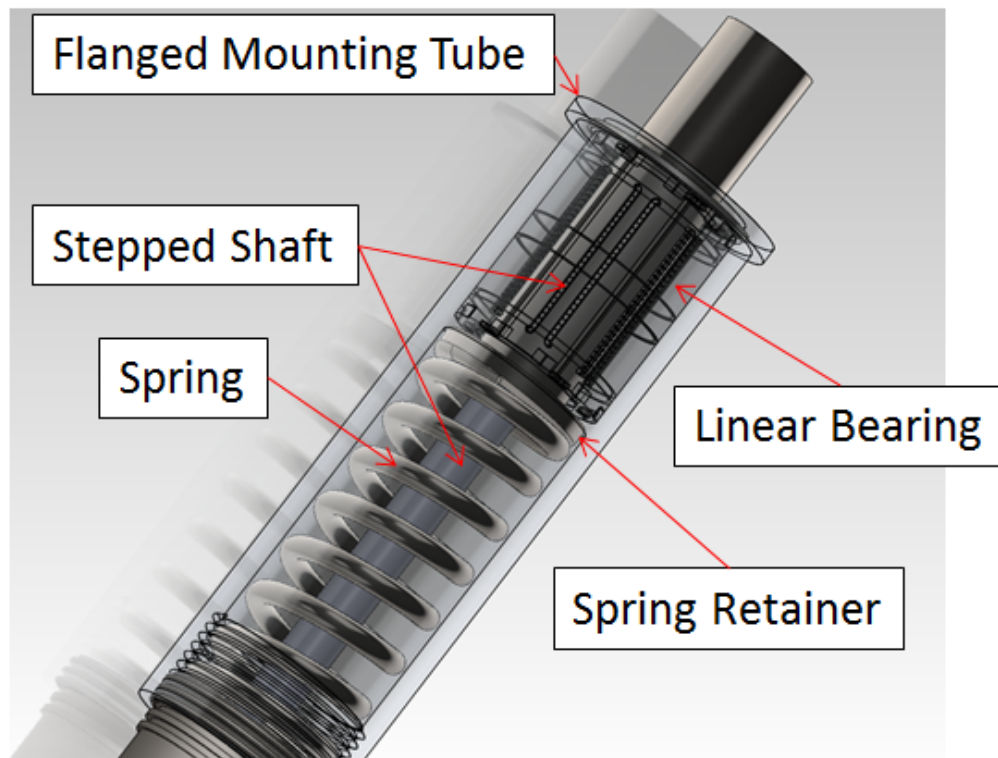


Figure 37: Flanged Mounting Tube with Stepped Shaft, Spring, Spring Retainer and Linear Bearing

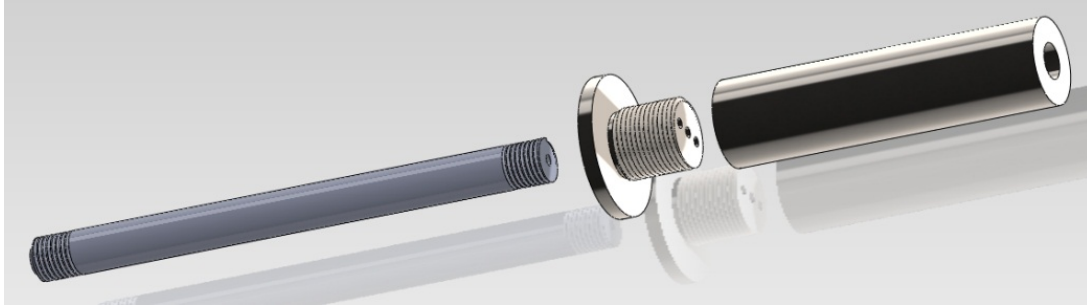


Figure 38: Three Piece Stepped Shaft Design with Spring Retainer

As for the spring itself, below are the desired specifications based on initial design criteria:

- Spring specifications used to find stock spring:
 - Spring rate: 150 lb/in
 - Minimum stroke before coil bind: 1.25"
 - Maximum O.D.: 1.25"
 - Minimum I.D.: 0.5

At the bottom of the damper an accumulator is required to allow for the expansion of volume as the piston rod enters the damper. The accumulator design chosen is a simple diaphragm. The diaphragm accumulator is a thin elastomeric sheet or a shaped cup that will deform with pressure. The removable damper bottom cap will also compress the diaphragm material for use as a gasket seal to seal the connection of the cap to the damper body. On one side, the diaphragm is in direct contact with the MR fluid; while on the opposite side, pressurized air creates a reaction force to ensure fluid is forced through

the MR valve while being flexible enough to compensate for rod volume. A check valve in the damper bottom cap will allow for adjustment of this pressure after assembly.

The bottom cap of the damper is the last piece of this design. The bottom cap must fasten to the flange of the damper body; create an air tight seal with the diaphragm flange; allow for the expansion of a flat diaphragm into a cavity in the bottom cap and allow for an air valve fitting. The flanges of the damper body and cap will be fastened using #4 black oxide screws. The inner edges of the damper body and cap will require a fillet to make sure no sharp edge cuts the diaphragm material. The design of the cavity need not be complicated, but the depth must be enough to allow for enough deformation to allow for the volume expansion needed when the piston rod enters the damper body. The total amount of volume is equal to the area of the rod times the possible stroke of the damper (0.138 in^3 minimum). With a bore of 1" and a potential volume expansion of 1/3 of the volume in the bore we will require .527" depth of the bore.

MR Damper Design Version 2.0 Changes

Each component and subsystem of the design was thoroughly reviewed by the project team to ensure that any future unforeseen problems were addressed before sending drawings out to machining facilities. The various details that have changed since the initial conceptual design were decided on based on cost-benefit analyses to the system performance, weight, cost, and reliability. Some decisions were straightforward, while others required more intense trade studies. The following sections outline the changes from top to bottom of the damper.

MR Damper Mounting Tube

The lip of the damper was changed to mimic the original plug in the guide tube. This allows the armored wing panel mechanism to fit in the same spot as in the OEM configuration. The new lip design is shown in Figure 39.

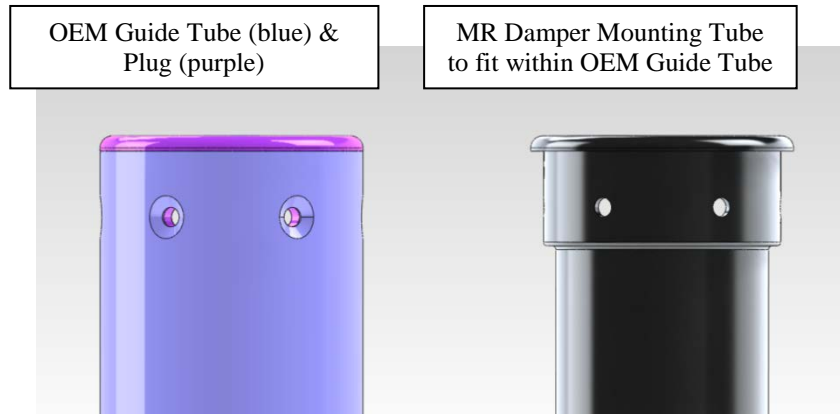

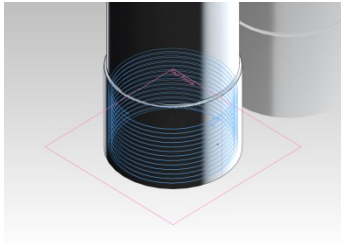


Figure 39: Lip Design Change

The method of restraining the damper was changed to use the existing rivet holes for this purpose. This will mimic the attachment of the current crossbar and plugs to the guide tubes in the OEM configuration. The riveted assembly has been analyzed using FEA (Figure 40) and the rated shear strength of the rivets. When loaded at close to 5 times the forces the dampers should produce, the design still showed a safety factor of 1.82. This design will later be changed to use screws instead of rivets.

Table 3: Loads and Constraints On Aluminum Spring and Bearing Holder

Fixture name	Fixture Image	Fixture Details
Fixed-3		Entities: 6 face(s) Type: Fixed Geometry
Load name	Load Image	Load Details
Force-2		Entities: 1 face(s), 1 plane(s) Reference: Top Plane Type: Apply force Values: ---, ---, -5000 N

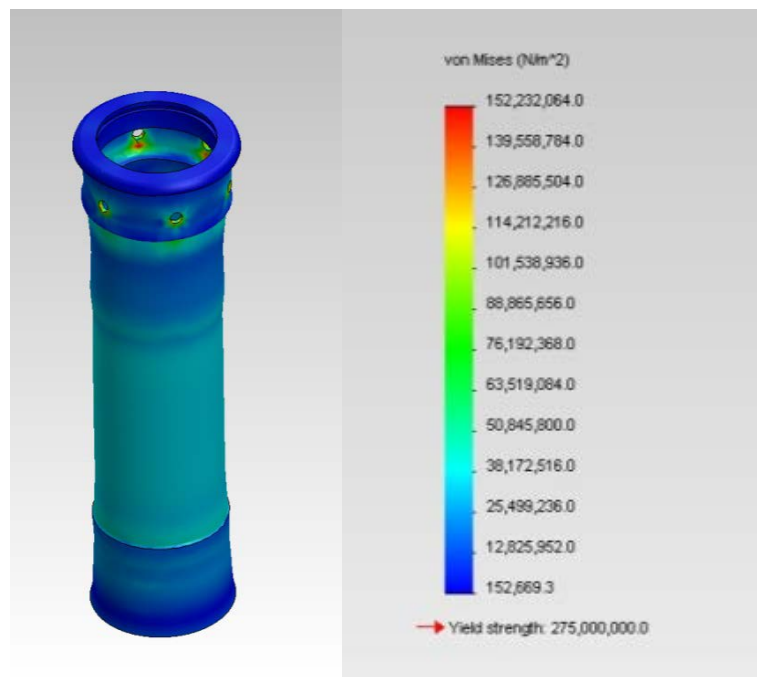


Figure 40: FEA Analysis of MR Damper Mounting Tubes

Spring Design

The spring options for the final design went through multiple review sessions before finalizing the design. The spring rate that was specified for the system was 150 lb/in, with the hopes of testing a range of springs from 150 lb/in to 200 lb/in. When the project team first assessed the state of stock spring catalogs at multiple spring manufacturers' websites, the options seemed numerous. After looking at the possibilities based on the amount of stroke required, the project team limited the options to just two off the shelf springs - both three inches long [30]. Meanwhile, custom spring design quotes were received for a two inch required stroke. The main decision sat with how the spring decision would affect the damper design. The project team decided that a weight study was required and the concept was fleshed out for each of the three possible spring designs (Figure 41).



Figure 41: Effect of Spring Options on Damper Integration Design

Changing the spring changed the design of various parts of the assembly. The aluminum mounting tube could be shortened or the outer diameter reduced to lower the weight required. The spring retaining parts were changed to fit the new spring design. The damper body section which threads into the aluminum superstructure was changed accordingly. The u-cup and bushing holder parts were also changed accordingly. The weights of all the components that would vary between the components were tabulated to decide on the best design (Table 4). SolidWorks was used to give accurate weights for each of the components.

Table 4: Weight Trade Study for Spring Selection

Spring Option:		LHL1250A05	DW Spring	LC135JJ08S
Part Description	Part	Part Weight	Part Weight	Part Weight
	Material	(lb)	(lb)	(lb)
Spring Weight	Steel or SS	0.2589	0.079	0.1064
Spring and Bearing				
Holder	Al	0.1633	0.1424	0.1297
Body Weight	1018 Steel	0.2849	0.2849	0.2548
Body Side Spring				
Retainer	Aluminum	0.0074	0.0074	0.0036
Piston Rod Spring				
Retainer	Alloy Steel	0.0472	0.0472	0.0395
3/8 Piston Rod Weight	Alloy Steel	0.1152	0.0878	0.1155
U-cup and Bushing				
Holder	Plastic	0.0069	0.0069	0.002
Total		0.8838	0.6556	0.6515

The physical dimension differences between the first two options varied only in two components therefore the project team made a decision based on possible future changes to the design. The body of the damper did not change between the DW spring and the LHL1250A05 spring design, therefore it was decided that if, for some reason, there

would be a need to switch to a three inch spring, the DW spring damper design required only fabrication of a new aluminum superstructure and 3/8" piston rod section.

The spring design was again changed based on the strength of the spring design at the maximum compression height. The design team initially trusted that the custom spring designed by the spring manufacturer would not take a set at the requested displacements. When the design was checked using a supplied computer application/tool, the program indicated that the spring may take a set at its solid height [31]. The design specifications were sent to two other spring coiling companies and both came back with the same concerns. When re-analyzing the spring decision based on the integrity of the spring at the maximum compression, the project team was left with only the larger three inch long off the shelf springs as a possibility. To allow for variation in the spring rate in future testing the project team has used the aforementioned spring assessment tool to design springs at the shortest possible length at intervals between 150 lb/in and 200 lb/in (Table 5).

Table 5: Spring Options for the AVASS System

Wire Size (in)	OD (in)	Active Coils	Inactive Coils	Free Length (in)	Material	Rate (lb/in)	Solid Height (in)	Load at solid (lbs)
0.162	1.215	5.6	2	2.5	Music Wire	151.424	1.231	192.127
0.17	1.215	6	2	2.5	Music Wire	175.349	1.36	199.898
0.17	1.215	5.3	2	2.5	Music Wire	198.508	1.241	249.922
0.1562	1.125	6	2	2.5	SST 17-7PH	150.028	1.25	187.595
0.1719	1.24	5.6	2	2.5	SST 17-7PH	175.947	1.306	210.004
0.1719	1.215	5.3	2	2.5	SST 17-7PH	199.596	1.255	248.523

The design was finalized with the 3 inch spring. The lead time and cost for these springs was considerably more than the \$20 per spring for the 3 inch spring available off the shelf and in stock. A spacer can be applied to use these spring designs with the first production damper design. The shorter spring can shave off up to two tenths of a pound from each damper assembly if new parts were made to use the springs above without spacers.

Rod Seal & Bushing Holder

Continuing down the damper assembly, the design for the U-cup and Bushing holder has been refined since the last progress report. Preliminary designs above show a brass bushing closer to the damper body and the u-cup piston rod seal after this. The project team believes that this would have caused high friction as the MR fluid was pushed between the rod and the bushing. To correct this, the u-cup was placed against the first opening from the damper body chamber. The bushing will sit directly above this, pressed into the u-cup and bushing holder part. A radial O-ring groove has been added to the damper body around this part as a secondary seal from MR fluid going up and around the u-cup and bushing holder. This assembly is held down by a snap ring and further by the spring retainer part which sits on the lip of the damper body and is stepped to also sit on the lip of the bushing. Keeping the bushing from moving is important to keep from damaging components and to prevent galling onto the shaft. The assembly is shown in place in Figure 42.



Figure 42: Rod Seal Assembly & Damper Body

Damper Body

The damper body has been left mostly unchanged, although features have been added to allow for proper preload of the spring. The first production damper body was designed with grooves for a snap ring to allow the aluminum structure to hit this snap ring when the spring has been fully pre-compressed. Two more positions for the snap ring were added to allow for tolerances in the assembly and various spring designs (Figure 42). This design would be changed further for the final damper design. The final version changes the snap ring design for a set screw used to set the preload. The system aligns holes in the aluminum superstructure with a threaded hole in the damper body. This design does not allow for the damper to rotate with respect to the aluminum superstructure.

Damper Accumulator

Special thanks go out to Stockwell Elastomerics for covering the cost of prototype flat silicon and Viton elastomer waterjet cut diaphragm and seal parts [32].

A simple diaphragm-type accumulator is placed at the bottom end of the damper to compensate for rod volume as the damper strokes. The project team plans to use simple flat-elastomeric diaphragms. As such, a method for testing the diaphragm system as an accumulator was developed and it was proven that a flat sheet of rubber will seal and have enough displacement to serve for this purpose. The project team had the diaphragm design water jet cut from sheets of nitrile and fluorosilicon rubbers. Parts to mimic the damper body and diaphragm cap, made of 1018 steel and 6061 aluminum respectively, were fabricated. The body side was connected to a syringe where the piston rod would usually enter. The syringe was used to push water against the diaphragm and measure the exact displacement allowed before it was too hard to push. A valve allowing compressed air to enter behind the diaphragm and a pressure gauge to measure the change in pressure were connected to the diaphragm cap part. The test setup is pictured in Figure 43.



Figure 43: Diaphragm Test Setup

At atmospheric pressure, the nitrile material allowed 2 cc of water to be displaced before becoming rigid, while the fluorosilicon only allowed 1 cc. The displacement required by the damper is $\pi \cdot (3/8'')^2 / 4 \times 1'' = .1104 \text{ in}^3$ (1.809 cc), or the volume of the entering piston rod. Already, the nitrile material allows for the required displacement. It was theorized that adding a static air pressure under the diaphragm would compress any air bubbles in the fluid and start the diaphragm bending in the opposite motion of actuation, thus allowing for a negative bias and extending the stroking displacement allowed by the diaphragm. Qualitatively, the project team can claim this has proven to be true. When adding even less than 10 psi to the diaphragm cap, the displacement seems to be at least 0.5 cc more than at atmospheric. The precision of the measurements is limited, however, by the sensitivity of the pressure gauge. The pressure gauge being used measures from 0-100 psi, and therefore it is hard to see changes in the pressure less than 10 psi. The

project team set out to understand whether we required a more robust diaphragm. With this testing, it was decided that the flat rubber diaphragm will work with our damper system as designed. Further pressure specifications will be added when the team starts characterizing the damper on an MTS machine.

MR Isolator Fabrication & Assembly Notes

All components for the first two MR isolators were received throughout January and February 2012. A photograph of the piston & rod assembly parts is shown in Figure 44. During the assembly process the U-cup seal is first passed over the 3/8" shaft and then the shaft is passed through the opening in the damper body to be threaded onto the piston which has already been wound with the appropriate number of magnet wire wraps to create the desired electromagnetic circuit and epoxied. The wear ring and wire seals are attached to the piston and the piston is inserted into the damper body. The bushing and U-cup holder, with bushing already pressed in, is passed over the back of the 3/8" shaft and pushed into place. The bushing and U-cup holder are held in by a snap ring and a lower spring retainer is passed over the shaft. The spring is passed over the shaft and the spring retainer/piston rod step is threaded on to the 3/8" shaft, finishing the main assembly of the damper. The wires are soldered to the small PCB for wire connections and the 3/4" shaft section can now be threaded on to the damper.

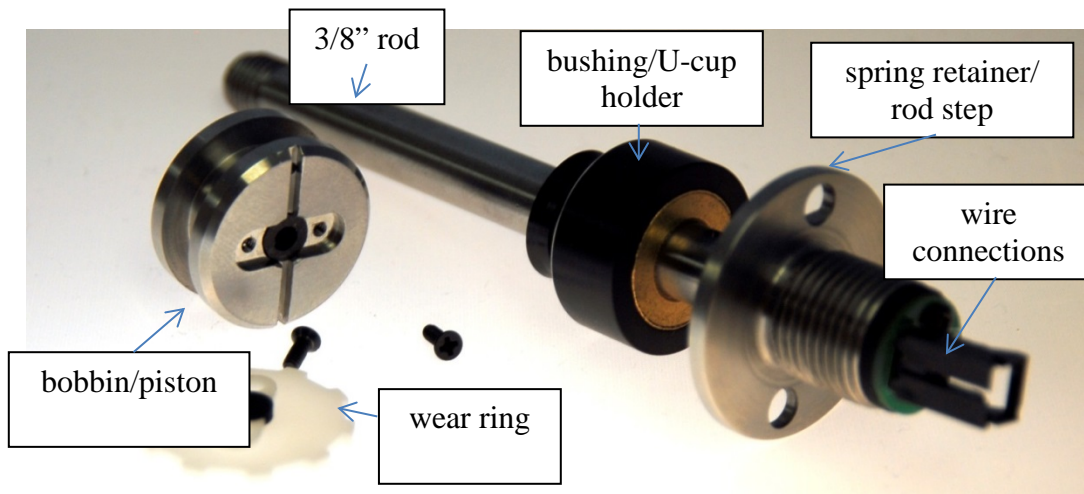


Figure 44: Assembly of Piston Rod to Piston

The damper body (Figure 45) is made of 1018 low carbon steel for its magnetic properties. The design of the damper body has a flange for the diaphragm compression and 1 3/8"-16 threads which mate the damper to the mounting tube (Figure 46). Inside the damper body top section, as seen in Figure 45, there is a groove for a radial O-ring and a snap ring groove closer to the top. The damper body has grooves for spring clips just below the 1 3/8" threads which were not used during assembly. These will be removed for future productions and replaced with a set screw locking mechanism to set preload on the spring. The flange at the bottom of the damper body was given a 1 7/16" hex design for the case that increasing preload was beyond a hand tightening procedure. It turns out that this is not the case and future designs will have a circular flange.



Figure 45: Damper Body



Figure 46: Spring and Bearing Holder/ Mounting Tube

The body side spring retainer, not shown, is made of aluminum and anodized black.

There is a small lip to keep the spring centered during assembly. The first step is a slip fit onto the steel damper body to keep the part centered. The second step sits on the flange of the bushing and provides a very smooth bearing surface to keep the friction down when turning the damper to preload the spring. The second step diameter was turned down during first assembly due to interference with features on the snap ring holding the bushing and u-cup holder. When preloading the spring, the damper body turns, but the piston and piston rod are allowed to stay stationary.

The spring and bearing holder/mounting tube, is made of 6061 T-6 aluminum which is then anodized. The 1 3/8" internal threads engage with the damper body while the top section has a bore for a linear bearing and holes for riveting to the guide tubes on the seat system. On assembly, it was noticed that the bearing fit well but has an external retaining spring which would get caught in the slot to make the required space for riveting the assembly in place. It takes some effort but is still possible to extract the bearing. It is not possible to rivet the tube into place with the bearing already installed. The project team later changed this to a threaded engagement as opposed to rivets. This part is anodized black to match with the color of the seat system and also to avoid direct contact with the steel of the damper body. The project team decided to ask the machinist to wait until this part was received back from anodizing to cut the threads on the steel damper body. This assured that both parts mated correctly.

The diaphragm cap, shown in Figure 47, is made of 6061 aluminum and will be anodized in future versions. This part has a bore for the expansion of the diaphragm as well as a high pressure check valve for adding pressure behind the diaphragm. The diaphragm cap has six through holes for #4 screws which

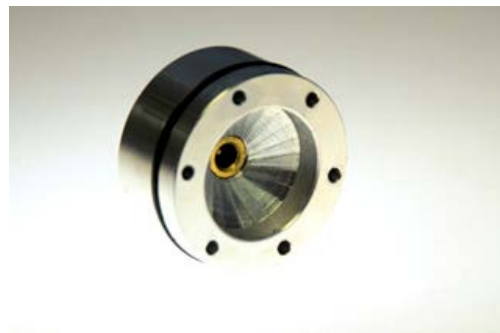


Figure 47: Diaphragm Cap

compress the diaphragm and hold the diaphragm cap against the damper body. It was noted that over compression and constant sealing pressure were very difficult to achieve

without a metal to metal contact to lock the piece at the correct compression. For this, the design of the diaphragm cap has been changed to include a pocket 0.05” deep leaving a 0.03” wide lip on the end where the diaphragm sits. This lip will meet up perfectly with the circular flange on future damper bodies and will create a secondary seal as well as an aesthetically pleasing closed design.

MR Isolator Testing

Upon assembly of the first two MR isolators, testing was conducted at the Smart Structures Laboratory at the University of Maryland on an MTS 810 load frame, which allowed for the characterization of the damper forces while changing one variable at a time. Testing outside of the seat also served to make sure that the AVASS dampers could be consistently checked for leakage and wear. The variables for MR damper test were the frequency of oscillation, the current passing through the coil, and the diaphragm pressure setting.

The project team designed a mounting structure to mimic the seat’s guide tubes. The design of the MTS mounting bracket uses the same rivets that will be used to mount the actual dampers to the seat. This will help to test the rivet connection as well as the damper. The final design is shown in Figure 48. The connection from the power supply is shown in the picture of the system on the MTS machine.



Figure 48: MTS Mounting Design CAD Model and set in MTS Machine

Initial testing was conducted with the diaphragm pressure set to approximately 150 psi. This was a conservative value which would allow testing up to maximum force levels using applied electrical currents up to a magnetic saturation, therefore giving the largest yield forces. The test was run at 0 amps, 1 amp and 2.5 amps for a preset frequency sweep. The project team wanted to make sure that a large range of frequencies was included, including the key 1/rev and 4/rev frequencies. The frequencies chosen were 0.5 Hz, 2 Hz, 4.3 Hz, 8 Hz and 17.2 Hz. All frequencies except 17.2 Hz were done with a 0.5" peak to peak amplitude around mid-stroke. The 17.2 Hz frequency amplitude was set at 0.1", very closely matching what the design team believes will be the final stroking at 0.2 g base excitation.

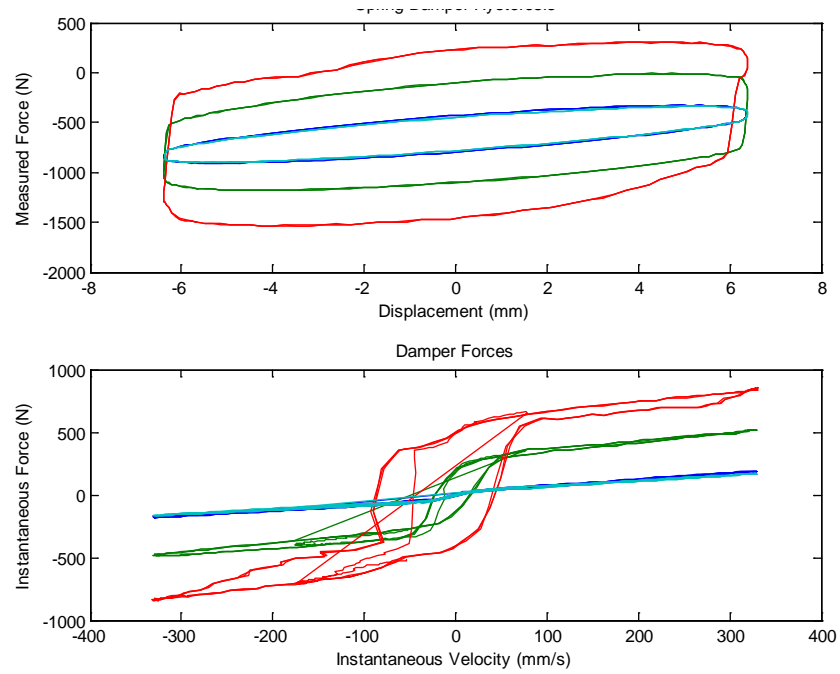


Figure 49: Damper 1 - 0.5 Hz

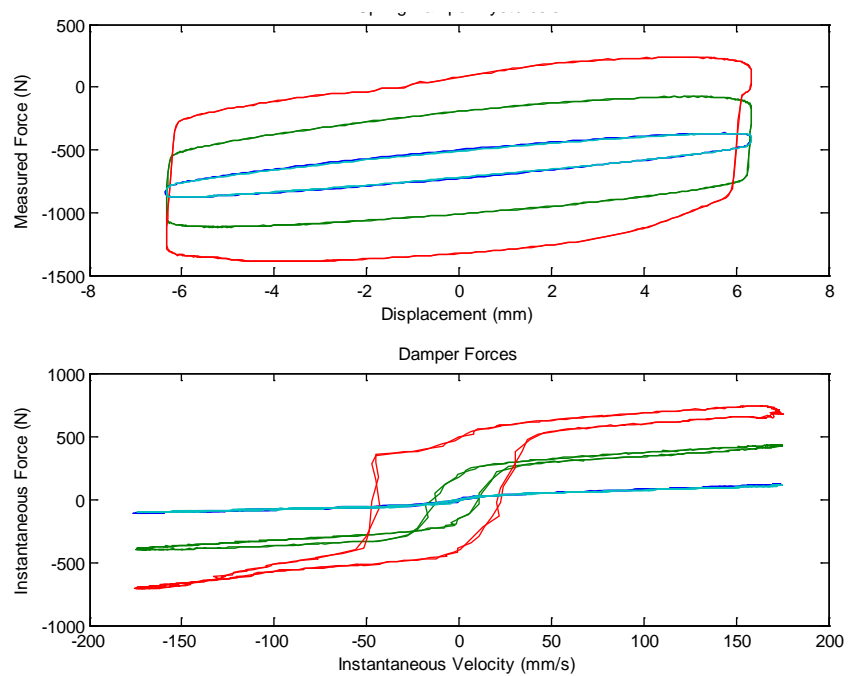


Figure 50: Damper 1 - 2 Hz

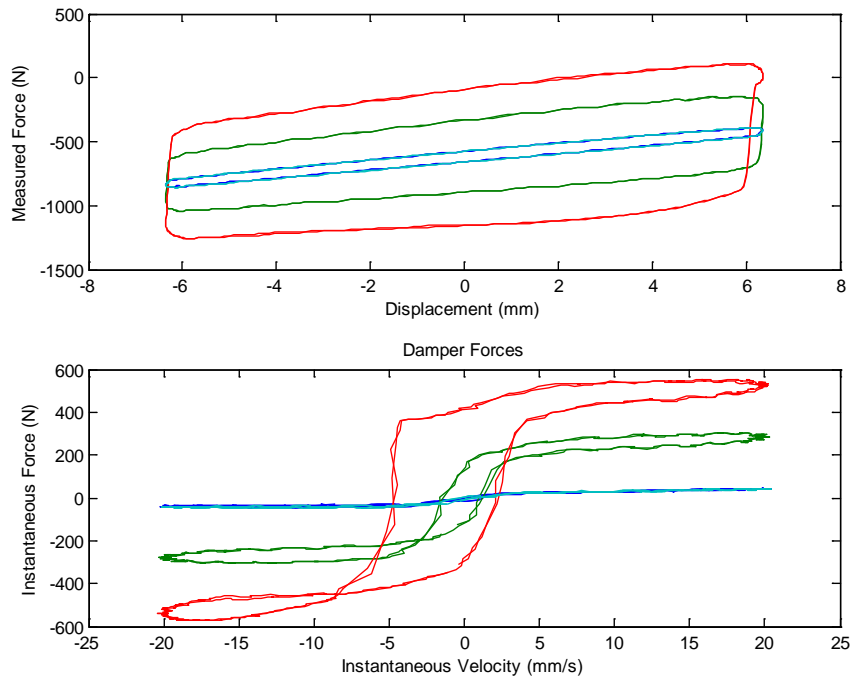


Figure 51: Damper 1 - 4.3 Hz

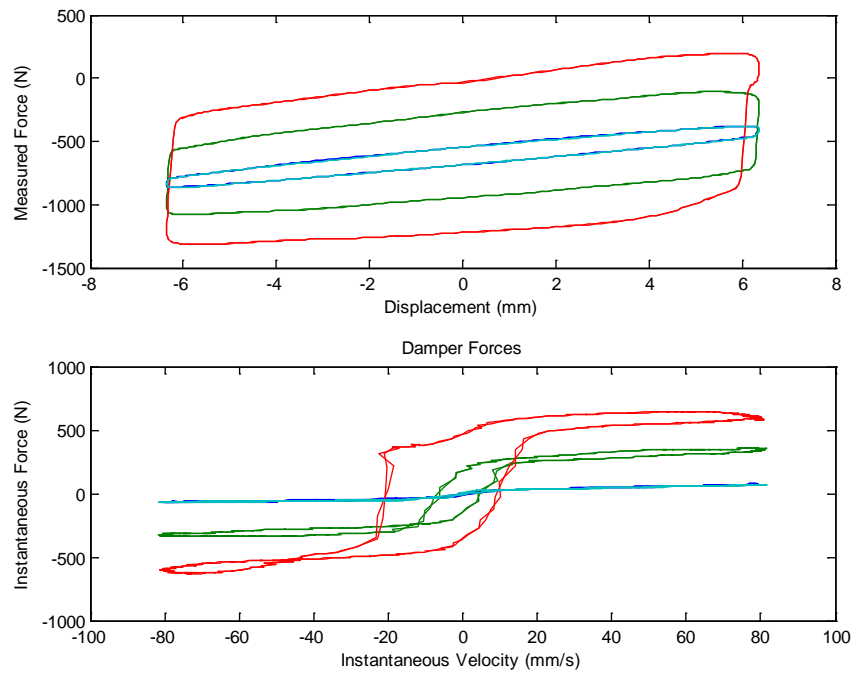


Figure 52: Damper 1 - 8 Hz

The data shows a damper that is quite clean, fairly symmetrical and which matches the desired characteristics. Hysteretic changes to the damper force response were within tolerable limits. Figure 49 through Figure 52 are using a 0.5" stroke. Figure 53 shows what is expected from cockpit vibration at the 4/rev with an overlay, in dark blue, of what the original specified damper characteristics were using a Bingham-Plastic model. These plots clearly show the change in yield force as current is increased. The damper's desired characteristics were 500 N Yield force at 2.5 Amps and 508 N-m/s damping. The damping measured by the slope of the F-v graph line, is slightly higher than the desired characteristic, but should be within a tolerable range.

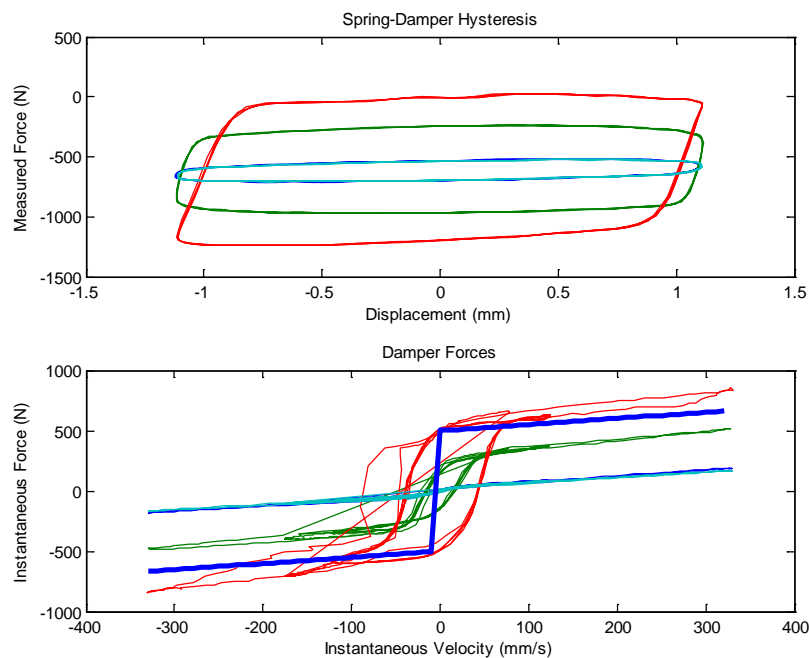
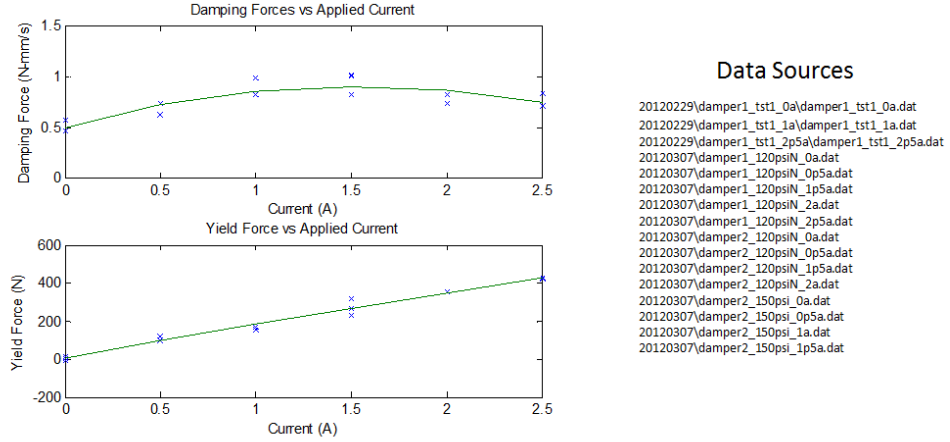


Figure 53: Damper 1 - 17.2 Hz Data; Dark Blue Indicates Bingham Plastic Model of Desired Characteristics

0 Amps: Light Blue, 1 Amp: Green, 2.5 Amps: Red



$$\text{DampingForce}(i) = -0.1698i^2 + 0.522i + 0.4993$$

$$\text{YieldForce}(i) = -6.295i^2 + 183.7806i + 7.8251$$

Figure 54: Damper Characterization Equations

Using this data, the dampers have been characterized using a second order equation to give expected damping and yield force as a function of applied electrical current. Figure 54 shows the characterization equations.

Study of the Effects of Varying Diaphragm Pressure on Damper Friction

Using a method of quickly switching between the first and second damper, the project team also hoped to test different diaphragm pressures and materials. In an MR damper, increasing the diaphragm pressure is important to providing a reaction force large enough to ensure that fluid is forced through the active valve area rather than simply compressing the diaphragm. Increasing diaphragm pressure also increases the internal fluid pressure, and seal manufacturers state that U-cup seals work better with a higher internal fluid pressure. Conversely, it is known that the U-cup seal is a large source of friction in a

damper, and that increasing the internal pressure increases the force on the piston rod and therefore increases the overall friction.

As such, the project team tested a variety of pressures to identify if there was a “sweet spot” in the trade-off between diaphragm pressure and friction. The testing guide tube was modified to be able to be able to adjust the pressure while the damper was still in the tube. Damper forces were recorded for the same frequency sweep, and at varying currents for a range of pressures between 0 and 150 psi. The effect of reducing diaphragm pressure was quite noticeable when increasing the desired yield force. Figure 55 and Figure 56 give a good example of what happens as the pressure is increased. Notice that the shape of the Force- Displacement curve has a boot shape where the damping force is greatly reduced. This reduction in force is due to the displacement of the diaphragm as the MR valve locks the fluid from passing through the gap between the piston and the damper wall. Displacing the diaphragm takes much less force with low pressure behind the diaphragm. The pressure needed behind the diaphragm is easily calculated as a function of the desired yield force. The key is to make the force from the pressure on the surface area of the diaphragm equal to at least the desired yield force.

As is stated above, the variation of pressure behind the diaphragm also affects the friction in the damper system. Dry friction in a damper is often called coulomb damping as it is another force acting against the direction of motion. This damping is different than the viscous damping as it requires a certain amount of force before the damper piston will start moving. This is modeled almost exactly like the Bingham Plastic model used for

modeling MR yield force. In a vibration case, reducing friction is of very high importance because it may negatively affect the systems ability to provide high frequency isolation. Figure 57 shows an overlay of all the data collected at different pressures at 0 amps. The thick lines displayed in the Force-velocity graph are a linear fit to the data and show a clear relationship between pressure and friction. If the vibration source will create 0.2 g vibrations, then the seat with a 5% Female occupant will experience a maximum force of $(0.8*103+20+60)*0.2=32.48$ lb. If the damper's static friction is above this point there will be no motion and no vibration isolation. The closer to being frictionless, the more the damper will be able to mitigate vibration and stroke in response to the impulses. If aiming for 90% isolation, the target maximum friction force should be $(1-0.9)*32.48=3.249$ lbs from two dampers. Figure 58 is a graph of friction, defined as the y intercept in the linear fit equations in Figure 57, versus pressure. Using a linear fit, this data shows that at a single damper requires 3.4 lbs of friction force before it starts moving at 0 psi.

Unfortunately, 0 psi would not be a useable figure since it would negate the point of the active MR damping by not allowing for enough controllable yield force. At 150 psi, the damper data fit gives a friction of 8.45 lbs. If there is a total of $2*8.45=16.9$ lbs of friction, only $100-16.9/32.48*100=48\%$ mitigation in vibration forces can be expected. Due to the way the linear data fit is constructed, these numbers are conservative, and the actual results will vary. It is important to note that the equation for yield force(i) from Figure 54, created with data at high diaphragm pressures, has a friction intercept at 0 amps of 7.825N or 1.76 lbs, which is lower than what found in studies of friction vs diaphragm pressure. In reality, the values are probably somewhere in between these two.

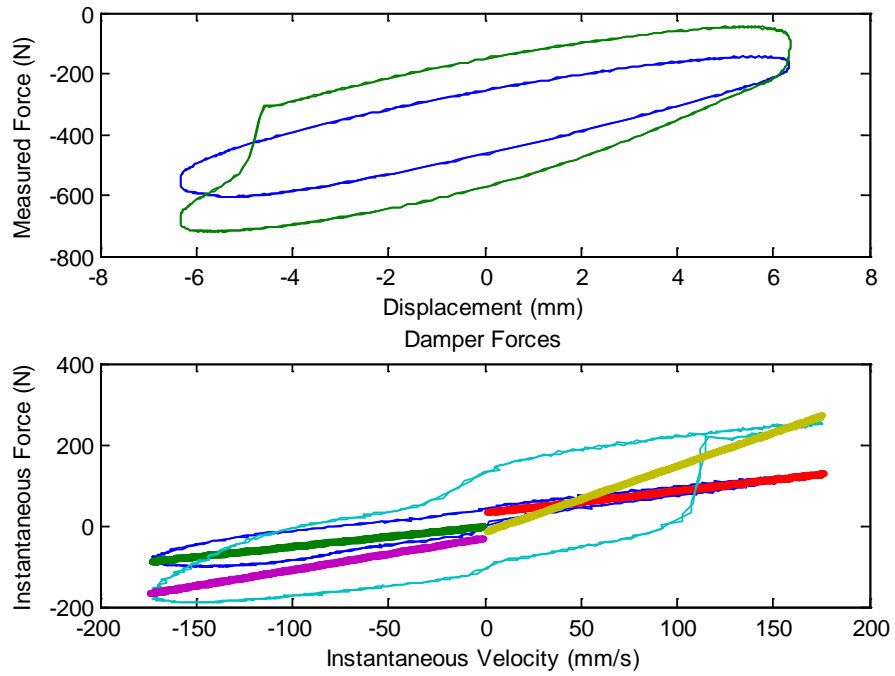


Figure 55: Damper 2 - 4.3 Hz, 0 PSI (0 amps, 1 amp)

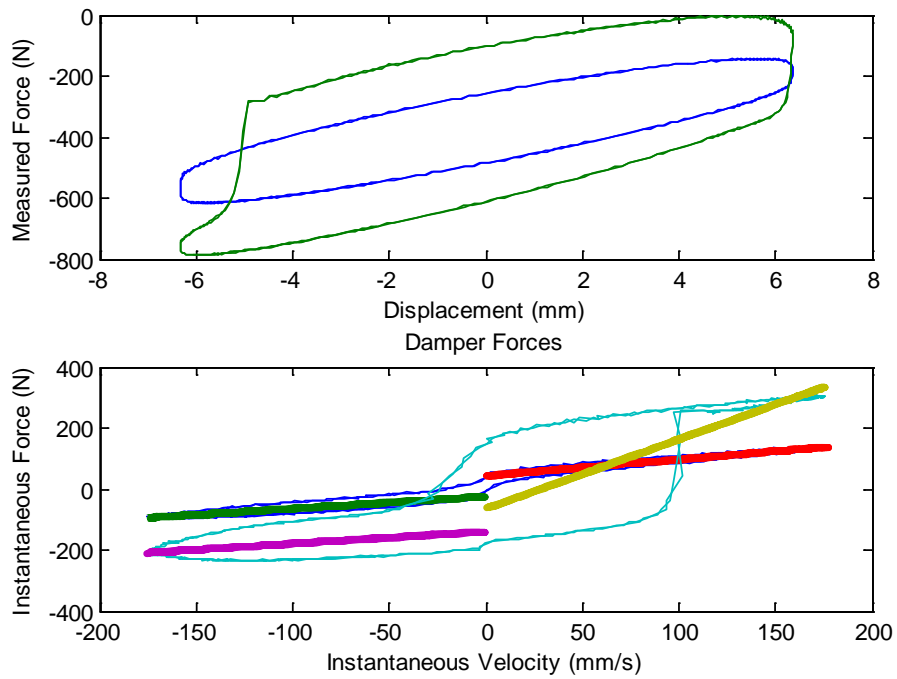


Figure 56: Damper 2 - 4.3 Hz, 40 PSI (0 amps, 1 amp)

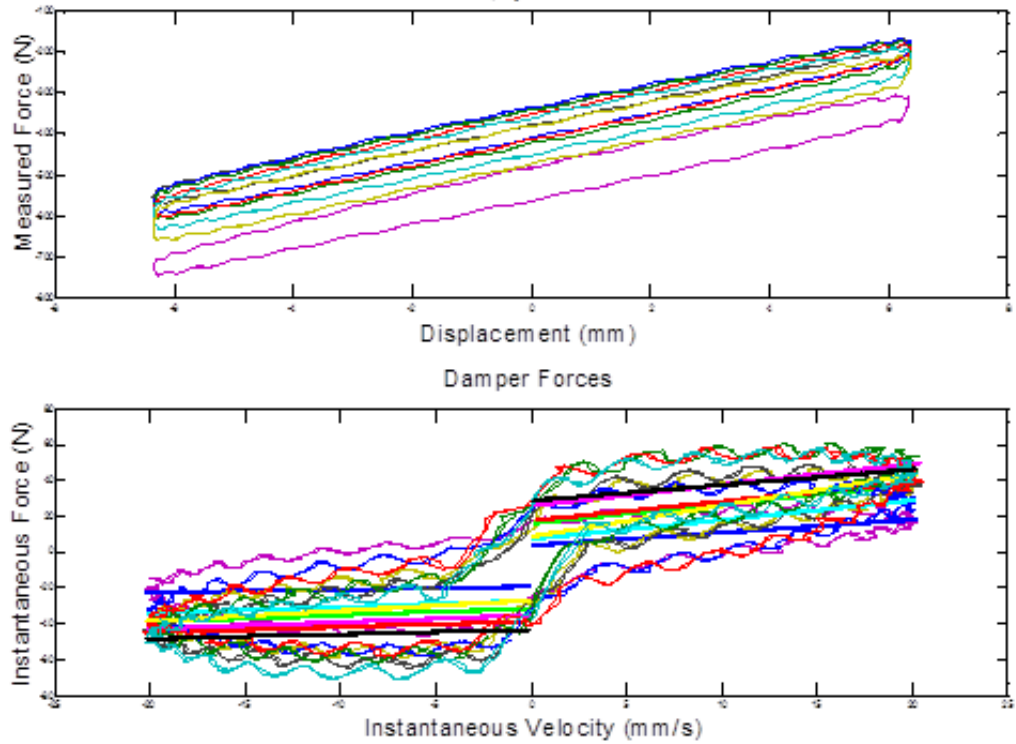


Figure 57: Variation of Friction at 0 Amps and Raising Diaphragm Pressures

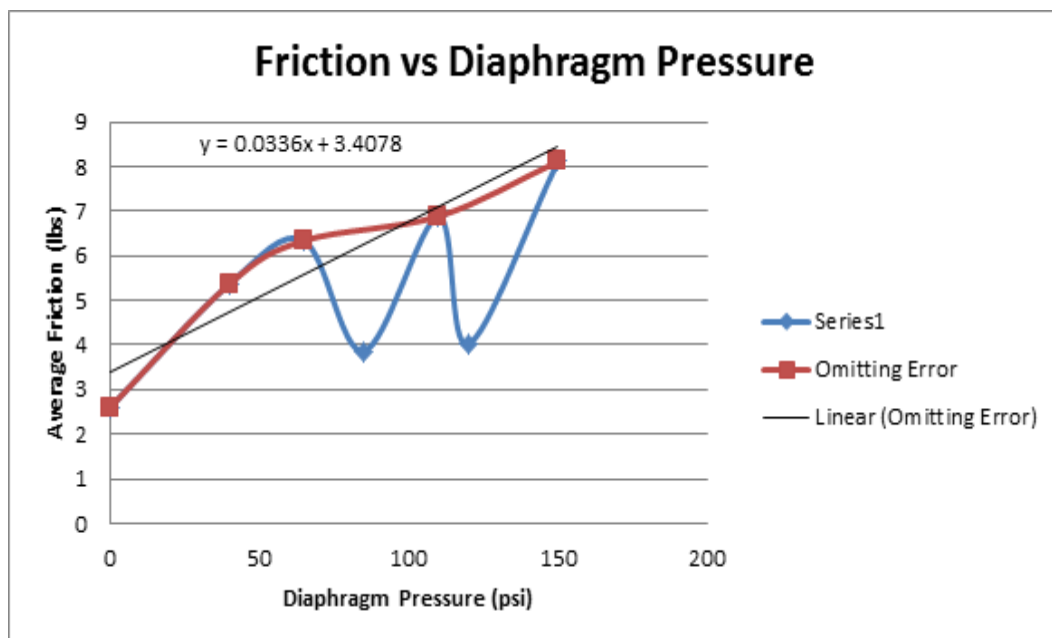


Figure 58: Friction vs Diaphragm Pressure

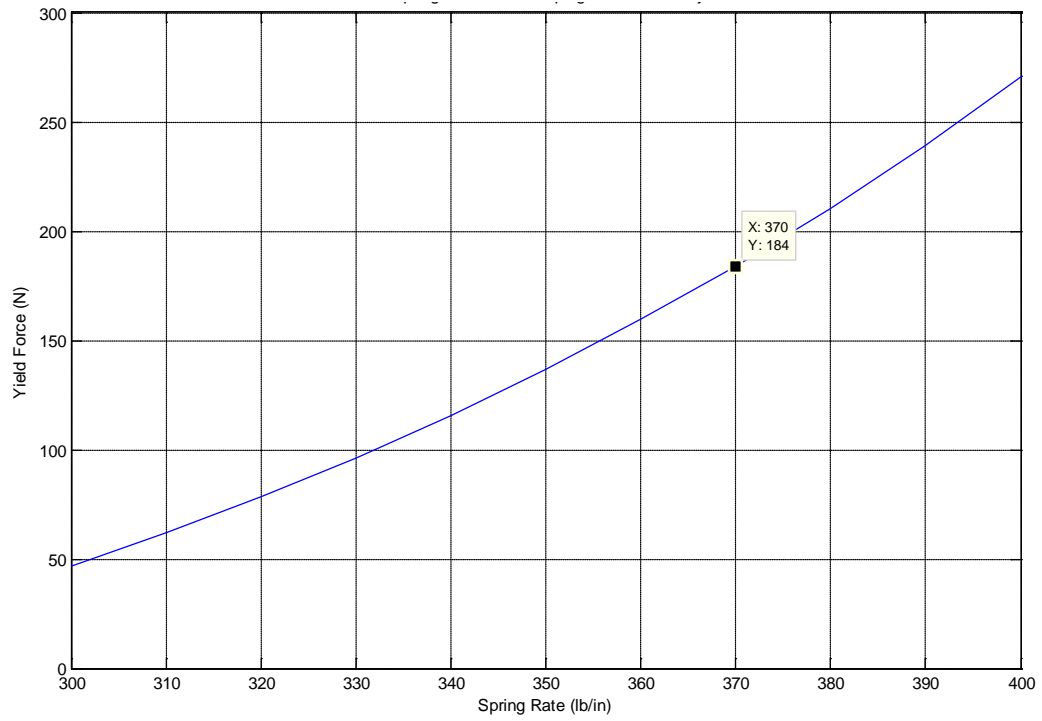


Figure 59: Required Yield Force at 0.2 g and 370 lb/in total spring force

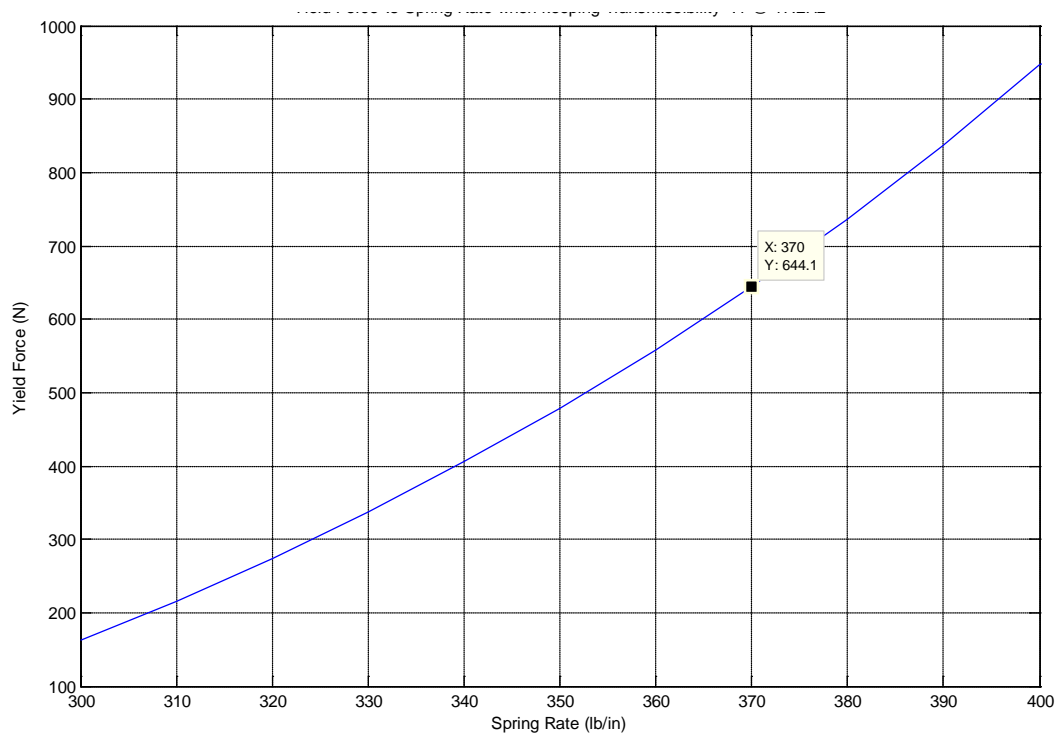


Figure 60: Required Yield Force at 0.7 g and 370 lb/in total spring force

Going back to the project team's original dynamic study, the true necessary yield force can be determined. The project team used the original MATLAB program to calculate the required yield force required at 4.3 Hz, or 1/rev frequency. Using 0.2 g and adding in a conservative maximum spring rate from the diaphragm helps us to make a decision with respect to testing. The diaphragm has a spring rate which is related to the stiffness of the material and the pressure behind it. This is added to the 150 lbs/in spring spring-rate and creates a total spring rate of approximately 185 lbs/in. Figure 59 shows the results of this analysis. The required total yield force will be 184 N, or 92 N per damper. To achieve 92 N (20 lbs) of yield force, only $20.72/(\pi \cdot 0.5^2) = 26.38$ psi of pressure is required behind the diaphragm. Using the equation from Figure 22, each damper would then have 4.29 lbs of internal friction. This is the smallest amount of friction believed to be possible in the damper implementation. Following the example used above, this will theoretically allow for 74% vibration force mitigation. The project team is currently considering other methods of providing a reaction force for the accumulator outside of pressure, such as internal springs, etc. which will allow for high controllable yield force without the added friction.

Further Changes for Future AVASS Systems

The first generation production AVASS system proved to be a very reliable design. No major changes were needed and future productions are expected to be very similar. With the opportunity to manufacture two more sets of dampers for dynamic testing, the project team has made small changes which only serve to make the system easier to assemble and more versatile.

The damper aluminum superstructure design has been changed to allow for use in both the MH-60R and MH-60S seat systems without sacrificing any performance. It was found that changing the fluid iron content to 26% from the designed 32% may allow for a low enough damping viscous force to use the exact same design with the unarmored MH-60R seat system. The internal diameter of the guide tubes used in the MH-60R are slightly smaller than the MH-60S seat, and the addition of a sleeve used only for the MH-60S installation allows for the installation of the same damper in either seat system. The rivet hole pattern for supporting crash load attenuating systems is also different from seat to seat. Both hole patterns can be present in the design of the aluminum superstructure without sacrificing strength. Finally, the seat bucket mass is quite different from the MH-60S to the MH-60R. The seat bucket weight must be accounted for by a preload in the spring to be able to make use of the full 1" stroke to account for changes between occupants. This preload setting is easily applied using a set screw which locks the aluminum superstructure at one of two positions.



Figure 61: MH-60R (left) and MH-60S (right) both with AVASS dampers installed

PAGE INTENTIONALLY LEFT BLANK

CHAPTER 5: ROLLER BEARING DESIGN

AVASS Bearing Bracket- Roller Bearing Design

The project team, in cooperation with BAE, has developed a twofold approach to moving forward with a modified guide tube bearing design. In an effort to maintain the current structural rigidity, a roller bearing which can be bolted to the existing bracket has been designed. The other approach is to replace the existing bracket with a set of roller bearings already in use on other BAE seat systems. This method requires the design of a completely untested bracket to match up with the mounting holes on the seat bucket. The rigidity of this new design would be calculated and simulated, but untested in high *g* crash loads.

BAE has offered to design a bracket system for the MH-60S seat which will use an existing roller bearing design. The proposed design is shown in Figure 62 below. The project team believes that a design like the one shown would be the best way to finalize the product. Unfortunately, the time involved in contracting and development would put the AVASS project behind schedule. The project team has taken the initiative to design a system which can be fastened to the current seat brackets to continue development within the AVASS contract schedule.

The project team's design will apply roller bearing support to the areas affected by friction on the bearing surface. Figure 63 shows a free body diagram of the seat system with a moment pivot at the single pin used for height adjustment. A table was constructed

to create a normal force design requirement for loads on the bearing design. Using a safety factor of 2, we chose bearings which indicated a load rating of at least 300 lbs. Due to the geometry of the seat pivot and bearing points, the bottom bearings will be taking a much larger load than the upper bearings.

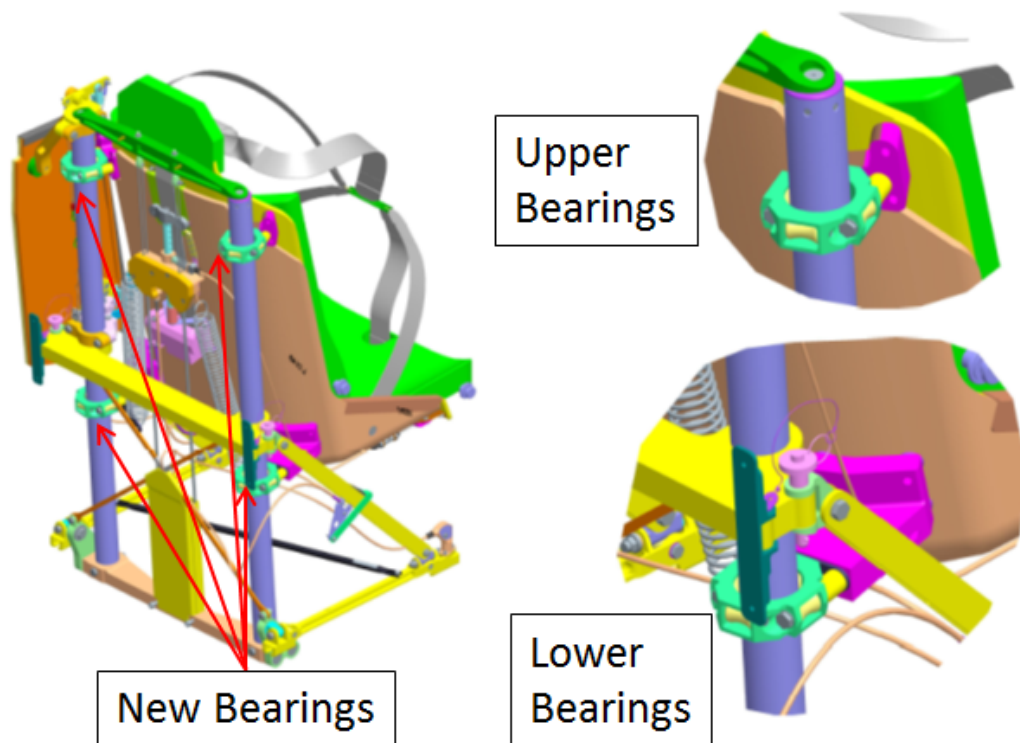


Figure 62: BAE Proposed Bearing Design

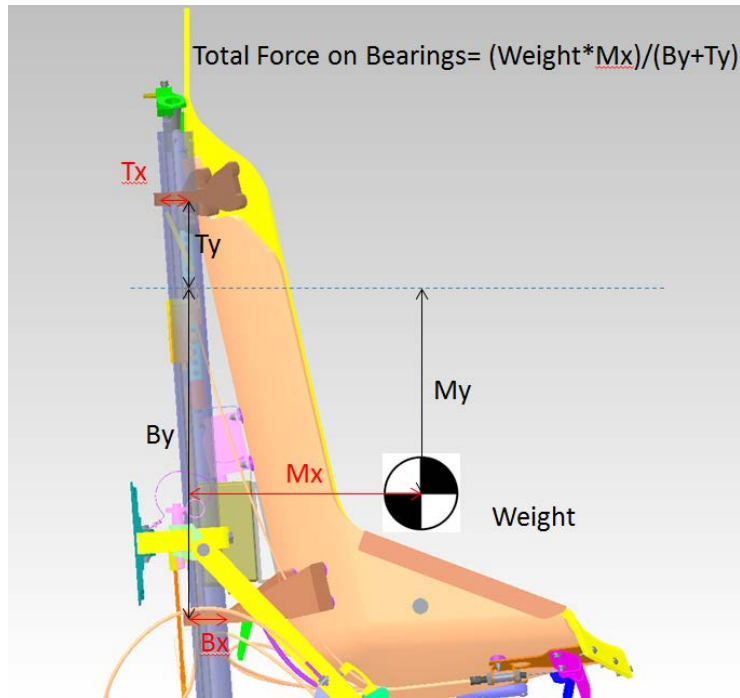


Figure 63: FBD of Seat System

	Occupant + Seat (lbs)	Mx (in)	By (in)	Ty (in)	Total Force on Bearings (lbs)	Ftop (lbs)	Fbottom (lbs)
95th Male	290	10	18.48	2.07	141.1192214	14.21493	126.9043
50th Male	240	10	15.5	5.0719	116.6639931	28.76293	87.90106
5th Female	170	10	13.5	7.07	82.6446281	28.40532	54.2393

Figure 64: Calculated Forces on Bearings

The top and bottom OEM guide tube bearing brackets are quite different, and require different methods for attaching a roller bearing. Figure 65 shows CAD representations of the top and bottom brackets. The top bracket has no existing mounting holes of any kind and has very little room to mount a bracket anywhere. The project team hoped to design a system which does not require drilling any holes or modifying any part in any way. The

bottom bracket has two mounting holes used for a bracket for attaching the seat height return spring. These holes can be leveraged in the design of the bracket. A roller bearing with appropriate load rating for a 1/4" shaft diameter was chosen for the roller. An initial design of the roller holds two of these bearings internally and was given a radius larger than that of the guide tube to make sure that any deformation would not cause a crimping force on the surface. A CAD model of the roller, to be made from HDPE is shown in Figure 66.

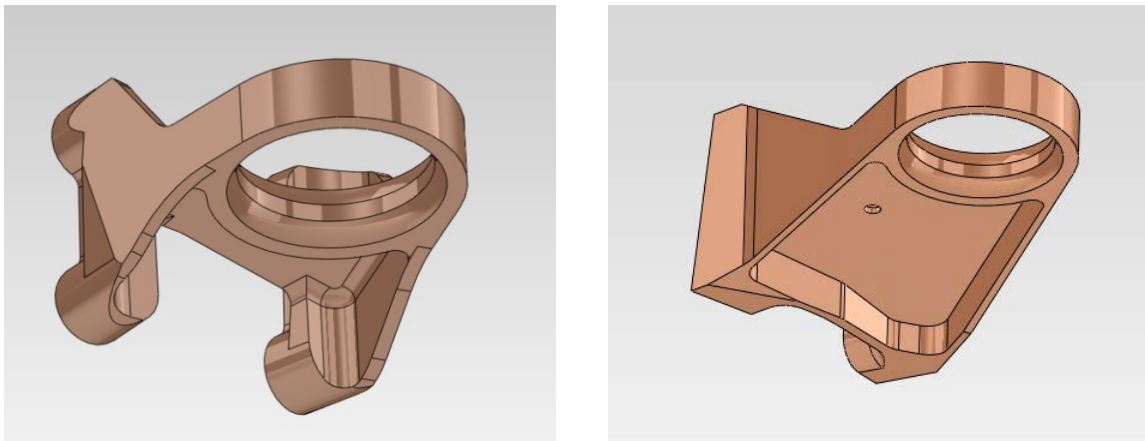


Figure 65: CAD Models of Top (left) and Bottom (right) OEM Guide Tube Bearing Brackets

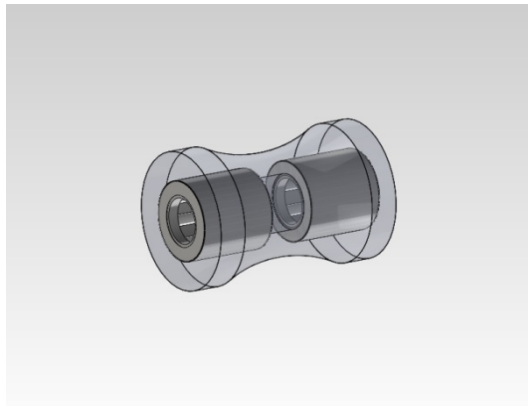


Figure 66: CAD Model of Roller with Bearings

The developmental top bearing bracket design, shown in Figure 67, will clamp around the bracket. Shims on the back side will allow for proper bearing alignment and loading. The design can be used for both sides by flipping the main body bracket piece over.

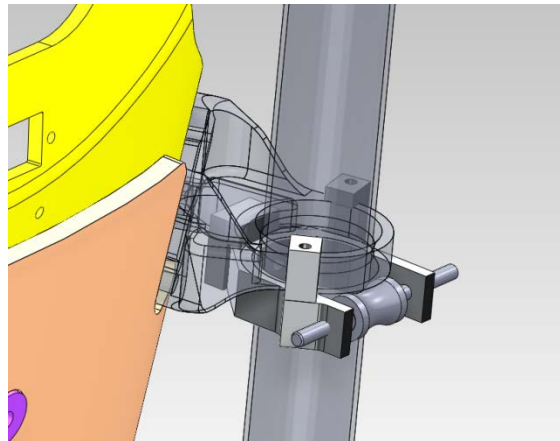


Figure 67: Top Bracket Roller Bearing Design Concept

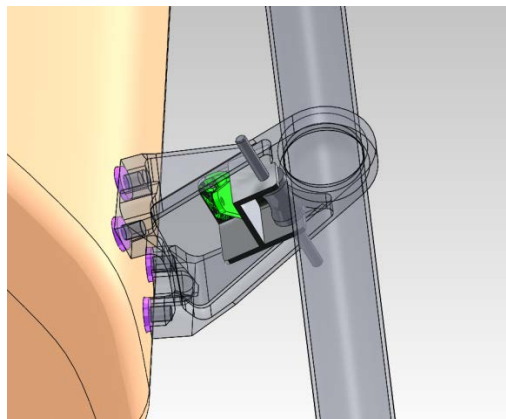


Figure 68: Bottom Bracket Roller Bearing Design Concept

Figure 68 shows a CAD model of the bottom bracket roller bearing design concept attached to the seat system. The design had a slotted connection at the bolt holes to allow

for shimming back and forth for loading of the bearing. This design proved to be problematic due to asymmetries in the OEM bracket designs and was not used. The project team designed these brackets quickly to reduce the time between testing sessions. It is important that the system is showing good vibration mitigation performance before moving on to Phase II, dynamic crash testing. The design of these brackets is only a first version and will change in the future to improve various aspects of their functionality. One specific problem we foresee is the loss of stroke due to the mounting position of these roller bearings. Both the top and the bottom guide tube bearing brackets required that the roller bearings be attached below the bracket, due to constraints at the top seat height position. In the event of a crash load which would normally stroke the seat to its originally designed maximum capacity, the roller bearing components, which are below the OEM bracket, will contact first and may reduce this stroke by up to an inch. This may be a good reason to move forward with the BAE bracket system, which replaces the existing bracket and will not reduce total crash load stroke.

Design and Installation of Roller Bearing Brackets

The design of the first version roller bearing brackets were fabricated and applied. The design of the top bearing design, Figure 69, was found to be acceptable for both the top and bottom bearings. The same exact design, with no changes, can be turned around and used on the bottom bearing brackets. Photographs of the final installation are found in Figure 70 and Figure 71.

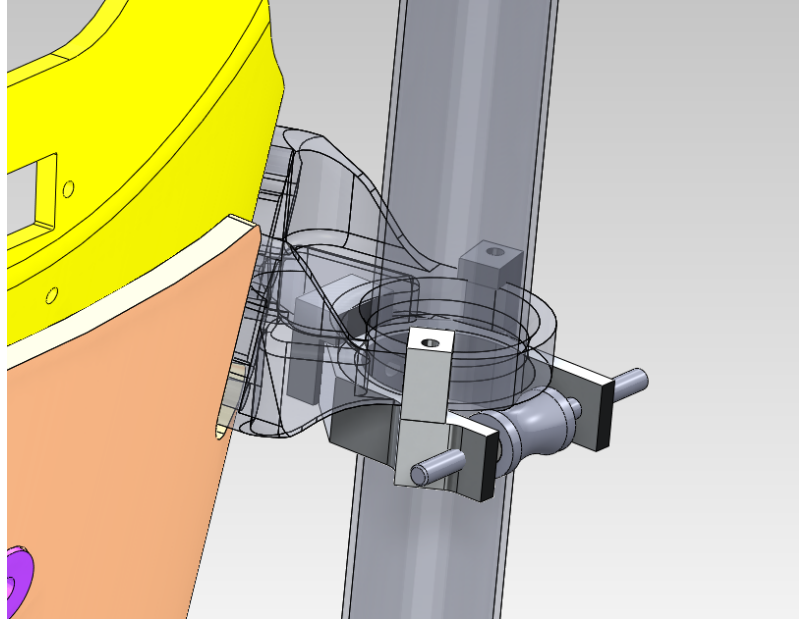


Figure 69: Top Bearing Bracket Design

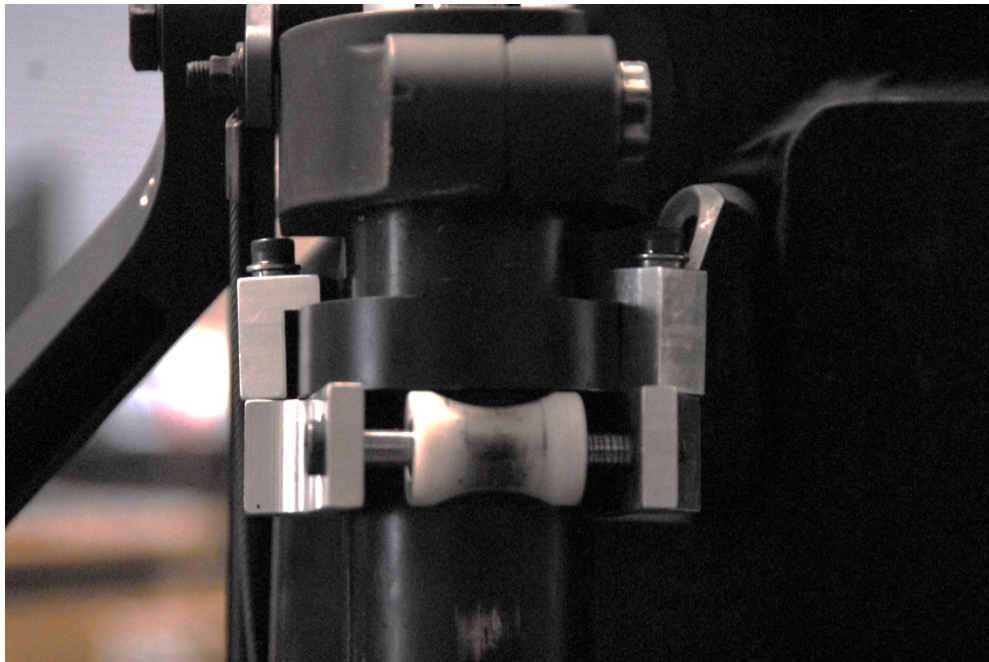


Figure 70: Roller Bearing Bracket on Upper guide Tube Bearing Bracket

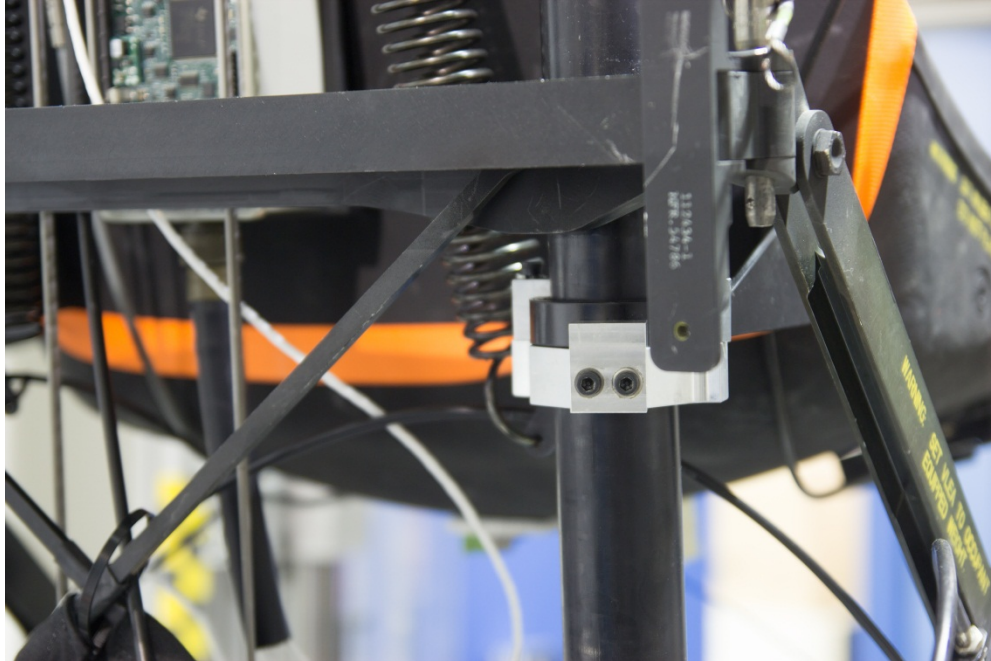


Figure 71: Roller Bearing Bracket on Lower Guide Tube Bearing Bracket

Proper installation of this bracket design is imperative to good performance. The design uses shims to load the roller bearing. The goal is to completely remove any contact between the ring of the original bracket and the guide post. If the bracket is over tightened, it is possible to have the opposite side of the bearing ring rub the guide post. If the bracket is too loose, the original friction will still be present. Shimming has been accomplished using washers of different thicknesses. Exact shimming is difficult to ascertain. Also, it is difficult to adjust the loading on the top brackets because the adjustment screws are only accessible in the space between the seat and the guide post. Improvements to the design are planned to allow for an acceptable prototype, but there are concerns about adding these brackets to the seat system as a final solution.

Attaching a bracket with a roller bearing to the existing bearing bracket potentially compromises seat height adjustability and crash EA stroke length. At the top most position on the OEM seat, the bearing leaves a 0.5” clearance between the bottom of the Armor bracket and the top side of the bearing bracket. It was found that the bearing bracket design with a socket head screw on top of the clamps restricted from reaching the top most position, this is shown in Figure 2. This can be solved by adding a countersunk feature. At the full down position, the MH-60S is designed with 11.5” of crash stroke. The roller bearing sits underneath the bearing bracket and its design adds 0.8” of height to the bearing bracket, which reduces the available crash EA stroke before impacting the middle cross member. Future iterations of roller bearing designs should attempt to put the roller bearing on the top of the bearing bracket. Sacrificing a height adjustment position is more acceptable, in the opinion of the project team and the project sponsor, than the effectiveness of the crash EA.

The same problems may be faced when trying to retrofit the rollers from BAE’s other seats to the MH-60S. The MH-60S bearing bracket, which does not have rollers, is thinner at the ring around the guide tube than any other BAE seat system that the project team has encountered. The diameter of the bearings used in the roller bearing system on the MH-60R, for instance, are larger than the thickness of the ring used as a bearing on the MH-60S. The design will have to make sure that the bracket position for the roller bracket is raised so that the lowest point matches the position of the lowest point of the current bearing bracket.

The material of the bearing may be another point of contention as we attempt to achieve a system which will last and perform. The material choice for the bearing will be important. The project team chose to use HDPE for its design for cost, weight and wear. The cost and weight were slightly improved over aluminum, which is used in the BAE design. The wear of the bearing both on the bearing and the guide tube is important for long service life. The guide tube is made of steel which is powder coated black. If the powder coat rubs off it could introduce a site for corrosion to occur. The HDPE did not wear completely through the powder coating in our tests, but deposits of black can be seen on the white roller wheels. It may be that a harder surface would not rub off as much of the powder coat. The project team would like to try aluminum in future versions of the roller wheels to compare the results.

Moving Forward After Successful Roller Bearing Tests

The results of applying roller bearing bracket V1.0 to the MH-60S with AVASS show a large reduction in transmissibility, matching simulated results using initial design specifications. The design of the MH-60S seat was not designed with low friction bearings at the guide tube, and the team has demonstrated that low friction bearings are necessary for optimal vibration reduction. The following figures show the transmissibility of the AVASS system before and after the installation of the first version roller bearing bracket design. It is interesting to note that before the friction was reduced, the single degree of freedom resonance peak is nonexistent and the peak is actually due to rocking in the seat frame. Once the seat is allowed to stroke in the direction of the dampers, by reducing friction, the single degree of freedom system transmissibility graph is quite

prominent. The reduction in transmissibility at higher frequencies is as designed. A further discussion of how the bearing brackets affected vibration performance is included in chapter 7.

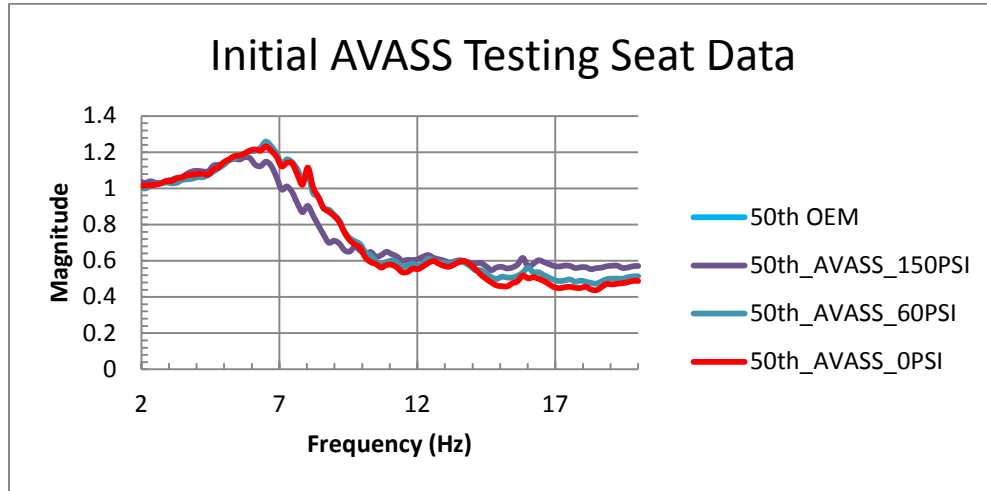


Figure 72: AVASS Before Roller Bearings

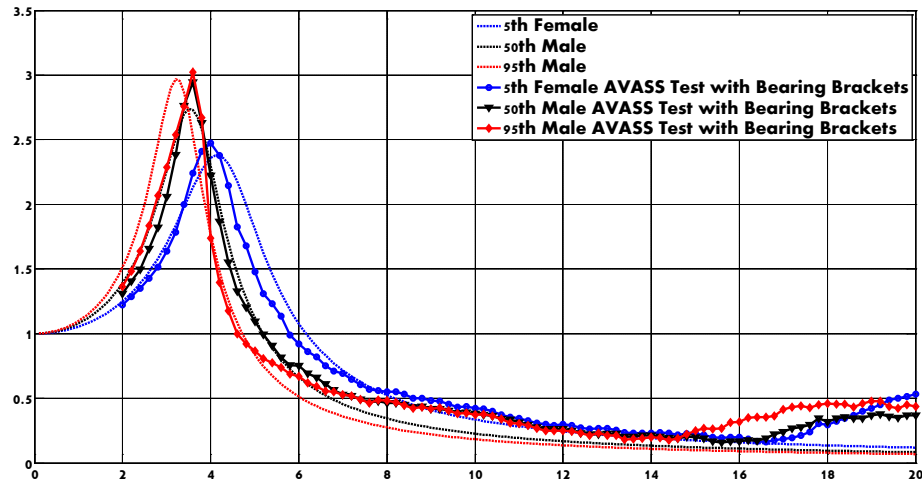


Figure 73: AVASS with Roller Bearing Brackets V1.0

The advanced state of AVASS integration into the SH-60S seat system, and its potential for commercialization, require that there be a discussion on the best way to integrate

roller bearings for production. Unfortunately, moving forward with the current roller bearing bracket design is impossible. The design was meant as a proof of concept and not a final component to the AVASS system. The main problem stems from an excessive reduction in crash stroke due to the height of the bracket which is attached below the OEM guide tube bearing. In an extreme crash scenario, the original bearing bracket would be the first thing to strike the frame after a minimum of 11 inches of travel. The first iteration of the roller bearing bracket reduces this stroke by almost a full inch. It is required that this reduction in crash stroke be minimized in the final low friction bearing configuration.

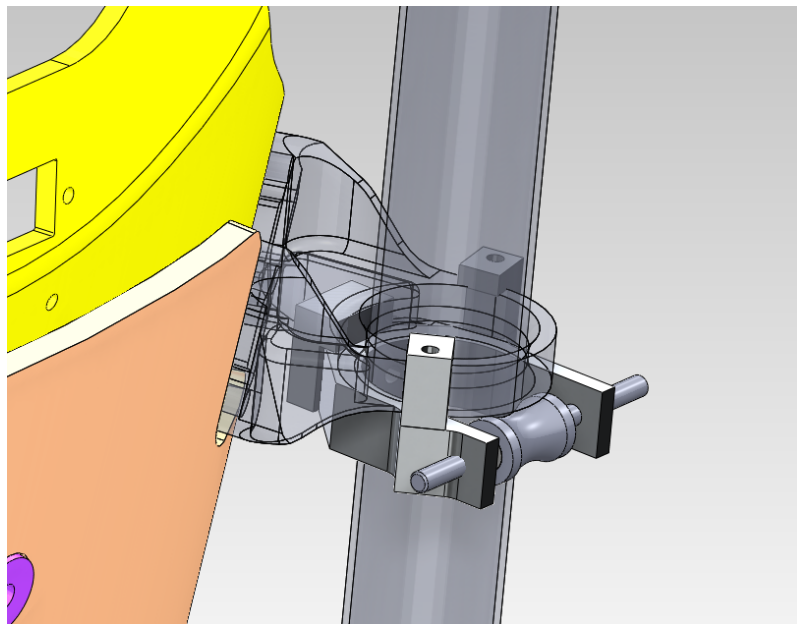


Figure 74: First Iteration Roller Bearing Bracket Design Methodology

A discussion of the requirements for the final version of the low friction bearing design is important as the project team decides how to continue. The main requirement is a low friction bearing contact which displaces the original guide tube bearing from the guide

tube. In order to do this, with expected tolerance deviation between MH-60S seats, either the bearing bracket needs to be completely replaced or a roller bearing bracket design must have adjustable preload. From experience using the first roller bearing bracket design during testing, the project team can say that ease of adjustability should be added to the requirements list as well. The adjustments should be made using easily accessible methods. The next requirement is related to keeping the functionality of the original MH-60S seat system. As discussed above, the MH-60S was designed with a wire bending crash attenuation EA which may require a significant amount of stroke down the guide tube. Keeping the designed in crash stroke as close to OEM is extremely important. Unfortunately, in the case of a roller bearing bracket applied with no modifications (i.e. new screw holes) to the existing bearing brackets, the system should be clamped at some part of the bottom of the bracket. Keeping this clamping thickness to a minimum is a requirement. The other function of the OEM MH-60S which the project team will keep in mind is the seat height adjustment. With the roller sitting on top of the existing bearing bracket, the seat will not be able to reach its full top position. The best situation with regards to a roller bearing bracket design of this type is to lose only one position of adjustability. The final requirements added to the list have been added to aid in design decisions. The project team has ranked the importance of cost and weight as shown in the list below.

The list of requirements is reiterated below:

- ▶ Must be adjustable for tolerance issues between seats.
- ▶ Adjustments should be easy to access

- ▶ Shim adjustments
- ▶ Must keep crash stroke as close as possible to OEM.
 - ▶ Must keep roller bearing design to a minimum thickness below the existing bearing brackets.
 - ▶ Thickness below bearing brackets to be $\leq 0.1''$
- ▶ Must lose only one top height adjustment spot at worst case
- ▶ Design for X Prioritization
 - ▶ Performance/Meeting Friction Requirements
 - ▶ Cost
 - ▶ Ease of Assembly/Installation
 - ▶ Weight

There are four OEM guide tube bearing brackets attached to the seat bucket which require rollers. These brackets are mirrored from side to side and differ greatly from top to bottom. The roller bracket designs can be mirrored from side to side, but will be completely different from top to bottom. It will be difficult to make parts which would be universal, although this would be beneficial for cost reduction purposes.

The total height of the roller to be used at the top bracket can be determined using the constraint put upon the design from the requirement to lose only one top most height position. The top most position has the OEM bearing bracket almost flush against the side armor clamp at the top of the guide tube. Figure 75 shows the position of the seat bucket, with the suspension at full extension, when installed in the second from the top position. In this position, the clearance to the side armor clamp at the top of the guide tube is just over 0.48". The roller and bracket assembly must not height taller than 0.48".

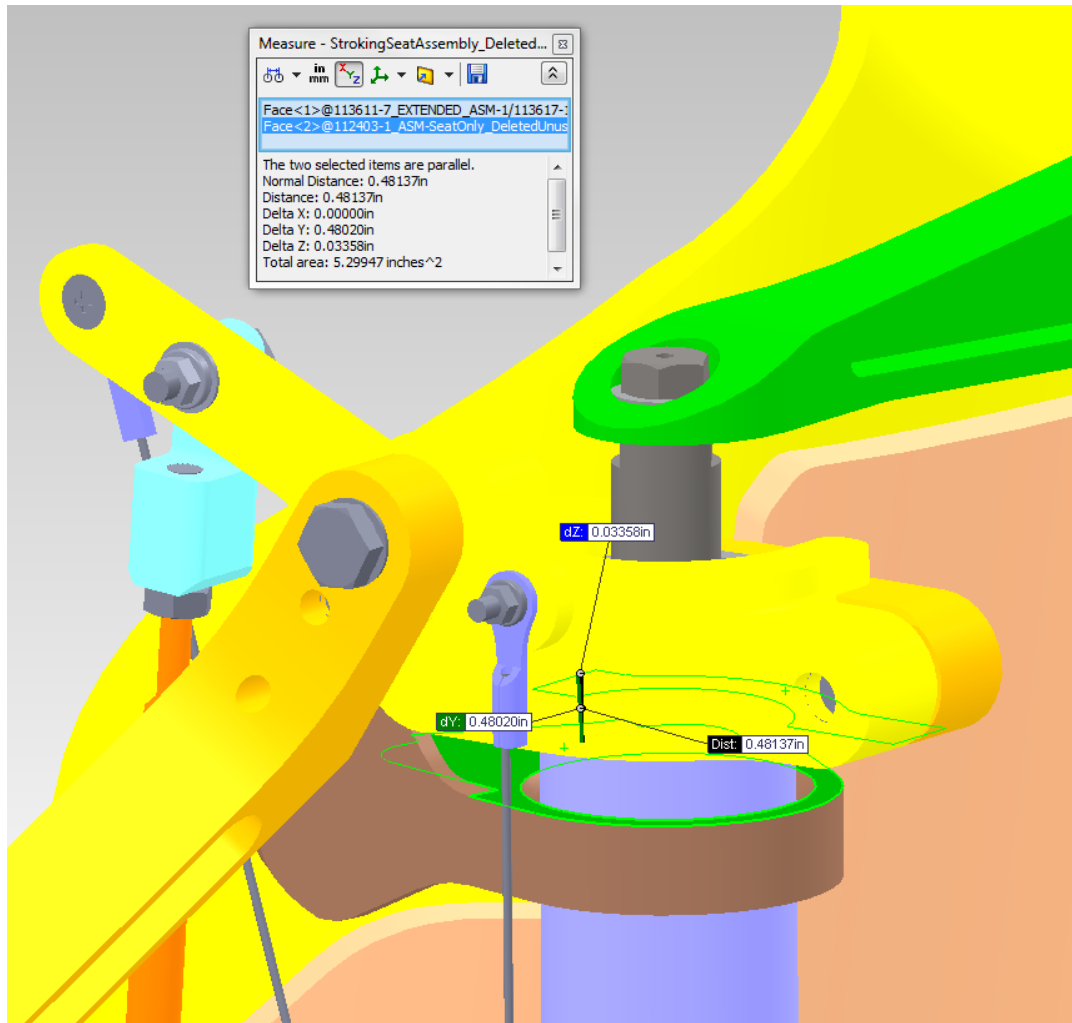


Figure 75: AVASS Seat At 2nd From the Top Position

This constraint causes a problem due to the known loads and COTS bearings available for this application. The roller shaft must be $\frac{1}{4}$ " diameter to meet the minimum strength requirements. The smallest outer diameter for a needle bearing which is rated for the loads and will accept a $\frac{1}{4}$ " shaft is $\frac{7}{16}$ " or 0.4375". This number is very close to our limit of 0.48" and would leave very little room for supporting structure for the bearing or roller. The final solution chosen for this design defining problem was to move the

bearings outboard and to have the roller slide over the shaft directly. This works due to the design of the side armor clamp at the top of the guide tube.

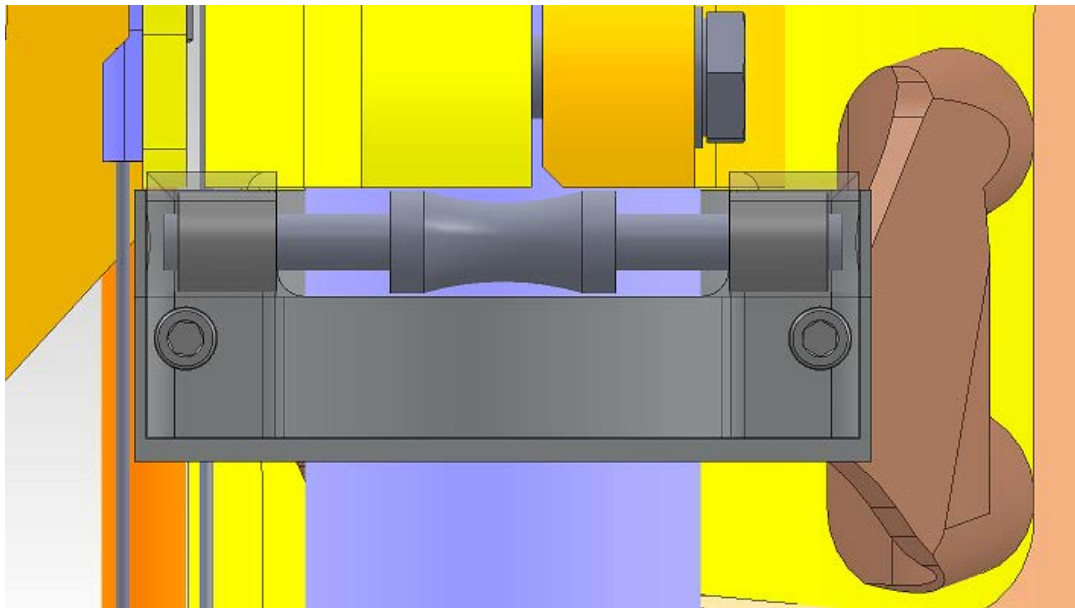


Figure 76: Second Iteration Roller Bearing Design for Top Brackets, Rear View (Adjustment Screws Easy to Reach)

The design of the brackets require that there be a method for securing the position of the roller and a positive reaction of the normal loads applied when the roller is pushed against the guide tube, not to be friction. This is a challenge because the design should also be designed with assembly in mind. Easy assembly of the system means not having to dismantle the OEM seat. Each part should be able to slide around the guide tube and should not have a closed circle over the guide tube which would require having an open end to the guide tube. The designs leverage the coupling from the top bracket to the bottom bracket to be able to provide the reaction surface. In general, the design philosophy is to create a solid base on which to attach a bearing bracket which can be tightened against the guide tube using screw adjustment from the back of the seat.

The components of each of the roller bearing brackets are to be designed with the potential to be manufactured with a 3 axis CNC machine from one side of the bracket. The CNC mill can be programmed to cut out the design of the bracket from one side, and then minor features like counter bores and tapped holes can be added after this operation. Although these brackets have the potential of having a large number of parts per seat system, this design for manufacturing method will hopefully reduce time and money expended during the production process.

The final design for the top bracket is shown in Figure 77 and Figure 78. The design hooks around the backside of the top OEM guide tube bearing bracket and is clamped to the bracket with 0.1” of clamping height. The adjustment screws point outward and will be used in tandem with shim washers to push the roller bearing against the guide tube to a to-be-determined preload. Due to the time constraints of the project timeline, these bracket components may be overdesigned and can still be optimized for weight in future iterations.

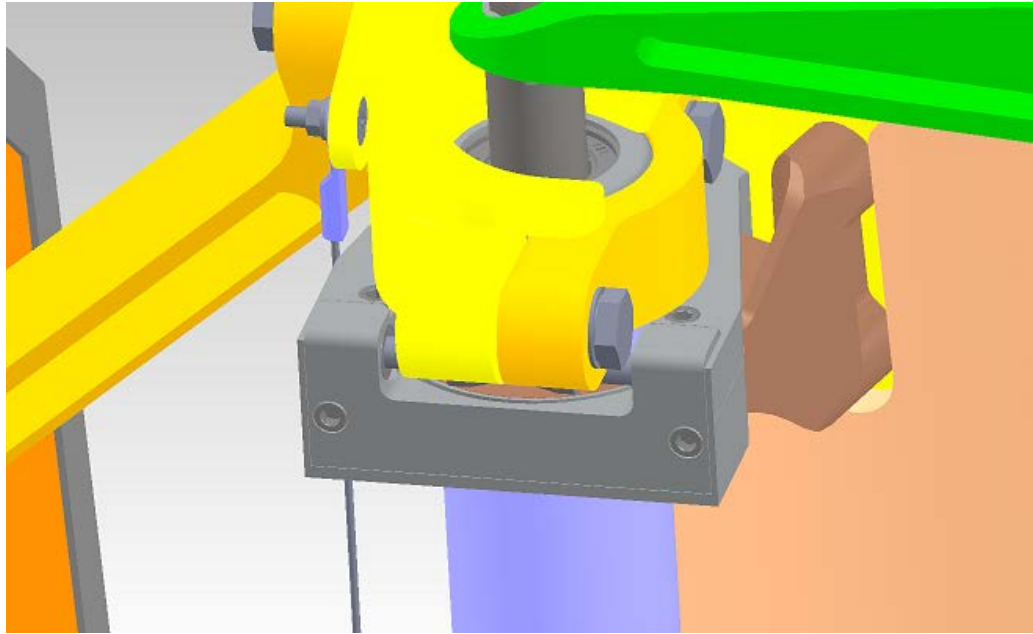


Figure 77: AVASS Roller Bearing Design for Top Brackets V2.0 Top Angle View

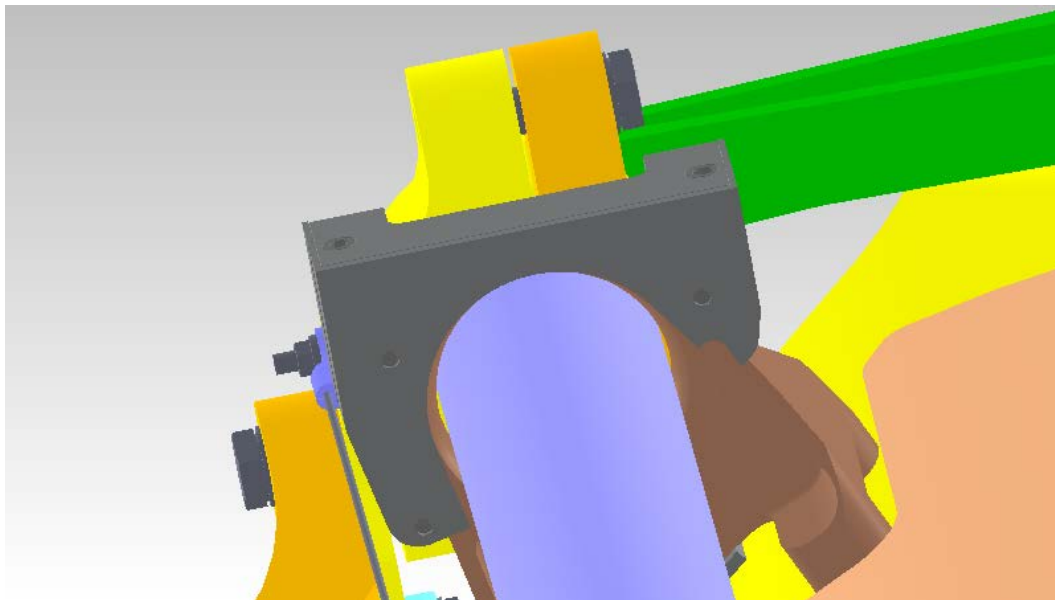


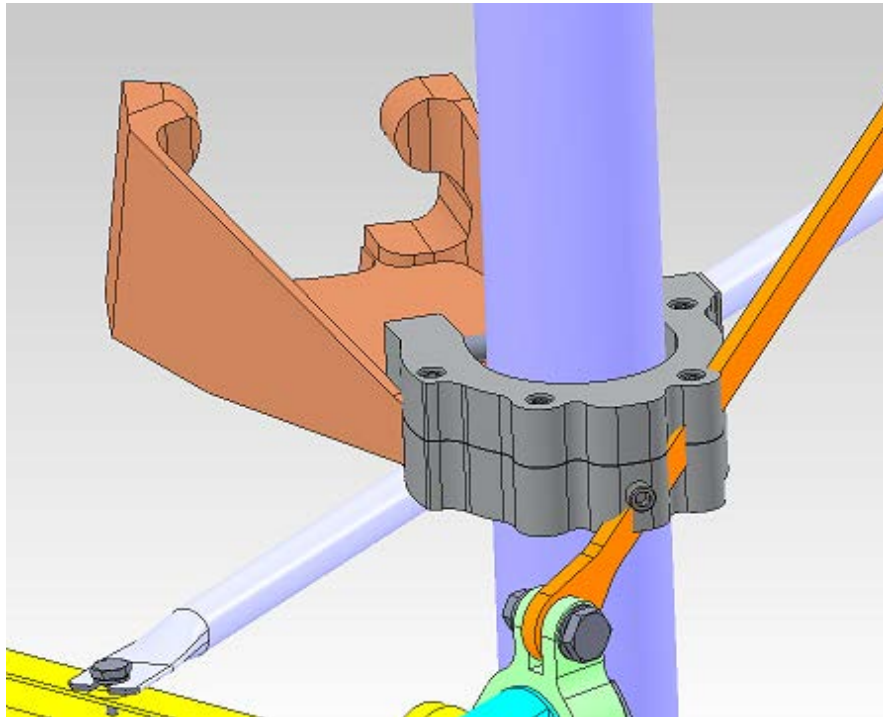
Figure 78: AVASS Roller Bearing Design for Top Brackets V2.0 Bottom Angle View

The bottom brackets required multiple iterations due to the design of the MH-60S seat.

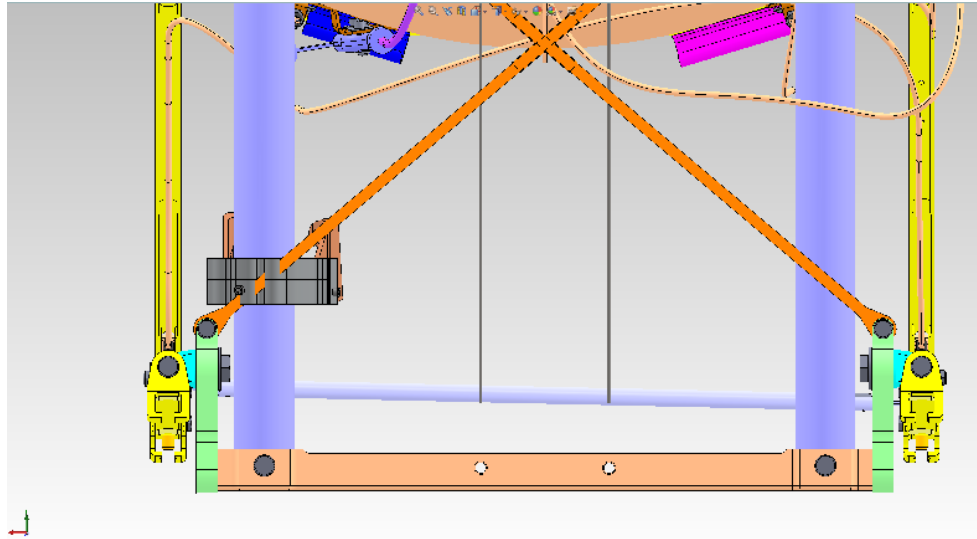
Initial impressions about the potential for roller bearing bracket designs for the lower

bearing brackets were that it would be much easier to design for than the top brackets due

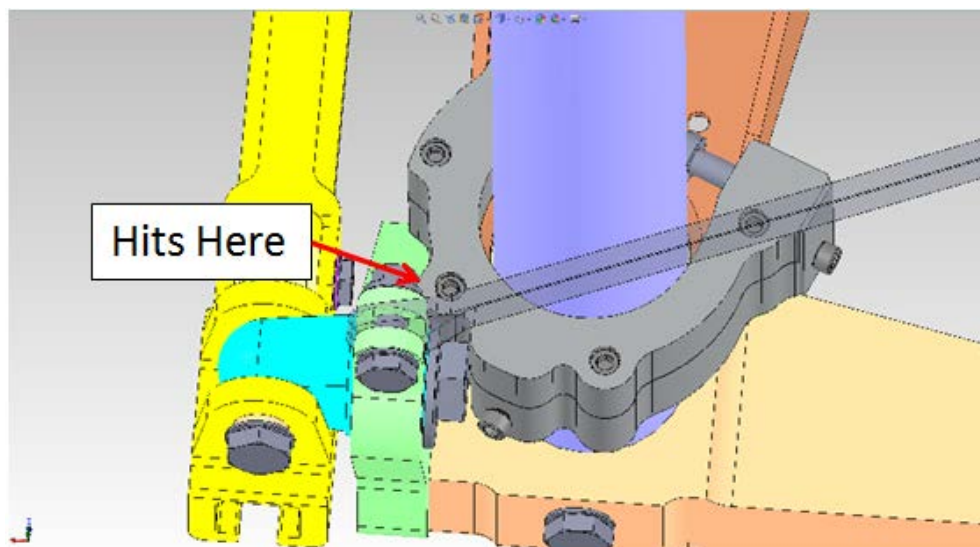
to clearance at the normal operating position. Unfortunately, after the first iteration of the design was completed, a final check on the clearance along the crash stroke of the bearing revealed new geometric constraints on the design. Figure 79 shows the aforementioned first iteration design hitting stabilizing x bars which are too close to the guide tube to allow the roller bearing design to pass without hitting.



**Figure 79: Problems with Clearance in 1st Iteration for
AVASS Roller Bearing V2.0 Lower Brackets**



**Figure 80: Problems with Clearance in 1st Iteration for
AVASS Roller Bearing V2.0 Lower Brackets**



**Figure 81: Problems with Clearance in 1st Iteration for
AVASS Roller Bearing V2.0 Lower Brackets**

Further down the guide tube, at the bottom of the stroke, there are still additional geometric constraints. The upright connection from the fore-aft seat position rails to the bottom crossbar connecting the guide tubes are also very close to the guide tube. This can be seen in Figure 81. The final shape of the constraint, from a top down view, is shown in

orange in Figure 82. Also shown is the bearing bracket used in the MH-60B seat, which was once seen as a potential solution for moving forward. The outline of the first iteration is still shown as well.

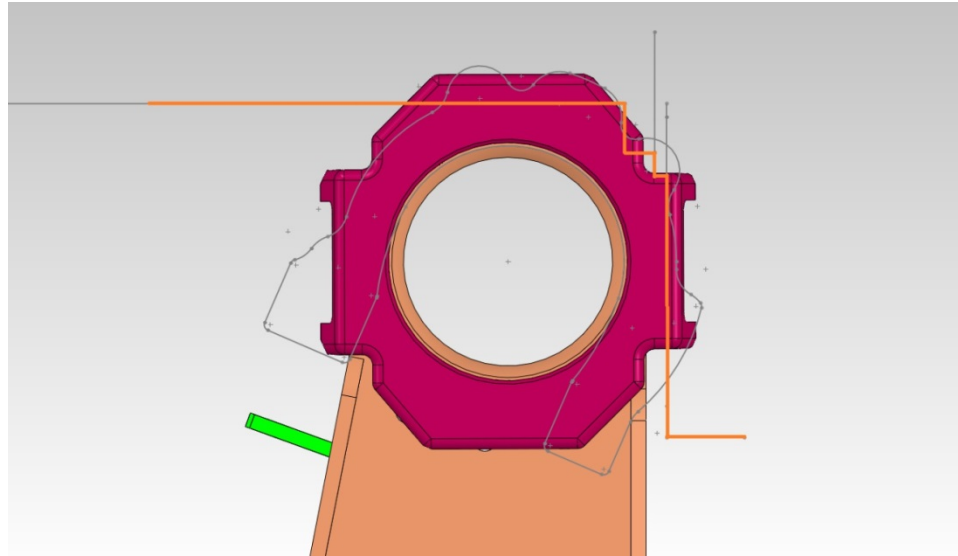


Figure 82: Geometric Constraints on the AVASS Roller Bearing Lower Brackets

Working with this new constraint, a new design took shape. The clamping screws created the backbone and clearance from this shape defined the rest. Figure 83 shows the top view of the final design for the bottom bracket design. Other clearance issues which also changed the design of the roller bearing bracket were the return spring position and screws used to mount the bracket where the return spring is attached at the bottom brackets. These screws and the return spring change position from side to side, but the left side bracket gives the most problems. There is a slightly different mounting hole pattern for these screws in one of the three MH-60S seat systems that the project team has access to. This deviation was accounted for in the design so that the same parts could be universal.

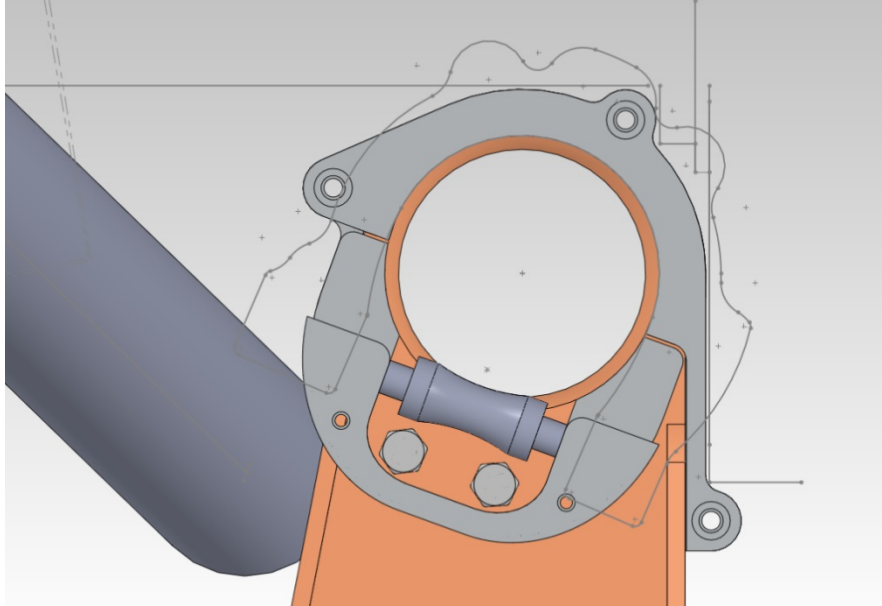


Figure 83: Design of Second iteration of AVASS Roller Bearing Bracket for Lower Brackets with additional Geometric Constraints

The final design of the lower bracket roller bearing is shown in Figure 84. A light weight part has been added to cover the needle bearing bore so that the shaft will not be able to leave the bearing side to side. There are 3 screws clamping the roller bearing bracket on the OEM bearing bracket and 2 screws for pulling the roller bracket against the guide tube for adjustment.

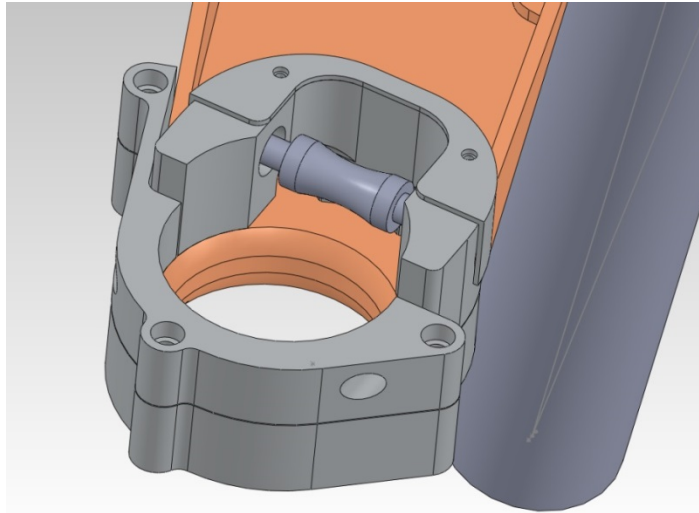


Figure 84: AVASS Roller Bearing Design for Lower Brackets V2.0 Top Angle View

The bottom roller bearing clearance above the OEM bearing bracket is much greater than the clearance above the top roller bearing. This space provides for the possibility of using a larger diameter roller bearing which can use inboard needle bearings. These inboard needle bearings may provide an extra reduction in friction. This is important due to the fact that the bottom bearings take a much greater normal load than the top bearings. The first iteration of the roller bearings were designed with rollers that used inboard needle bearings. The project team made certain that the design of the bottom roller bearing bracket could be used with the first iteration roller, as shown in Figure 85. This configuration will be included in the test plan.

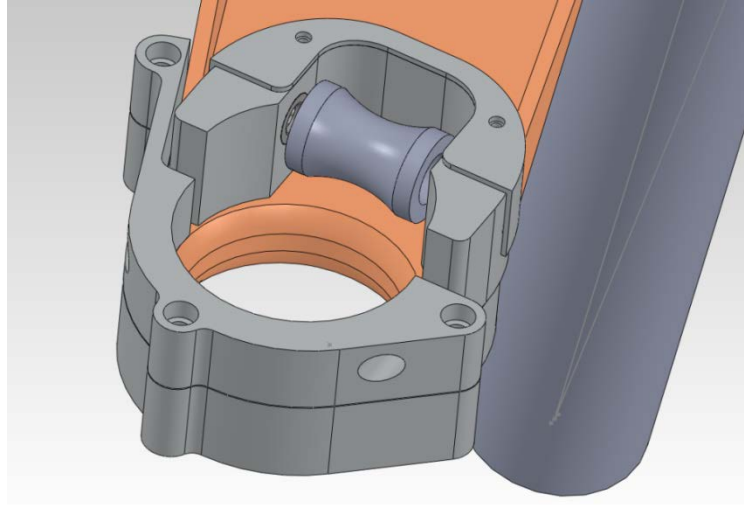


Figure 85: Larger Roller in AVASS Roller Bearing Design for Top Brackets V2.0 Top Angle

The assembly of the AVASS bearing bracket design is very straight forward. Attach the clamp to the appropriate bearing bracket. Each roller bearing bracket closely fits only one of the OEM bearing brackets making incorrect installation impossible. Once the roller bearing clamps are in place, use shim washers to try to push the roller against the guide tube and keep separation of the OEM bearing surface at all points round the guide tube. It is possible to push so much that the guide tube will start to rub against the opposite surface, so this shimming must be tested to make sure that friction is kept to a minimum.

There are two mirrored sets for each of the top and bottom brackets per seat system, making for 18 parts per AVASS system. The total weight added to the system, including shafts and hardware, is approximately 2 lbs. Drawings for all parts are found in the appendix to this report.

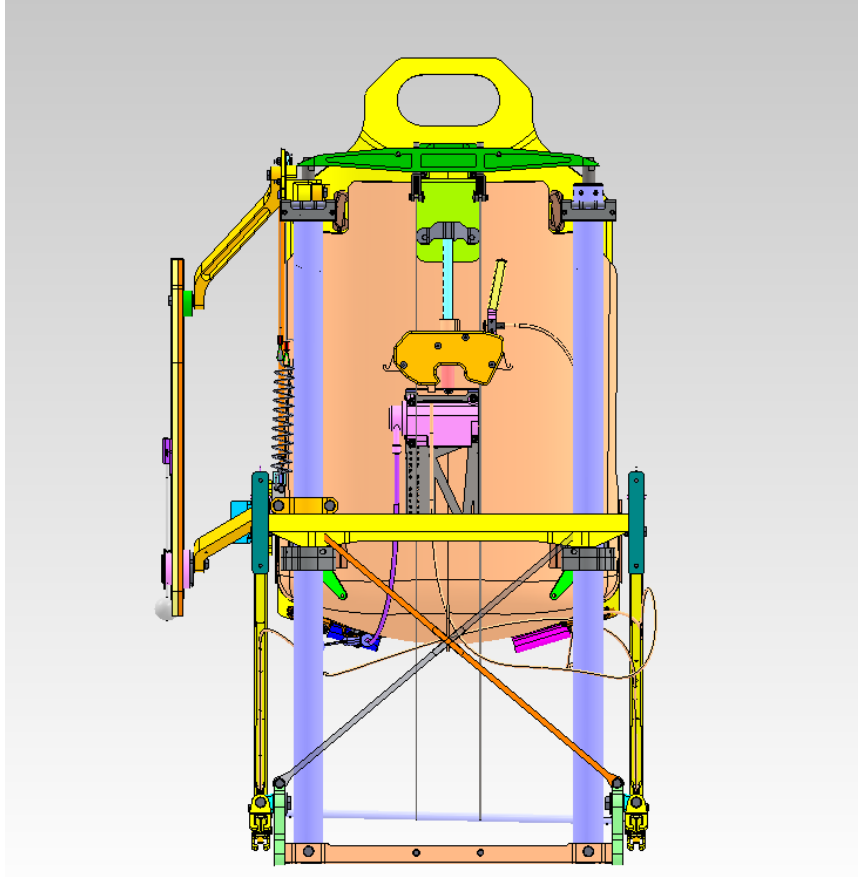


Figure 86: AVASS Roller Bearing Design V2.0 Fully Installed

Documentation of Roller Bearing V 2.0 Assembly

The first machined components of the final design for roller bearing brackets to be used with the SH-60S for the AVASS system were delivered to the project team in late November, 2012. The components are documented in photographs below. All machined parts are 6061 Aluminum.



Figure 87: Lower Assembly - Bottom Brackets



Figure 88: Lower Assembly - Top Brackets



Figure 89: Lower Assembly - Bearing Holders

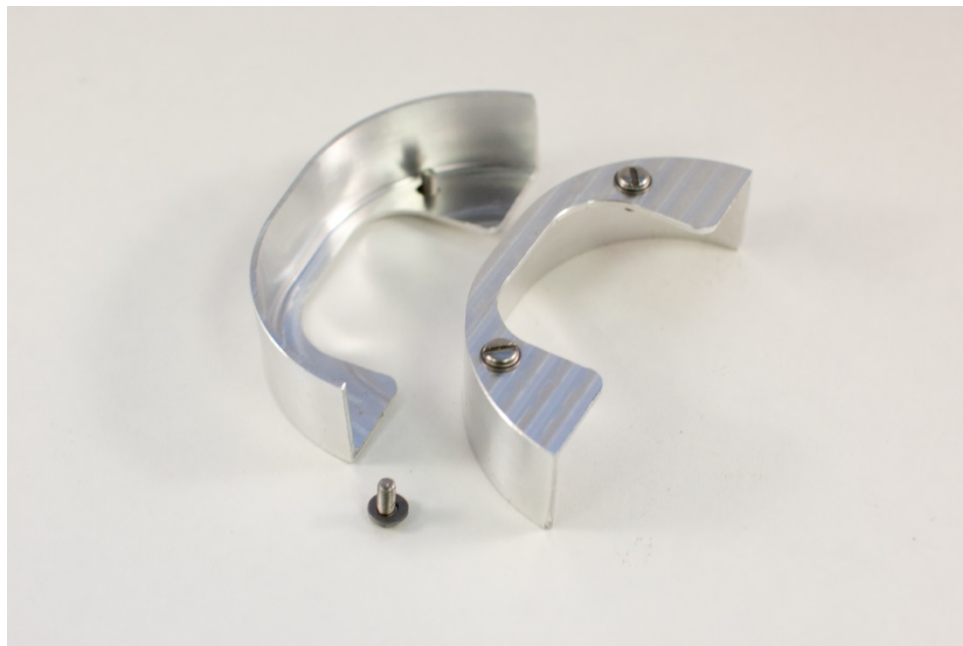


Figure 90: Lower Assembly - Axle Covers



Figure 91: Lower Assemblies - Angled View



Figure 92: Lower Assemblies - Top View



Figure 93: Lower Assembly - Comparison to SH-60B OEM Roller Bracket



Figure 94: Upper Assembly - Bottom Brackets

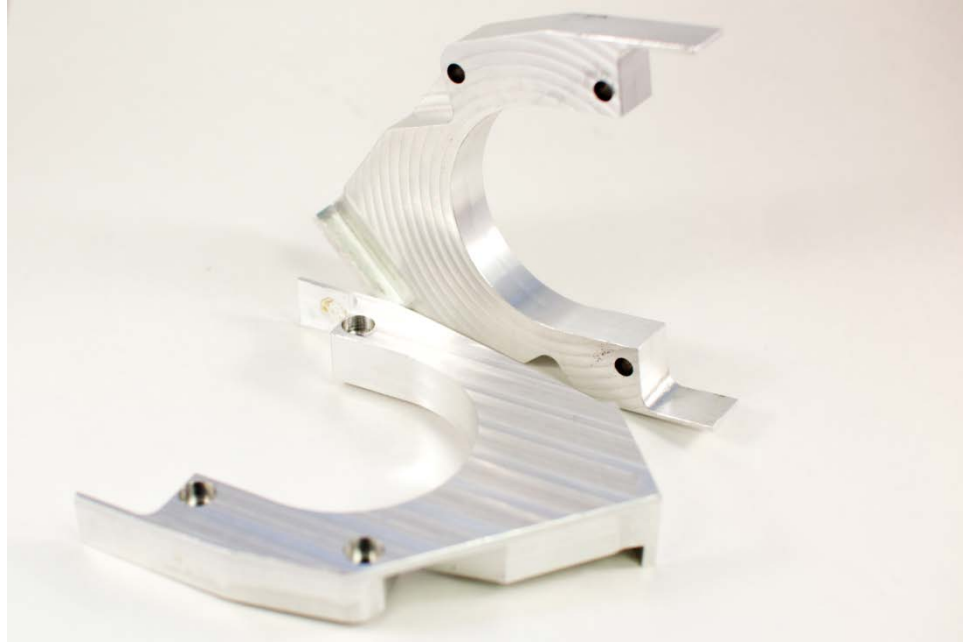


Figure 95: Upper Assembly - Top Brackets



Figure 96: Upper Assembly - Bearing Holders



Figure 97: Upper Assemblies - Top View



Figure 98: Upper Assemblies - Alternate View



Figure 99: Left Side Upper Assembly - Installed On Seat - Top View



Figure 100: Left Side Upper Assembly - Second From Top OEM Position Clearance

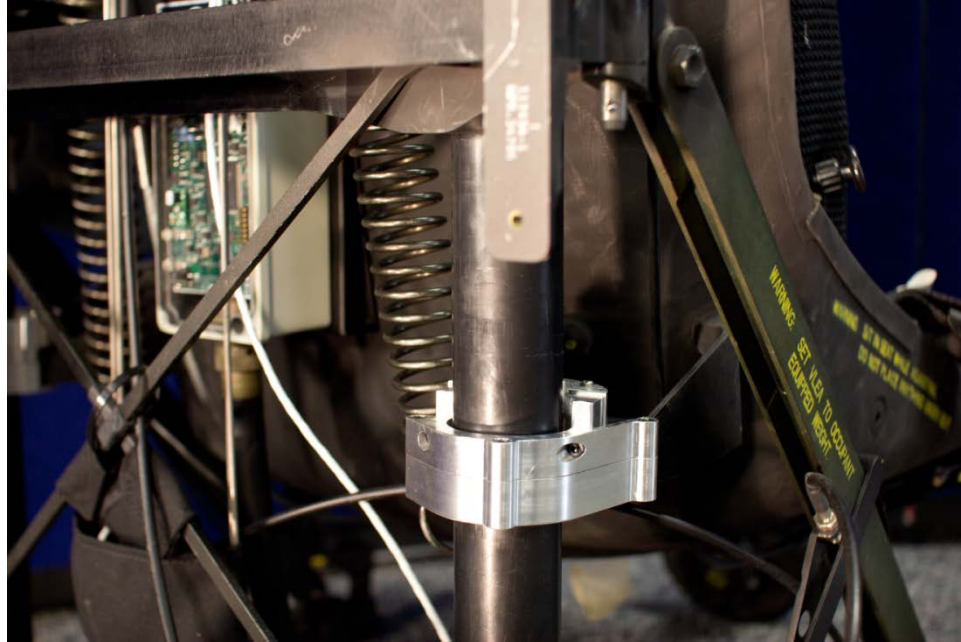


Figure 101: Right Side Lower Bracket - Installed On Seat

All parts mated as required and the fit is excellent. All four brackets together weigh about 2 lbs. Only minor modifications were required to adjust the preload of the rollers. The lower bearing holder was shortened by 0.03” to allow for a larger adjustment range. This change was added to the model drawings; to be implemented into the next two sets of brackets. Plastic spacers were implemented around the adjustment screws to set the preload distance. As was explained in the design criteria discussion above, applying this roller bearing design comes at the cost of the top most position.

Assembling all four brackets onto the seat system takes no more than 15 minutes. No disassembly of any part is required. If the seat is lowered to its bottom most position, all screw heads are accessible for tightening. The bottom brackets for both upper and lower assemblies are designed to fit snugly around the form of the existing OEM brackets. The

top bracket can then be moved into place and aligned with the bottom bracket. The clamping screws can be hand tightened to serve as guides and hold the system in place. The top and bottom brackets are tightened before applying the bearing holders. The bearing holders have built in stability and support for alignment. Spacers should be put in place before tightening the adjustment screws. Applying correct and even torque on the adjustment screws will help align the roller properly.

The AVASS bolt on roller brackets are designed to lower friction while maintaining the structural strength of the OEM system. The OEM MH-60S has been qualified safe using criteria from MIL-STD-58095A. The seat system with AVASS applied will be required to pass the same criteria. Clamping these brackets around the existing brackets in no way weakens them. Bending loads on the roller bearing axles will only be applied until the original bearing surface is in contact with the guide tube. At this point, the load path will be the same as the OEM seat.

A problem which was encountered while designing the lower brackets was clearance along the crash stroke. In an effort to confirm that the design does indeed have sufficient clearance, the seat, with brackets installed, was detached from the crossbar clevises and lowered through its crash stroke. Documenting photos are shown below. There is a very tight tolerance on the right side X bar which comes close to the bottom of the right guide tube. In an effort to reduce the likelihood of any problems during dynamic testing, a chamfer has been added to the lower part of the lower brackets. All other points give sufficient clearance.

Starting at the top of the stroke there are no problems. The first clearance issue is with the spring used for retracting the armor plate. The spring is pushed out of the way with very little effort, but a modification can be made to the lower spring perch to move it out of the way permanently. The need for the modification of the lower spring bracket is accentuated at the bottom of the stroke. The modification proposed is shown in Figure and does not negatively affect the performance of the seat in any way. Next, the lower right side (looking from the back) X-bar is actually bent in towards the guide tube and actually rubs as it allows the bracket to move past it. As was discussed earlier, a chamfer is being added for the case that this may hit during dynamic testing or a crash incident. Finally, the head of the screw attaching the rail to the lower crossbar comes very close but does not seem to have any issues.

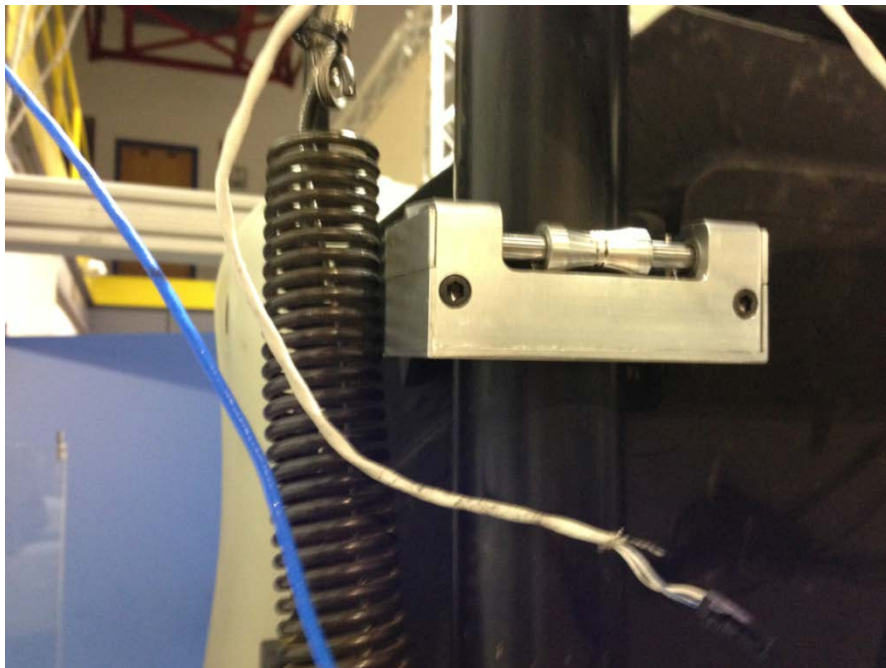


Figure 102: Upper Bracket - Armor Side - Spring Clearance Issue on Crash Stroke

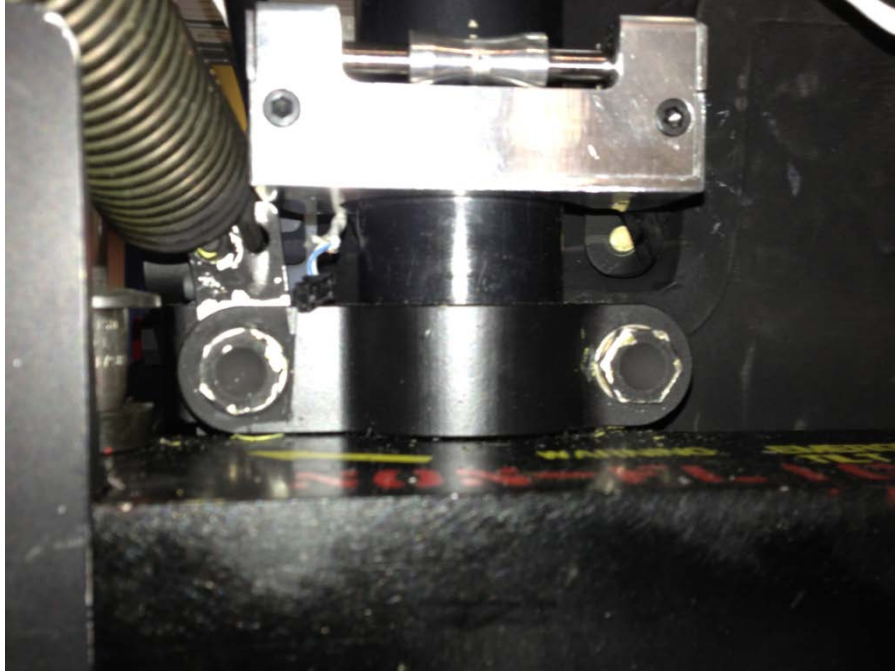


Figure 103: Upper Bracket - Armor Side - Armor Spring Bracket Clearance Issue

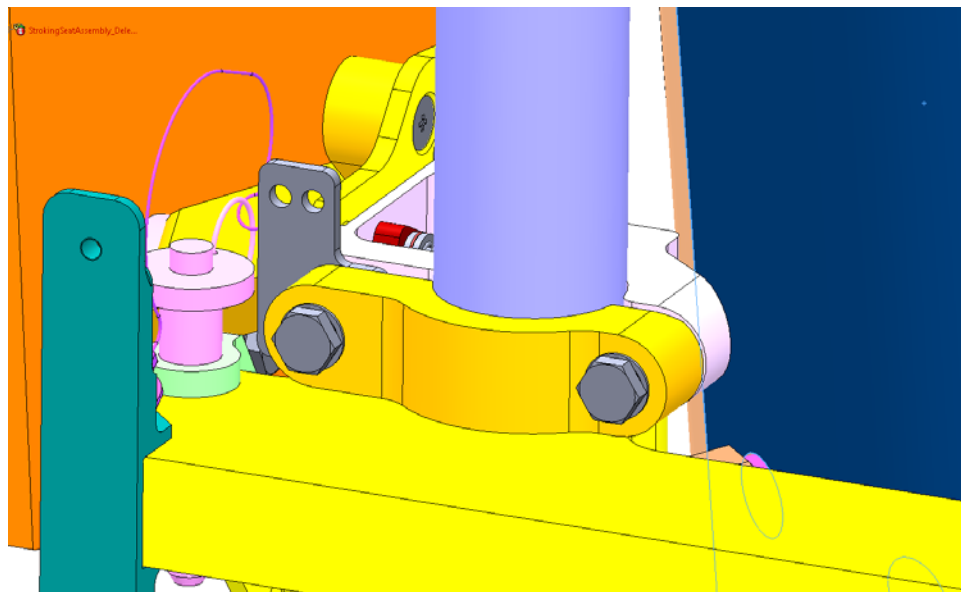


Figure 104: Proposed Armor Spring Bracket Modification

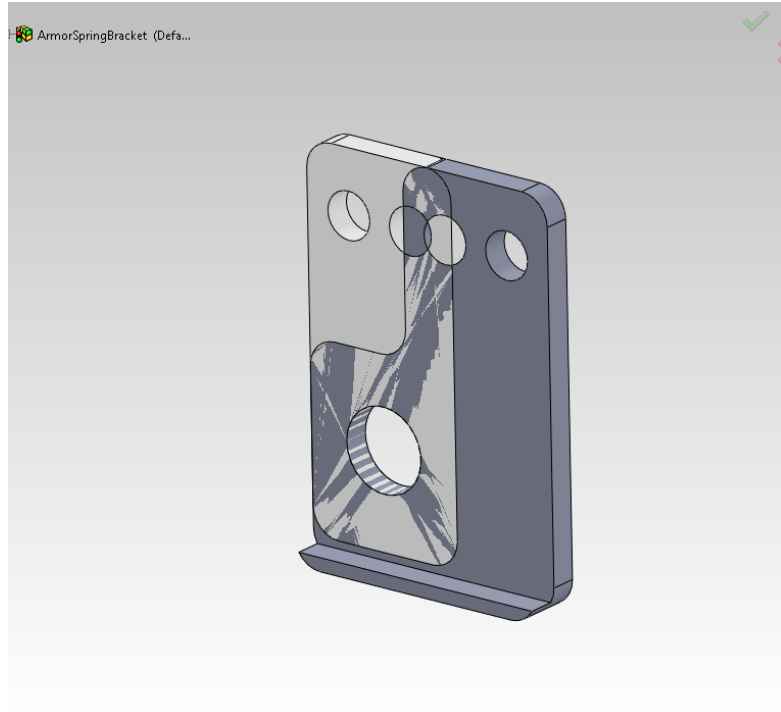


Figure 105: The Proposed Modified Armor Spring Bracket Over the Original bracket

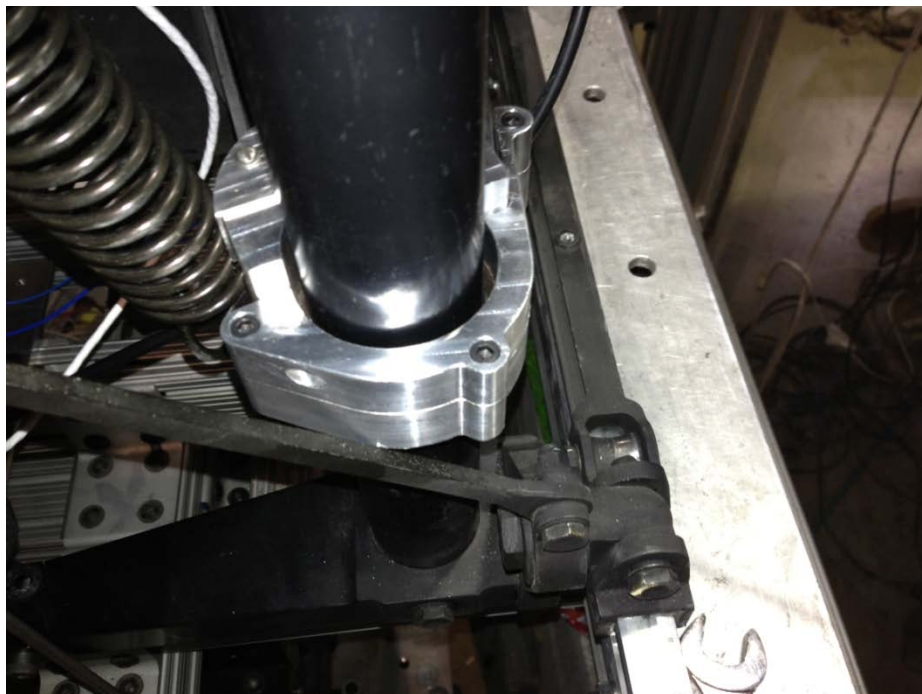


Figure 106: Lower Bracket - Right Side (From the back) - X-bar Clearance Issue



Figure 107: Lower Brackets Clearance on Full Down During Crash Stroke

AVASS Roller Bearing V 2.0 Performance Verification Testing

The prepared MH-60S seat system with AVASS and V 2.0 of the roller bearing brackets was tested on the vibration stand at the University of Maryland to assure proper performance. All tests during this session were run uncontrolled with 50th male mass BART ballast. The BART anthropometrically correct weight ballast system is discussed in Chapter 6. Figure 22 is a plot overlaying the best results from past testing and the results from this test.

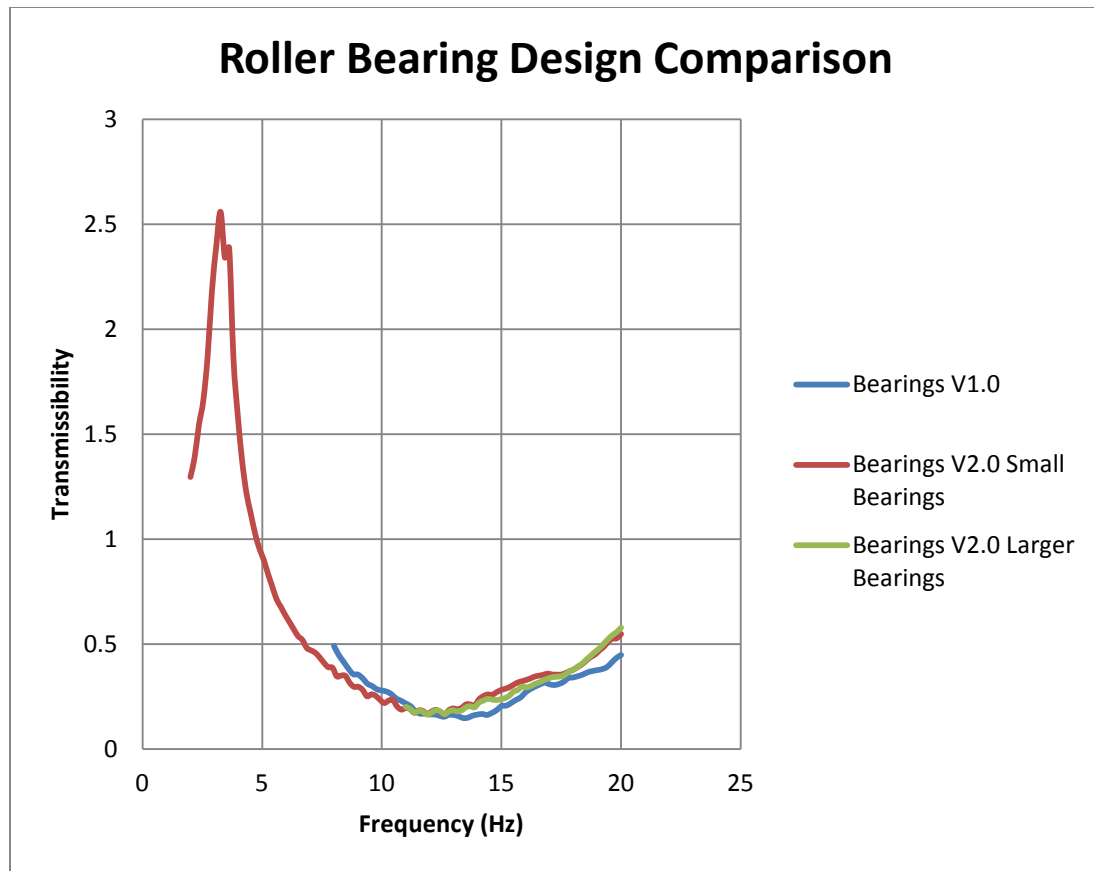


Figure 108: Comparison of V 1.0 and V 2.0 Roller Bearing Performance

The lower bearing bracket design allows the possibility of using a larger diameter roller, such as the roller used in V 1.0. The plot in Figure 22 shows a green line labeled “Bearings V 2.0 Larger Bearings”. This line shows the performance of the system with the V 1.0 bearings in the lower bearing brackets. The graph shows a small rise in transmissibility from the V 1.0 and V 2.0 with Larger Bearings, but this is all within error of the measurement method.

The project team believes that the performance is quite good and matches reasonably well with the performance of the first version of the roller bearing system. Overlaying the

plots shows similar dynamics and comparable levels of vibration reduction. In an effort to reduce variation in parts and problems in assembly, the team has chosen to continue with small bearings at all the bearing brackets. The material may be changed in the future, but all four brackets should have the same rollers.

CHAPTER 6: TESTING METHODOLOGY

Vibration Testing of the MH-60S Seat System

Two types of vibration performance evaluations are being conducted:

- 1) Frequency response evaluations using stepped-sine inputs, and
- 2) Transient evaluations using representative H-60 flight data.

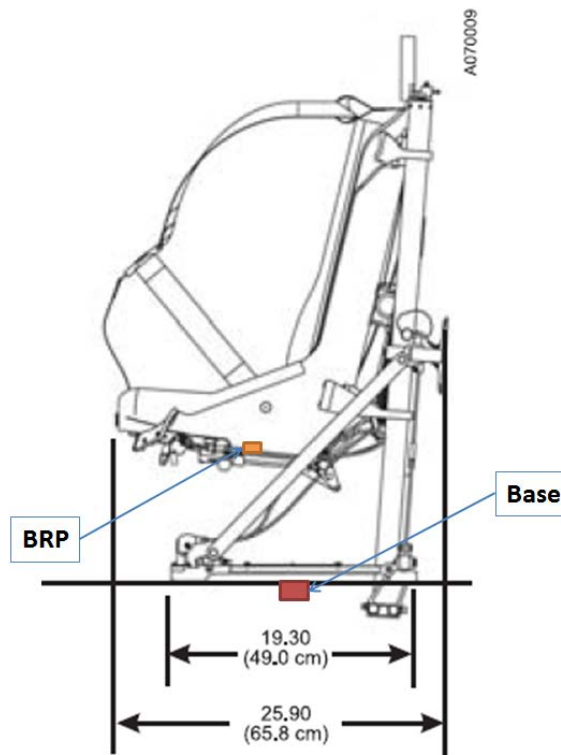


Figure 109: Sensor Mounting Positions for Testing

Output accelerations at the buttock reference point (BRP) and at the floor are used to create a transmissibility curve or frequency response plot, which is a measure of output acceleration divided by input acceleration at each frequency. The system used to

construct the transmissibility curve includes Siglab electronics and software, an MTS controller and a hydraulic actuator. The MTS actuator is capable of frequencies from 1 to 40 Hz and a total stroke of 6 inches. The vibration test stand at the Smart Structures laboratory at the University of Maryland was originally designed and built for the SAMSS program. Since then, a large number of projects have been able to benefit from its use. A photo of the test area is shown in Figure 110.



Figure 110: University of Maryland Smart Structures Laboratory Vibration Test Stand

The Siglab controller is programmed to sweep through a set of given frequencies while attempting to match desired 0.2 g input accelerations for each frequency. Five averages of the root-mean-square (RMS), filtered, input and output accelerations are used to calculate the transmissibility values. When limited to the range from 2 Hz to 20 Hz, each vibration sweep takes about one hour to conduct. Multiple sweeps can be completed for each mass level to assure repeatability and to avoid errors. When appropriate, the project

team was able to increase input levels and limit the range of frequencies tested. These changes allowed for testing of hypotheses in a shorter time span.

For transient vibration performance evaluations, the project team is using data provided by the U.S. Army Advanced Applied Technology Directorate (AATD) for the UH-60 Blackhawk. While there are known differences due to the H-60 variants and payloads, this data is useful for establishing approximate levels of n/rev vibrations (which should be representative of all variants). Provided are time domain accelerometer measurements and associated power spectral density (PSD) plots. The PSDs allow for an attempt at recreating the time signal by generating inputs at the noted frequencies. A Simulink block diagram is used to generate sinusoidal waveforms with 4.3 Hz and 17.2 Hz content to match the power at each frequency. A dSpace system is used in an open loop to control the hydraulic actuator in the shock and vibration test stand to recreate this signal at the floor accelerometer. Accelerometer measurements at the BRP for both the OEM MH-60S and the MH-60S with AVASS can be directly compared to show reductions in power at specific frequencies.

Occupant test masses were initially achieved with the use of sand bags calibrated to specific weights. The total effective weights evaluated were 120lbs., 180 lbs., and 230 lbs., respectively for the 5th percentile female, 50th percentile male, and 95th percentile male. These weights are in accordance with suggested values for the amount of the occupant's total mass supported by the seat plus adding between 38 and 54 lbs for personnel supported equipment [12]. Anthropometrically correct weight ballast was

acquired at the end of testing with V1.0 of the AVASS roller bearing design. The BART ballast system is detailed in the following section. In general, the seat restraints were used to keep the masses restrained during testing. The project team also varied the height of the seat according to mass in order to match a realistic scenario. The theory is that the heavier the occupant, the taller he or she is, and therefore they will have to sit lower to maintain a proper line of sight.

Smart BART Test Ballast

Sand bags for testing proved to be prone to error due to the distribution of mass across the stroking mass. The weight was distributed between three or four bags of set mass and placed on the seat bucket as well as possible. At first, the sand bags were placed on top of the seat bottom cushion, strapped back against the seat back cushion using the existing five point harness. Observations of the sitting position of humans led to the conclusion that the mass distribution may be affecting the performance. A test with different variations, including without the seat back cushion to push the center of mass further back and stacking the cushions so that the leg mass would not resonate on the seat cushion, shows a large variation in measured transmissibility (Figure 111). A more reliable and repeatable mass distribution was desired for continue testing.

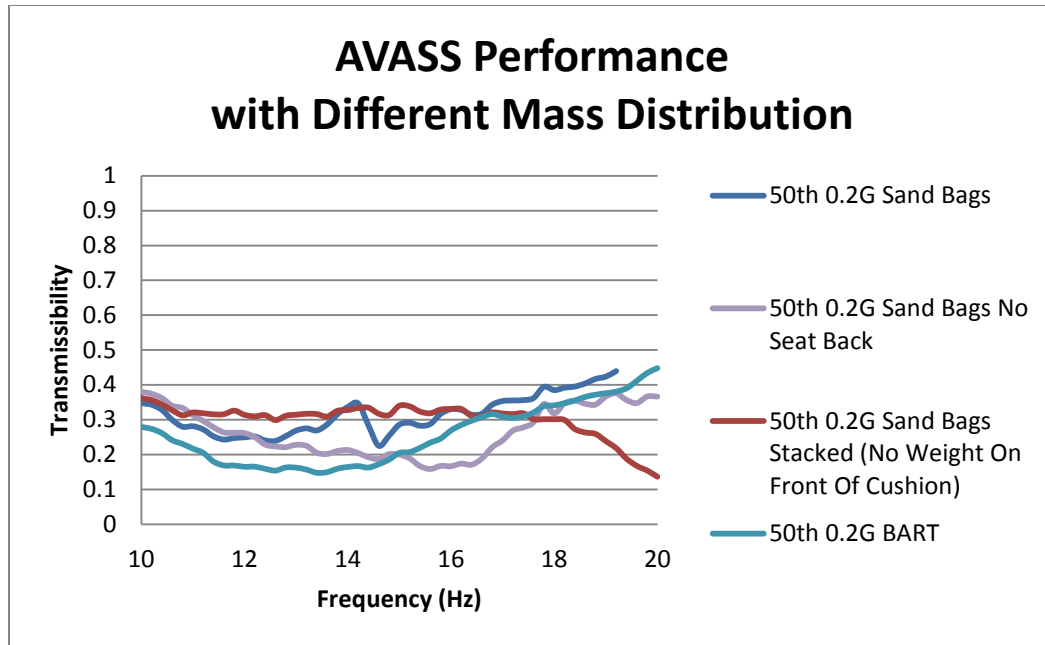


Figure 111: AVASS Performance with Different Mass Distribution

In an attempt to reduce error in performance measurement due to incorrect weight distribution, a Star Bart with Arms from ETD was acquired from Roto West in California [33]. This pose able hard plastic dummy can be filled with water to mimic the weight distribution of a human occupant. The dummy is 70.1” tall has freedom of rotation at the shoulder, elbow, hip and knee and weighs 192 lbs. full of water. The project group ordered the dummy and proceeded to do its own analysis of these claims for internal documentation.

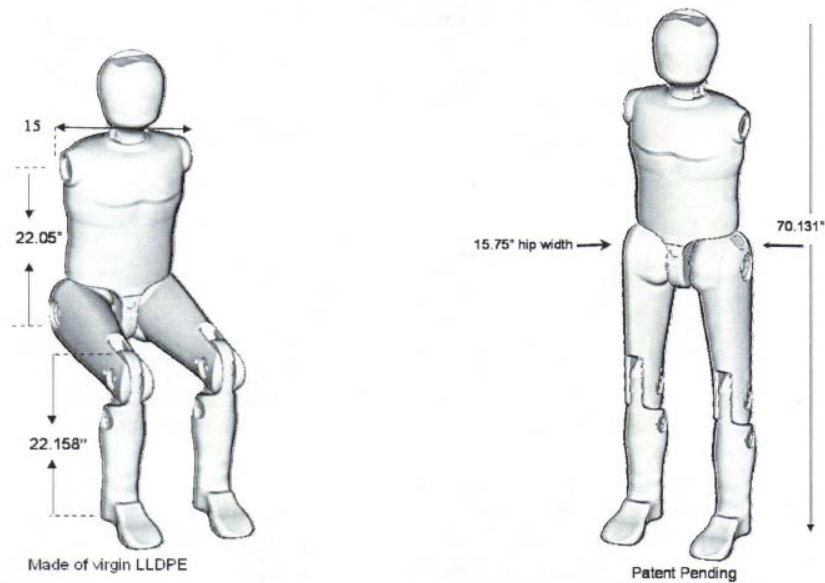


Figure 112: Star Bart with Arms

The dummy is easy to assemble and fill with water. It is made of a hard white, translucent, plastic. Each part can be filled individually and assembled on the seat. The parts come with NPT threaded plugs which allow for draining and filling with quick seals. The dummy comes with a sheet giving a suggested weight at full and giving the dimensioned image shown in Figure 6.



Figure 113: Photo of Star Bart Taken Apart

The table below (Table 6) lists measured weights. The final weight is very close to the advertised weight. It is also very close to the equipped 50th male weight. There are small air pockets visible in each of the body parts after filling which may reduce the weight measured versus the advertised weight number.

Table 6: Table of Star Bart Component Weight Composition

	Dry Weight (lbs)	Full of Water (lbs)	Water Weight (lbs)	Water Volume (gals)
Torso	12.00	91.50	79.50	9.52
Hip Bolt	3.52	3.52	0.00	0.00
Left Shoulder Bolt	0.28	0.28	0.00	0.00
Right Shoulder Bolt	0.28	0.28	0.00	0.00
Left Upper Arm	1.32	5.10	3.78	0.45
Right Upper Arm	1.30	5.00	3.70	0.44
Left Arm Bolt	0.27	0.27	0.00	0.00
Left Lower Arm	1.05	3.50	2.45	0.29
Right Lower Arm	1.04	3.50	2.46	0.29
Right Arm Bolt	0.27	0.27	0.00	0.00
Left Upper Leg	4.04	23.50	19.46	2.33
Right Upper Leg	4.06	23.50	19.44	2.33
Left Knee Bolt	1.46	1.46	0.00	0.00
Left Lower Leg	3.08	12.50	9.42	1.13
Right Lower Leg	3.10	12.90	9.80	1.17
Right Knee Bolt	1.46	1.46	0.00	0.00
Total:	38.55	188.56	150.01	17.97

These weights are useful for determining how closely the Star Bart with Arms mimics the weight distribution of a human. The project team found anthropomorphic data relating the *relative weight and length of body segments for adult men and women* [4]. This table is shown in Figure 114. In order to use this table, the parts of Star Bart had to be matched to the chart segments as well as possible. The torso, hip bolt and half of each of the shoulder bolts should be equivalent to the trunk and head and neck added together. The upper arm, half of the elbow and shoulder bolts should be equivalent to the upper arm. The lower arm, and half of the elbow bolt should be the same as the forearm and hand together. The upper leg and half of the knee bolt should be equal to the thigh. Finally, the lower leg and half of the knee bolt should be equivalent to the shank and foot together. A bar graph relating the table values to the measured Star Bart with arms weight by percentage is found in Figure 115.

TABLE A.2.3. Relative weight and length of body segments for adult men and women

Body segment	Men		Women	
	Weight	Length	Weight	Length
Whole body	100	100	100	100
Trunk	48.3	30.0	50.8	30.0
Head and neck	7.1	13.8	9.4	
Thigh	10.5	23.2	8.3	24.7
Shank	4.5	24.7	5.5	25.6
Foot	1.5	4.2 ^a	1.2	
Upper arm	3.3	17.2	2.7	19.3
Forearm	1.9	15.7	1.6	16.6
Hand	0.6	10.4	0.5	10.4

Weight and length measurements reported are percentages of body weight and body length, respectively.

^aThe number is associated with height of the foot not its length.

The data were gathered from de Leva (1996) and the skeletal anthropometric measurements by Santschi et al. (1963).

Figure 114: Relative weight and length of body segments for adult men and women

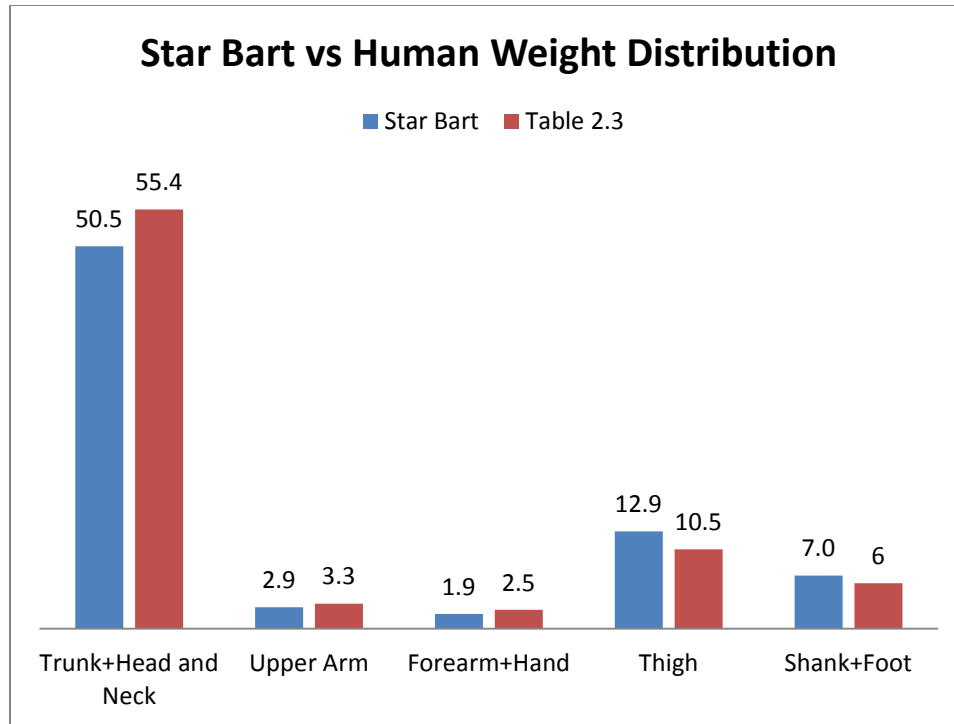


Figure 115: Anthropomorphic data versus Star Bart measured data

Testing with the Star Bart with Arms is as simple as sitting it down and using the seat belts to hold him down. Test masses have been 80% of the nude weight of the occupant plus equipment weight. For the 50th male, the test mass should be around 185 lbs. This is almost the exact weight of the nude Star Bart with Arms. In order to account for the 20% weight loss, the project team removed the lower leg section of the dummy. This accounts for 15% of the weight of the dummy. We added weight strapped to the chest of the dummy to simulate the equipment weight. The results from sine sweep tests with the Star Bart with arms are discussed in chapters 7 and 8.

CHAPTER 7: AVASS REPORTED RESULTS

This chapter summarizes the results of testing completed throughout the program, not including the final configuration. The data was used to draw conclusions for assessing the quality of the AVASS system and recommend changes. This information was submitted in bimonthly reports to project sponsors.

OEM MH-60S Test Results

Following the methodology described in chapter 6, a full suite of tests was conducted on the OEM MH-60S for observation and future comparison. Figure 116, Figure 117, and Figure 118 show the frequency response characteristics for the 5th percentile female, 50th percentile male, and 95th percentile male equivalent sand bag test masses in the baseline OEM seat configuration, respectively. During testing, all mass levels demonstrated a very noticeable rocking motion harmonic between 6 Hz and 8 Hz. The exact harmonic frequency is slightly different depending on seat position and mass. In theory, the lower the mass, the higher the harmonic frequency should be. This is noticeable in the plots.

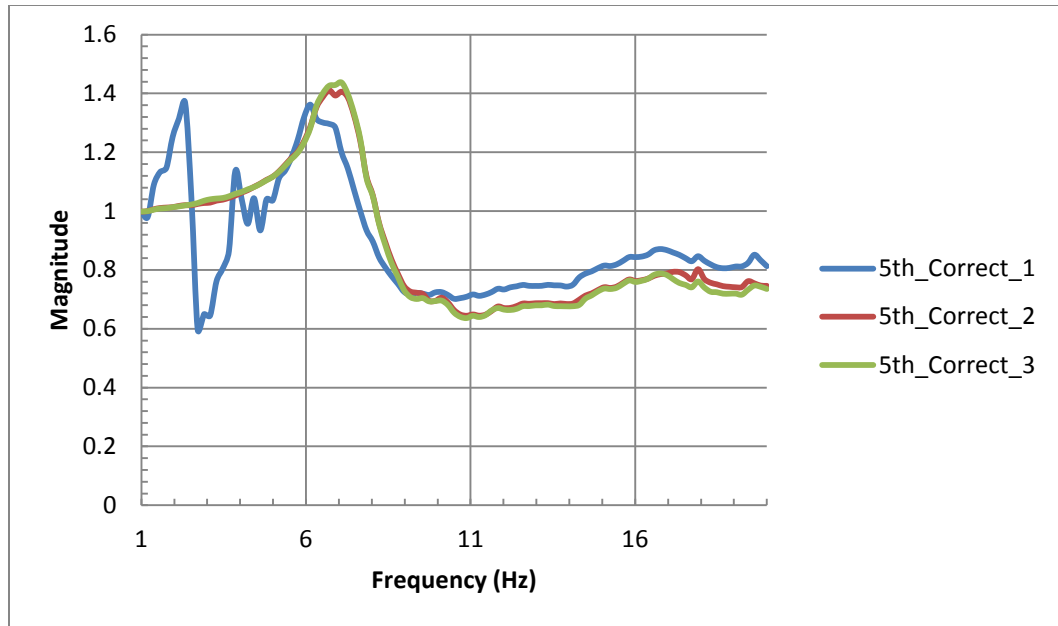


Figure 116: Frequency Response of MH-60S Seat in Baseline OEM Configuration for 5th Percentile Female with Seat at Highest Position

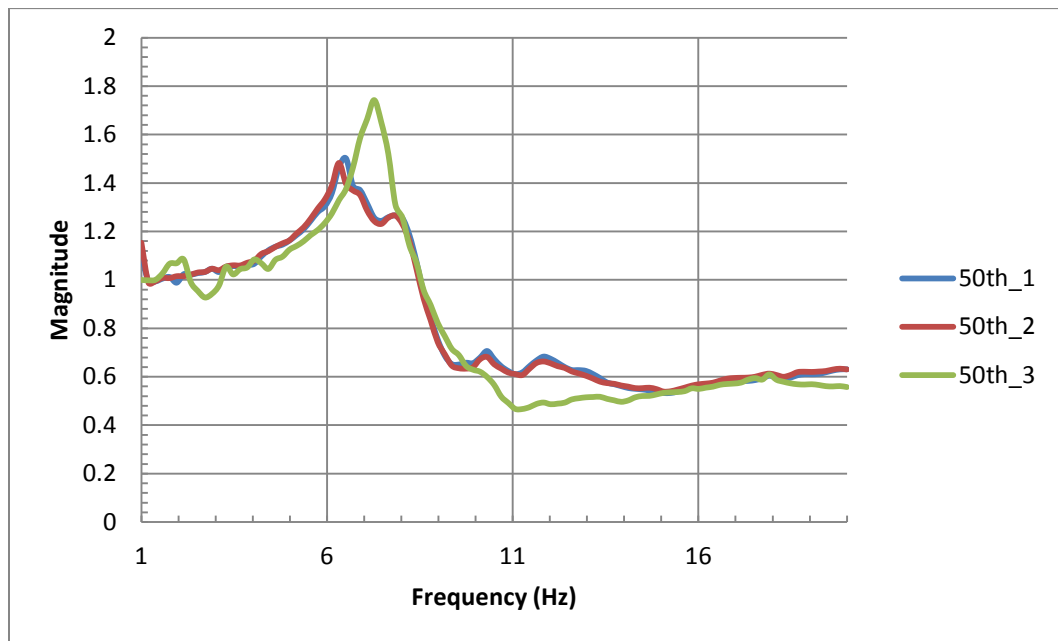


Figure 117: Frequency Response of MH-60S Seat in Baseline OEM Configuration for 50th Percentile Male with Seat at Middle Position

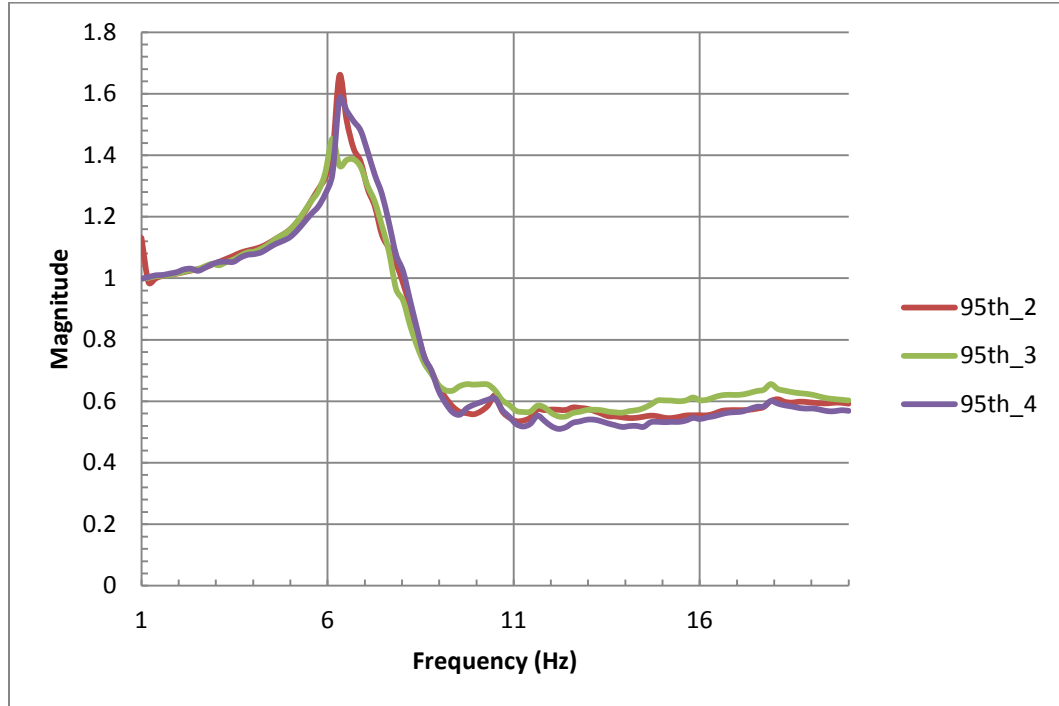
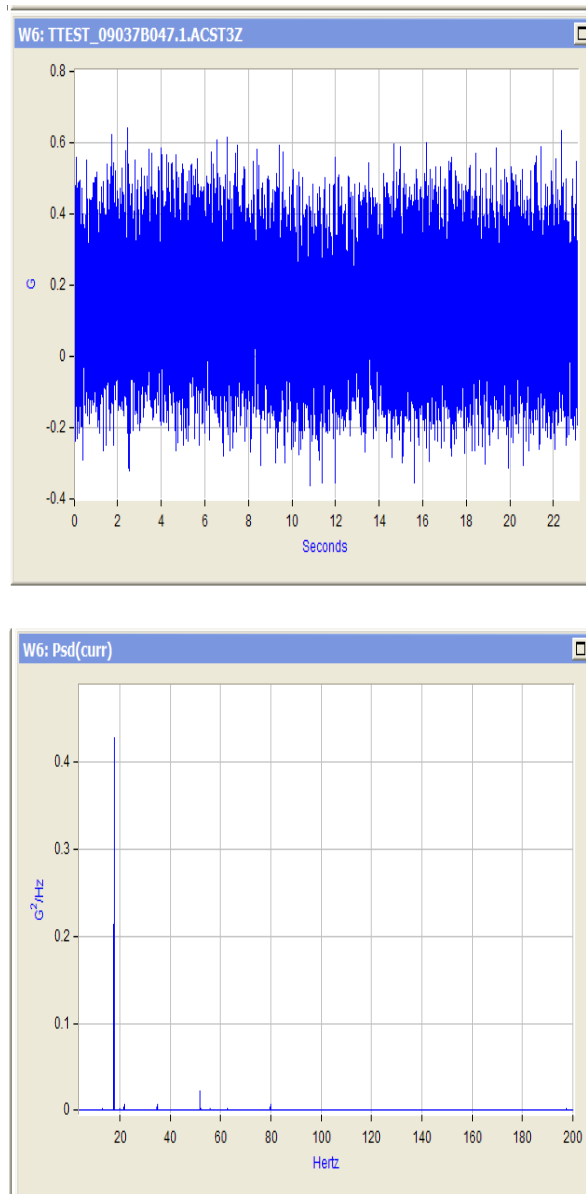


Figure 118: Frequency Response of MH-60S Seat in Baseline OEM Configuration for 95th Percentile Male with Seat at Lowest Position

The dSpace system was calibrated to output transient signals which match up with the appropriate plots described in Chapter 6. With the OEM MH-60S on the vibration test stand, the following wave forms were generated. The data gathered at the seat will be used for comparison with the performance of AVASS in further testing.



**Figure 119: Vertical Vibration Data at the Cockpit Floor from UH-60 for a 30 Degree Bank at 130
Kias Flight Condition**

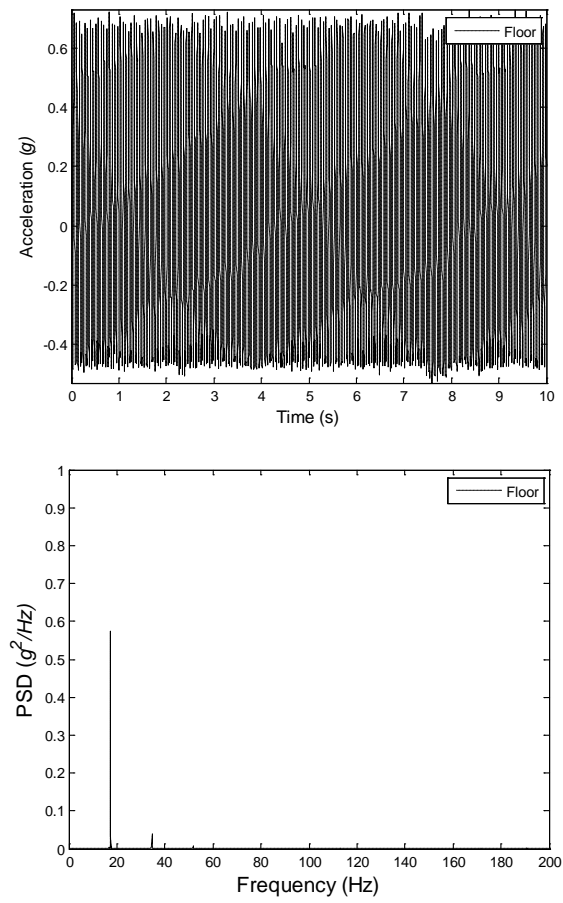


Figure 120: Reproducing the Representative Flight Vibrations in Shock and Vibration Test Stand

AVASS Preliminary Vibration Stand Testing Plan

The test plan for vibration testing the AVASS system mirrors the testing of the OEM SH-60S crew seat test plan finalized in January of 2012. The main objective is to create transmissibility plots at a set g level, 0.2 g , for a variety of occupant masses. The occupant masses for testing are 5th Female, 50th Male and 95th Male, each at predetermined seat heights matching testing on the OEM seat. The goal is to be able to standardize the tests and leave no doubts about the results when directly compared.

A list of possible issues moving forward was created to identify contingencies for possible future scenarios. The most likely performance reducing factor is friction. Friction in the damper was discussed previously, and is mostly due to the internal pressure in the fluid. Decreasing the accumulator pressure will have a direct effect of reducing friction caused by the u-cup seal. A way to quickly and accurately vary the pressure in the accumulator in between tests was devised. This will be a method of determining whether reducing the friction in the damper is enough to allow for good vibration mitigation. The second predictable source of friction is from the Guide Tube Bearings, shown in Figure 121. Although BAE calls these brackets bearings, they serve to restrict the motion of the seat in lateral directions more than to allow for a low friction vertical motion. There is a .03" radius clearance from the guide tube to the bearing surface. The cantilevered weight of the seat and occupant create a line force on one side of the guide tube leading to high friction forces. In an effort to potentially reduce the cost of the system, the project team hopes to test the system as-is. In the case of noticeable

reduction of expected performance, the project team acquired a variety of low friction tapes to be applied directly to the guide tube. The project team does not expect that low friction tape will be a final part of the retrofit design. The tape will only be used to demonstrate the effect of lowering friction from the Guide Tube Bearings. The final contingency, which will be a task for after preliminary testing, will be to design a better bearing surface for this specific application.



Figure 121: OEM Guide Tube Bearing Design

AVASS Preliminary Testing Results

The unfortunate reality is that the testing results do not match expected performance with vibration excitation of 0.2 g. Vibration mitigation performance at the 4/rev frequency is up to 30% better than the OEM seat, but not at the 90% vibration mitigation which is the goal of this program. The accumulation of friction between the two sources, the damper and seat bearings, is large enough to stop the seat from stroking as is required to reduce vibration transmissibility. The expected transmissibility is plotted in Figure 122.

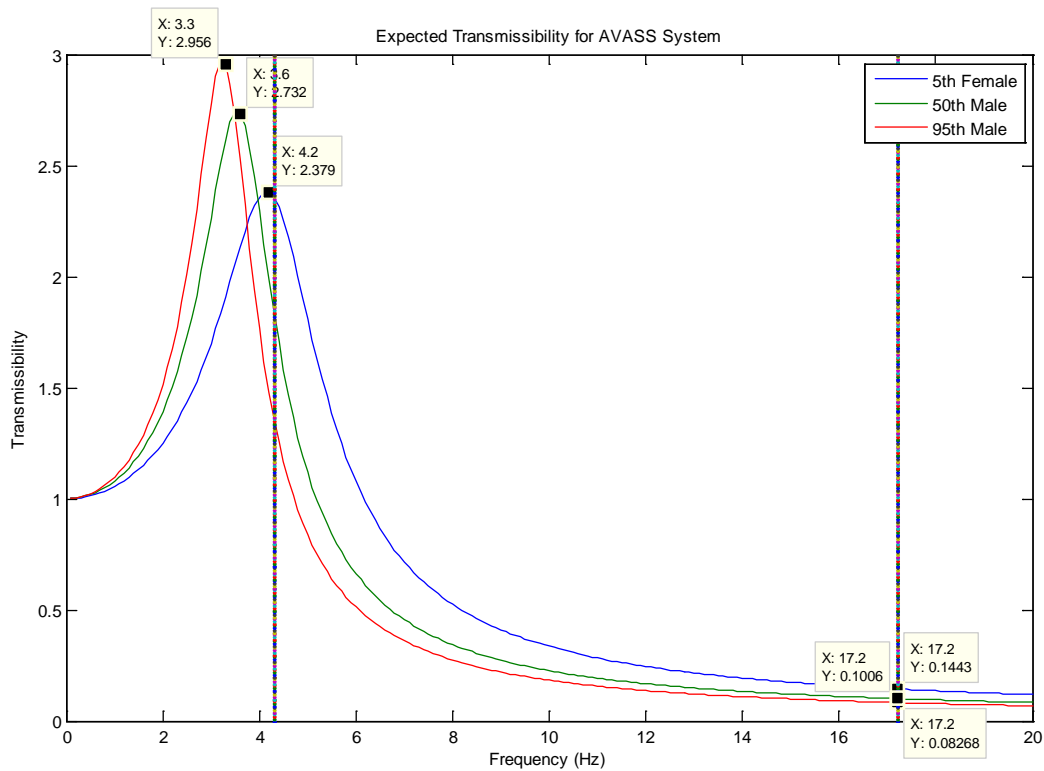


Figure 122: Expected Field-Off AVASS Performance

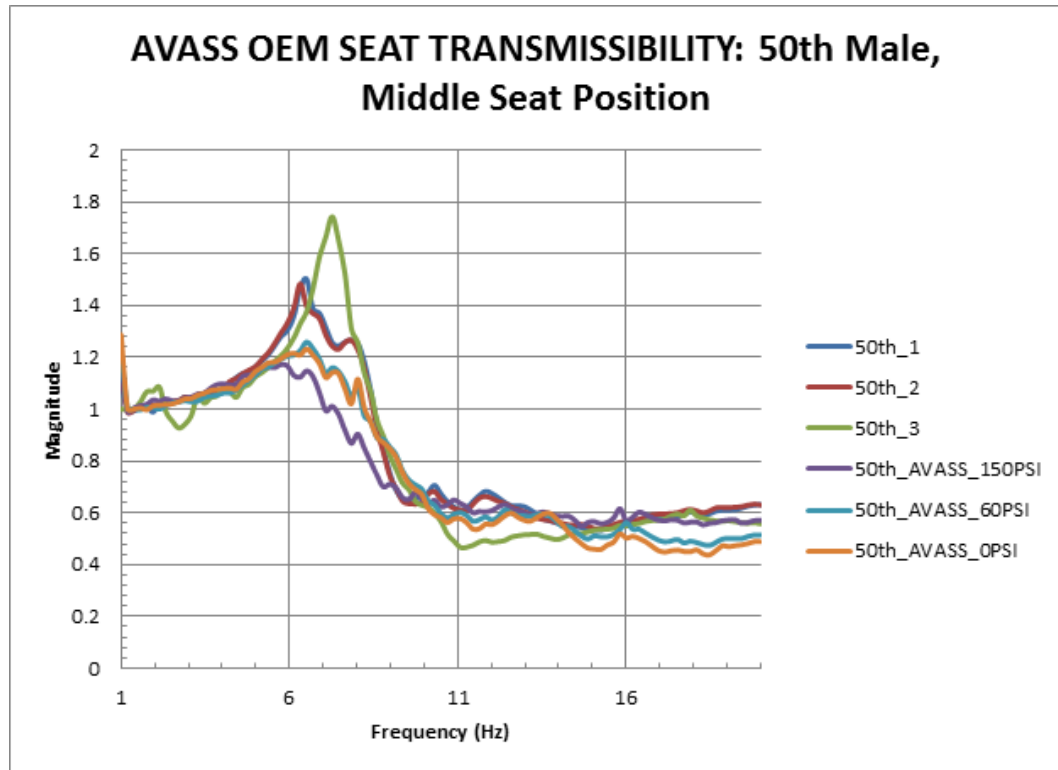


Figure 123: Initial Testing Results at 0.2 g

The initial results are plotted in Figure 123, overlaying OEM testing and AVASS testing at different accumulator pressure levels. The resonance seen in the plot is not the desired resonance from vertical motion; instead it is the rocking mode which the project team has proposed to mitigate. It is interesting to note that the pressure differences do exactly what the project team predicted would happen with higher friction. Increasing pressure decreases the transmissibility at frequencies near resonance and increases the transmissibility near the 4/rev frequency.

In an effort to demonstrate the possibilities when lowering friction, the contingency was to use low friction tapes directly between the Guide Tube and the Guide Tube Bearing. A variety of low friction tapes were used. Figure 124 shows photos of example applications.

Some tapes had good friction performance but low wear performance. Completing a complete frequency sweep with these tapes was found to be nearly impossible due to premature wear failure of the tape. In general, it was observed that the thicker the bearing tape, the better the wear resistance. Unfortunately, over time and at small vertical displacements as seen in higher frequency sine vibrations, the thick tapes would allow the bearing surface to indent itself into the tape. This virtually nullified movement at high frequencies and is an obvious jump in the transmissibility plots at high frequencies. A plot of all of the tests is seen in Figure 125.



Figure 124: Low Friction Tape Application

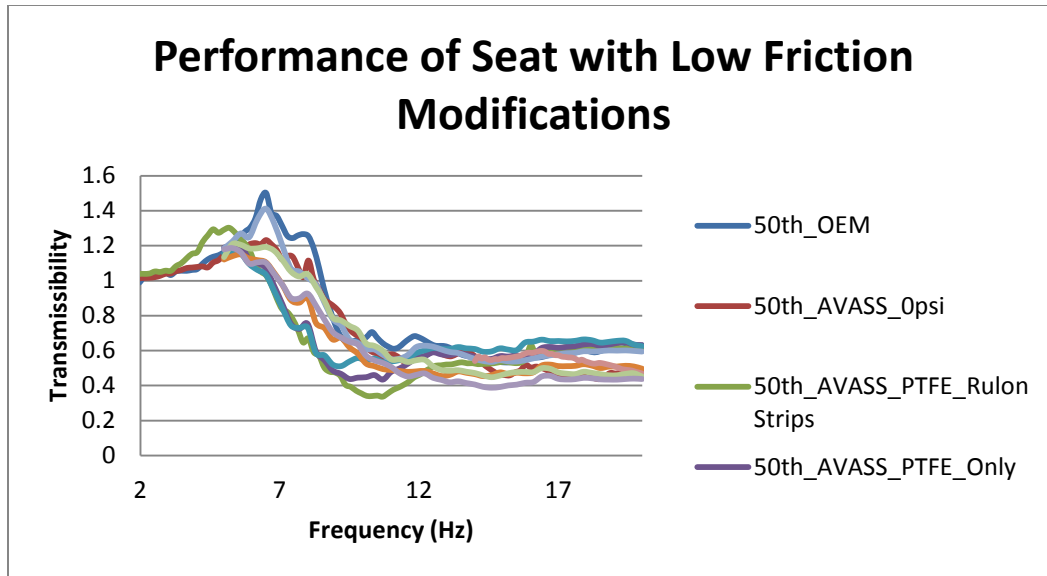


Figure 125: Low Friction Tape Modification Comparison

In order to continue testing and make the best use of the time on the test stand, a low friction tape with the best high frequency performance and wear was chosen. The tape chosen is a 1" wide UHMW (ultra-high molecular weight) tape with a thickness of 0.012". In order to further aid performance, white lithium grease was applied on top of the tape. This tape is shown in Figure 124, on the right hand side. The tape was applied along the length of the guide tube used in the range of seat height positions on both the top and bottom. On the top the tape is applied to the backside of the guide tube while for the bottom brackets the tape is applied to the front of the guide tube.

The test results below serve to further persuade the reader that, with further reduction of friction, the system will continue to improve. The system was tested with a controller using an algorithm developed for SAMSS system with gains calculated for MH-60S masses. Figure 126 demonstrates that an increase in peak force level to 0.3 g shows a

large reduction in the appearance of the rocking mode and is starting to look more like the expected transmissibility graph. The jump in transmissibility near 14 Hz is due to restricted motion from indentation into the tape. The project team hopes to see the graph continue downward with a different approach to friction reduction. Note that in all controlled instances the transmissibility is near one at resonance. 50 PSI seems to be a good pressure setting to reduce the rocking mode and allow controllability. The project team will optimize gain and filter settings for the control algorithm once performance has been maximized in the passive state.

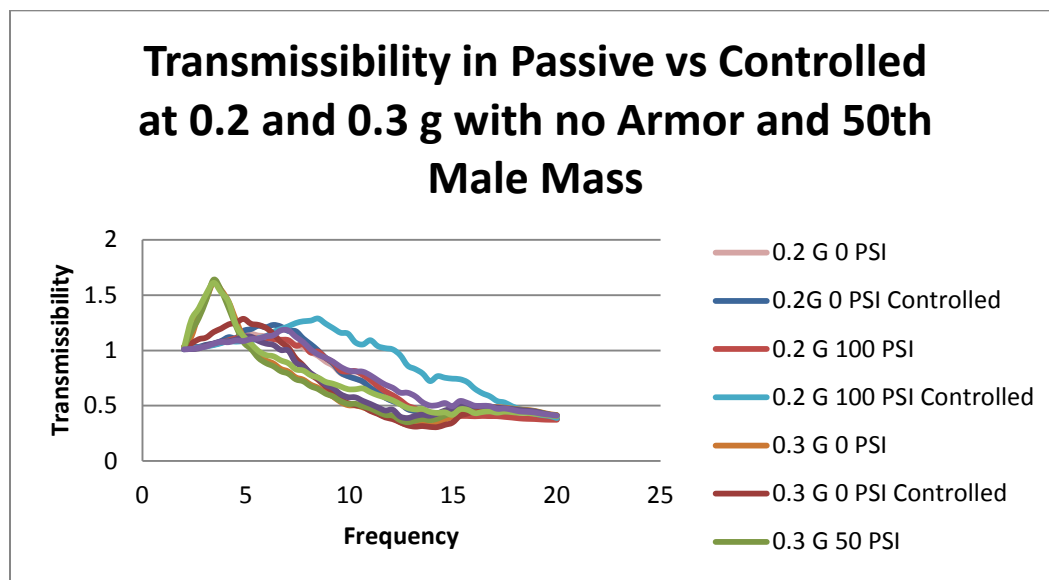


Figure 126: 50th Male Performance Comparison

Vibration Testing with Roller Bearings and Sand Bag Mass

As a necessity for continuing forward successfully, the first version of the roller bearing brackets, detailed in Chapter 5, was developed and applied for testing as a possible solution. The effect of reducing friction was immediately noticeable with the controller off, as the seat system started to stroke more at resonance than ever before. As the frequency rose, the transmissibility followed the expected single degree of freedom plot down closer to the 90% vibration attenuation goal. A plot of AVASS expected performance overlaid with the project team's results are shown in Figure 127.

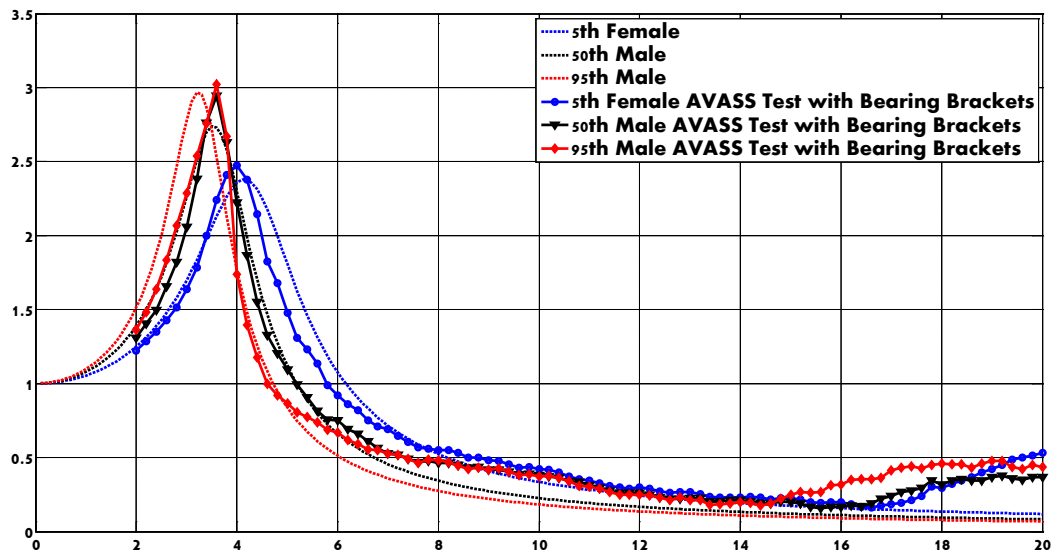


Figure 127: Transmissibility of System with Bearing Brackets versus Single Degree of Freedom

Theory

The plotted transmissibility for the system with the roller bearings started to deviate from the expected performance between 5 and 7 Hz. This deviation is still probably due to small amounts of friction in the system. The absolute lowest transmissibility seen in

testing reached below 0.1. The lowest transmissibility at 17.2 Hz is about 0.187, or 81.3% vibration attenuation, this is an increase of about 30-40% in vibration attenuation from the OEM seat system. Interestingly, there is a rise in transmissibility seen as the frequencies approach the 4/rev frequency which is stopping the performance from being even better. The project team intends to investigate this rise in transmissibility and propose a solution if necessary.

All masses should experience similar performance for vibration attenuation. As with the OEM system, the system dynamics change subtly with seat height and occupant mass variations. Each occupant mass is given a specific seat height for testing. The heaviest mass is at the full down position, the lightest mass is at the full up position and the 50th male is at the middle position. The difference between the plots is now quite small at high frequencies.

A visual inspection of all parts of the seat system during high frequency vibrations was conducted to attempt to determine the source of any possible dynamic resonances. Specifically, it was noted that the mass at the front edge of the seat cushion and the armor plate attachment to the guide post were vibrating at higher amplitudes than the seat bottom and maybe even the base. This observation is a good sign that these subsystems may be at, or near, a resonance frequency. In essence, it is possible that the energy input to the base is being multiplied through some sort of support with a spring like effect to these masses.

The system was tested with changes to the seat cushion and with and without the armor plate attachment to note changes in the dynamics. It was noted that removing the armor plate had very little effect on the system although it was noticeably vibrating on its mounts. On the other hand, changing the cushion had extreme effects on the system. The seat cushion is designed with an inflatable air bag at the front that is adjusted with an air release bag. Opening the valve locks in atmospheric pressure. Applying a load, such as leg mass resting on it, increases the pressure and creates an air spring. This spring rate is creating a resonance with the leg mass. Removing the air pressure as much as possible reduced the effect greatly. Removing the seat cushion completely is out of the question, but changing the material to something with a higher spring rate and more damping may be a good suggestion. It is possible that this load, and the related dynamic result, is greatly reduced in practice by the occupant's feet being firmly on the control pedals.

As a side note, there may be a way to lower the transmissibility for higher frequencies without affecting the stiffness of the seat system adversely. In SAMSS, a rubber sleeve was used over the pinned connection to the damper rod eye. This soft pin allowed for a softer spring rate at very low displacement vibrations and helped high frequency performance. It is proposed that the AVASS seat take advantage of this knowledge and apply this method to the pins at the clevis connection for the wires of the VLEA. Allowing the system to ride on a soft spring at this point could allow the system to stroke a bit more than it does right now at high frequency vibrations.

AVASS Tests of MR Controller Performance

The seat performance was tested with the controller on to verify that the MR force levels could bring the resonant peak down to the OEM values. The project team does not expect the system performance at low frequencies to be better than OEM values, but it should be able to match them. Each damper was monitored with a current sensor. Gain values were adjusted to make sure that the current through the damper coils was at a reasonable level. Values were tested on either side of a median value to test its effect. A graph of transmissibility with the gains tested on the control system is shown in Figure 128. The final chosen gain value was 1300. This value matched the low frequency vibration transmissibility of the OEM system and showed very little reduction in performance at high frequency performance from the passive case. Later, with a more anthropomorphically correct test mass and this same gain value, the system would see results which deviated less between controlled and uncontrolled cases.

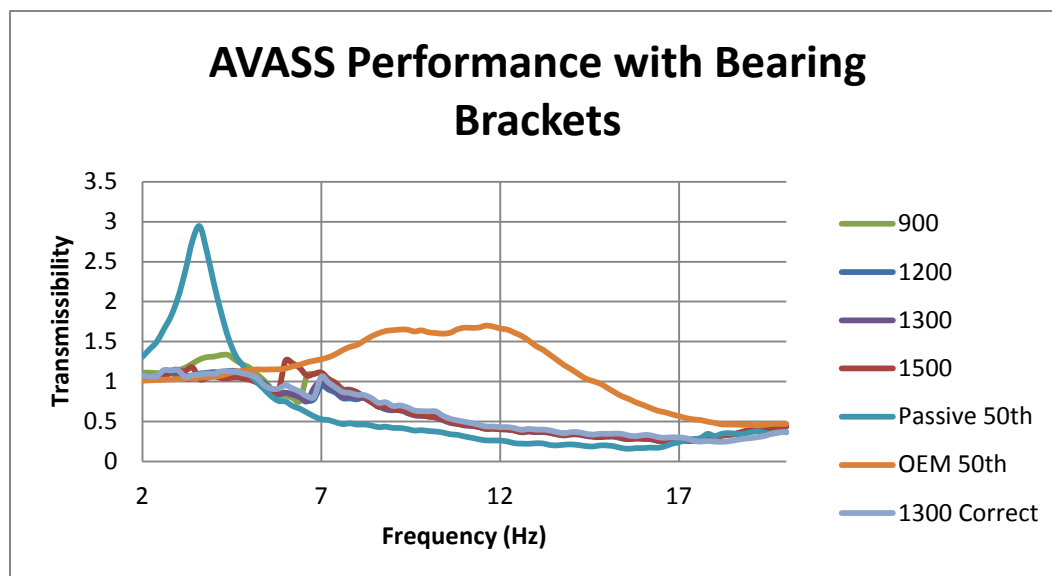


Figure 128: AVASS Control Gain Testing Results

It was found through testing that the positioning of masses can have a large effect on the derived transmissibility of the system. Initially, there was an idea that the sand bag mass C.G. was too far forward compared to a human body. At this point the seat back cushion was removed to test for any significant effects. The OEM seat looked to have less rocking and the high frequency jumps in transmissibility were less noticeable. Next, the idea that the mass at the airbag portion of the seat cushion was bouncing independently and creating a change at high frequencies was tested. The sandbags which were normally placed on the edge of the seat, where the thighs would rest, were placed on top of the larger sandbags. This concentrated the mass closer to the pin holding the load at the VLEA. This had two effects. The high frequency resonance performance seemed to be without any bumps at all mass levels, but the transmissibility was higher. Also, the rocking mode was observed to be worse even though it is not visible in the sine sweep data. The only positive result of this test was that the 50th male showed transmissibility still reducing after the 4/rev mark. This could be a sign that the rising transmissibility is indeed a dynamic issue and not a friction issue. This result also meant that our hypothesis that the rise in transmissibility was caused by the mass at the end of the seat cushion was probably correct. The question to answer is, “can we actually state that the system is being made to perform better with these results?” To get closer to the answer without moving into human testing, test ballast which could more closely resemble a human body mass distribution was required. The BART anthropometrically correct test ballast discussed in chapter 6 was thus acquired.

Figure 129 is a plot of the results from testing the AVASS system with V2.0 Dampers and V1.0 bearing brackets using the BART test mass. The system was tested only at the 50th male to identify changes in seat performance while using a different mass distribution. The project team observed small changes in the dynamics of the system. The transmissibility plot now reaches a new low, although at a different frequency. The plot also starts to rise faster and more consistently than in previous testing. Overall, the project team is positive that these test results are more representative of the final product under human use. Moving forward, the project team will continue to test with the BART system.

The system was also tested to identify if there was any advantage to reducing damping forces to increase high frequency performance. Two sets of identical V2.0 dampers were tested. One set was filled with MRF-132, as has been intended for use with AVASS, the other was filled with MRF-126 which was used for SAMSS. The method of fastening the damper to the guide tube was changed from a riveted system to a threaded system, allowing for a quick change of dampers between testing periods. As expected, there is a reduction in transmissibility across the entire transmissibility plot after 6 Hz. It was also shown that the system is controllable using the MRF-126 fluid. This performance may lead to a discussion about whether MRF-126 fluid may be more suitable. The trade-off is that MRF-126 is known to have particle settling issues.

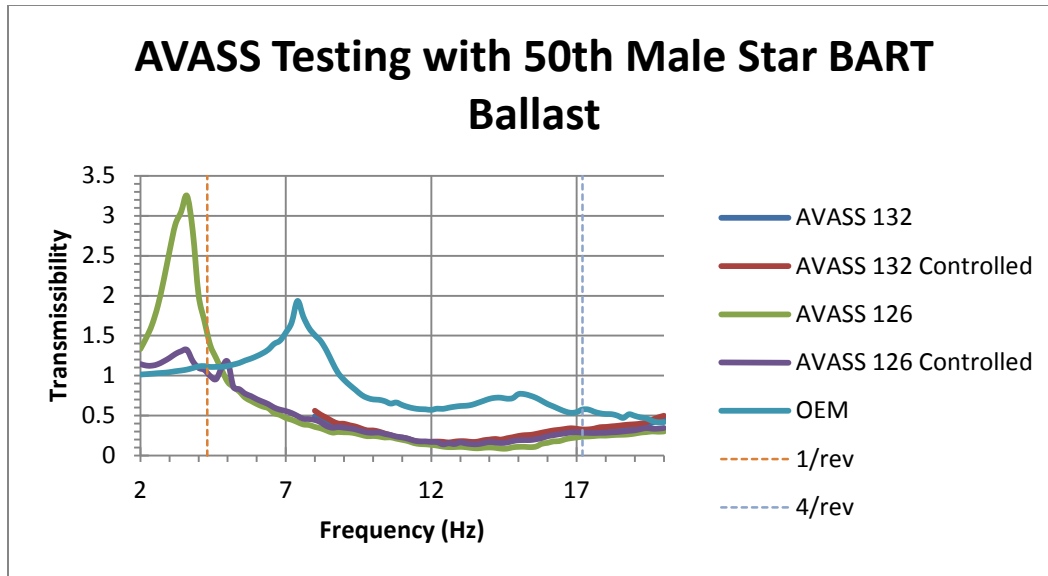


Figure 129: AVASS Sine Sweep using 50th male Star BART Ballast

The controlled system with Star BART was also tested with transient vibration signatures to try to recreate the vibrations seen on the helicopter. The project team recreated the tests performed on the OEM seat at the beginning of the chapter. The exact same vibration signature was used to test the AVASS system. Figure 130 through Figure 135 show plotted results from this testing. It is evident that the AVASS configuration is better than OEM. More analysis is being conducted to make a final decision between using the MRF-126 or MRF132 fluid. On first look, the MRF-132 fluid performs slightly better. This is leading the team to stick with using MRF-132 to avoid settling issues.

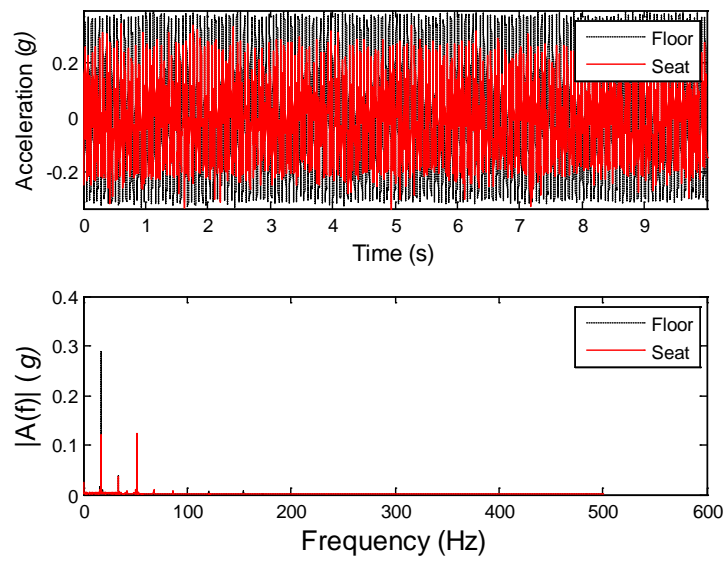


Figure 130: OEM Transient Testing

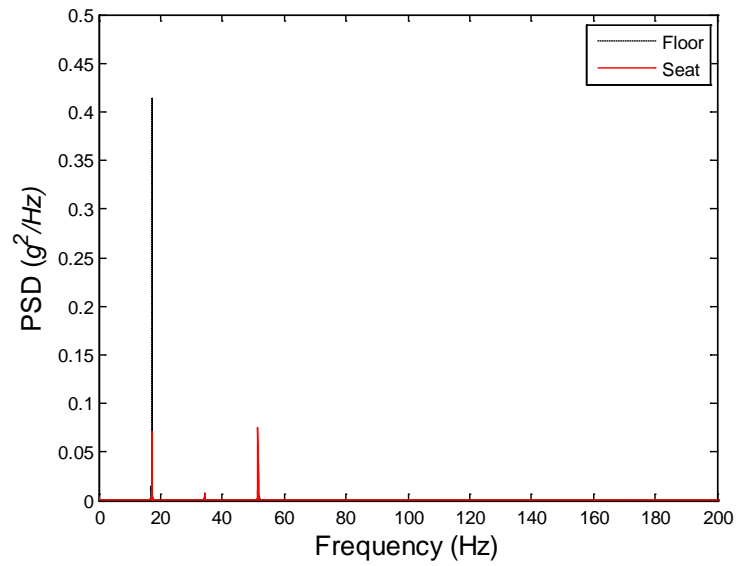


Figure 131: OEM Transient Testing PSD

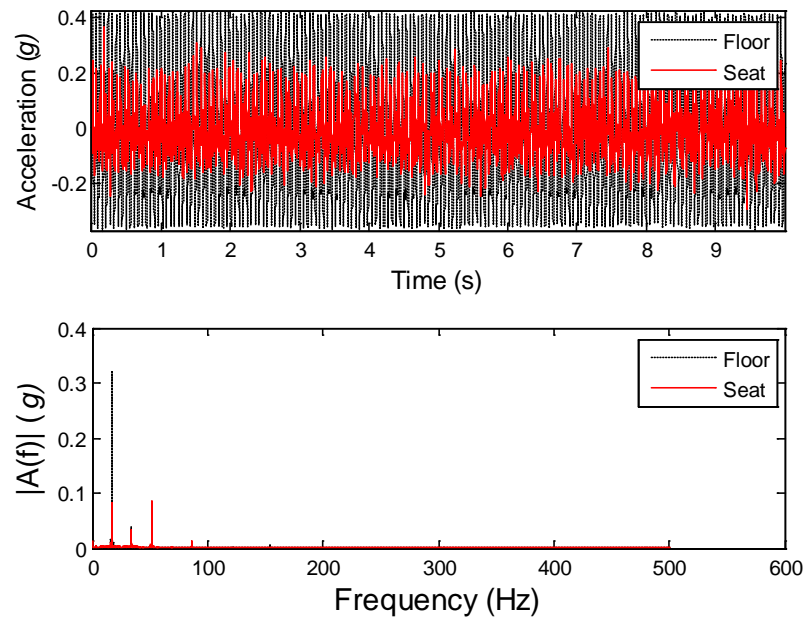


Figure 132: AVASS with MRF-132 Transient Testing

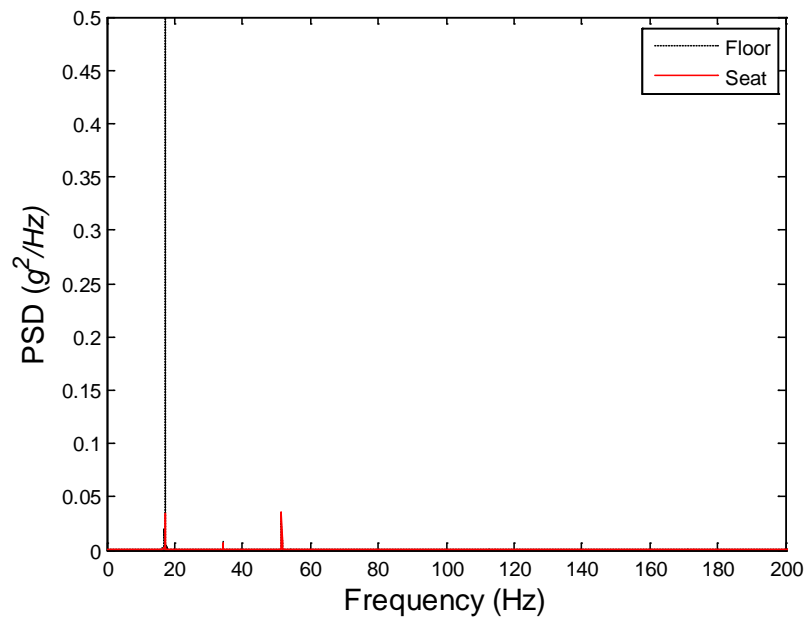


Figure 133: AVASS with MRF-132 Transient Testing PSD

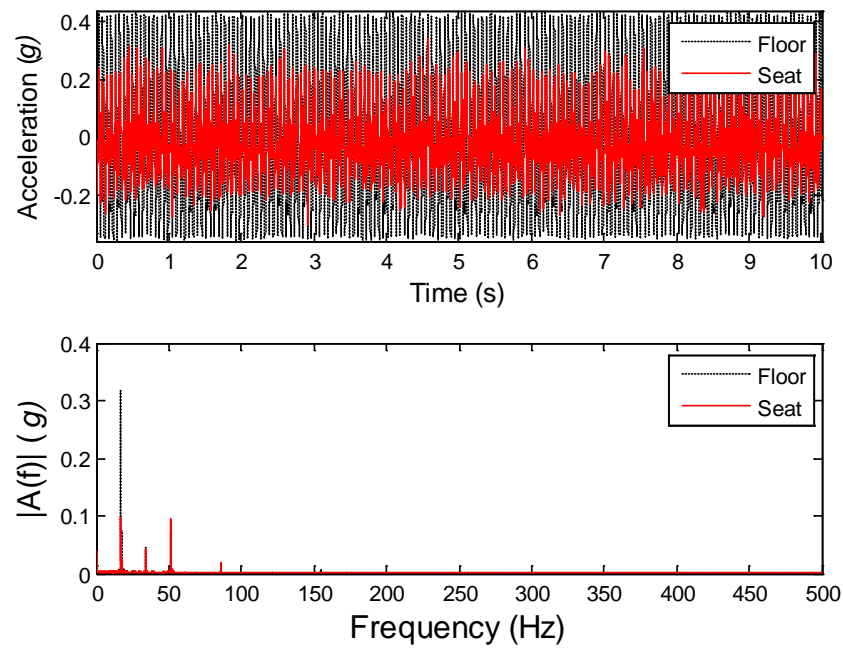


Figure 134: AVASS with MRF-126 Transient Testing

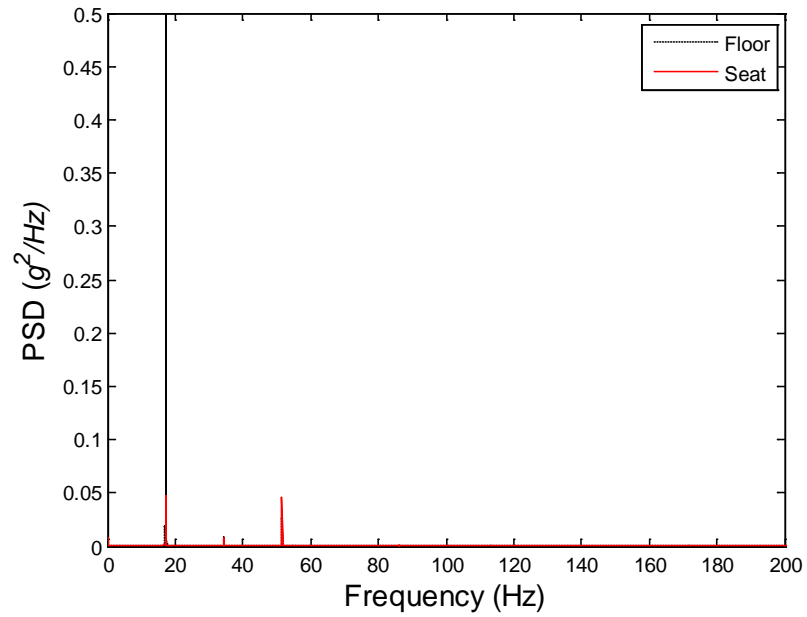


Figure 135: AVASS with MRF-126 Transient Testing PSD

Final AVASS Modifications

In December of 2012, with only a small amount of time before the end of the period of performance and the need for final AVASS characterization, final performance increasing modifications were proposed. At this time the latest MR controller electronics were still unavailable for AVASS testing. While the team was not able to test AVASS fully working during this testing session, it took advantage of the time on the vibration stand.

SAMSS had recently entered flight testing, bringing questions about measurement of transmissibility using the electronics enclosure position as opposed to the seat pan. Transmissibility measurements were taken at various places on the seat bucket for comparison. Comments from SAMSS and experience from AVASS testing showed that cushion dynamics can make a large difference on the transmission of vibration to the occupant. Transmissibility plots have been created using seat cushion accelerometers between the BART ballast and different cushions to study this effect. Finally, the project team took this time to test a theory about high frequency vibration reduction by applying freedom of motion to the clevis pin. A quick brief about each of these studies is discussed below including plots when needed.

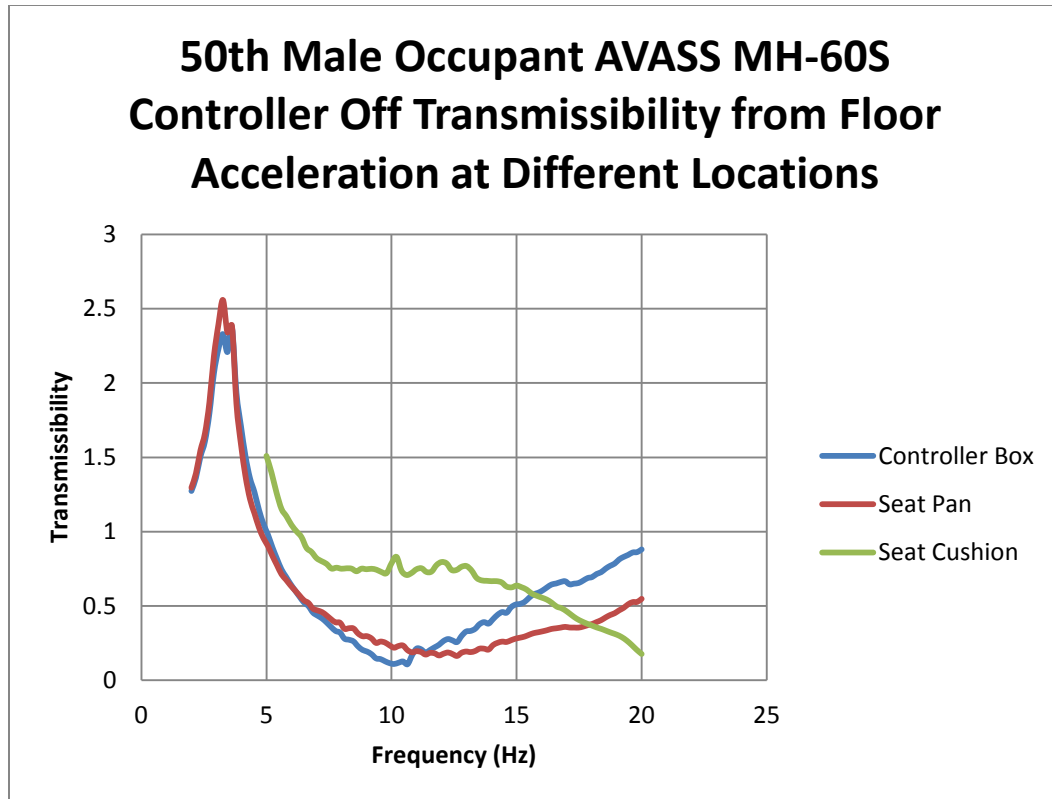


Figure 136: AVASS SH-60S Transmissibility from Floor Acceleration at Different Locations

Figure 136 is a comparison of the transmissibility of floor vibrations to different points on the seat bucket. The three positions that were studied were at the controller box, on the back of the seat bucket halfway up the backrest, at the bottom most point of the seat pan, directly underneath the occupant but attached to the composite seat bucket, and directly between the occupant and the seat cushion. Figure 137 details these positions further. The first point of interest is that the seat pan shows a different transmissibility than the controller box. This is the same as what was found during SAMSS testing. The effect is caused by the added degree of freedom of the seat pan flexing due to the weight of the occupant. Next, we see that the seat cushion transmissibility appears to be worse than the seat pan along most of the spectrum in question.

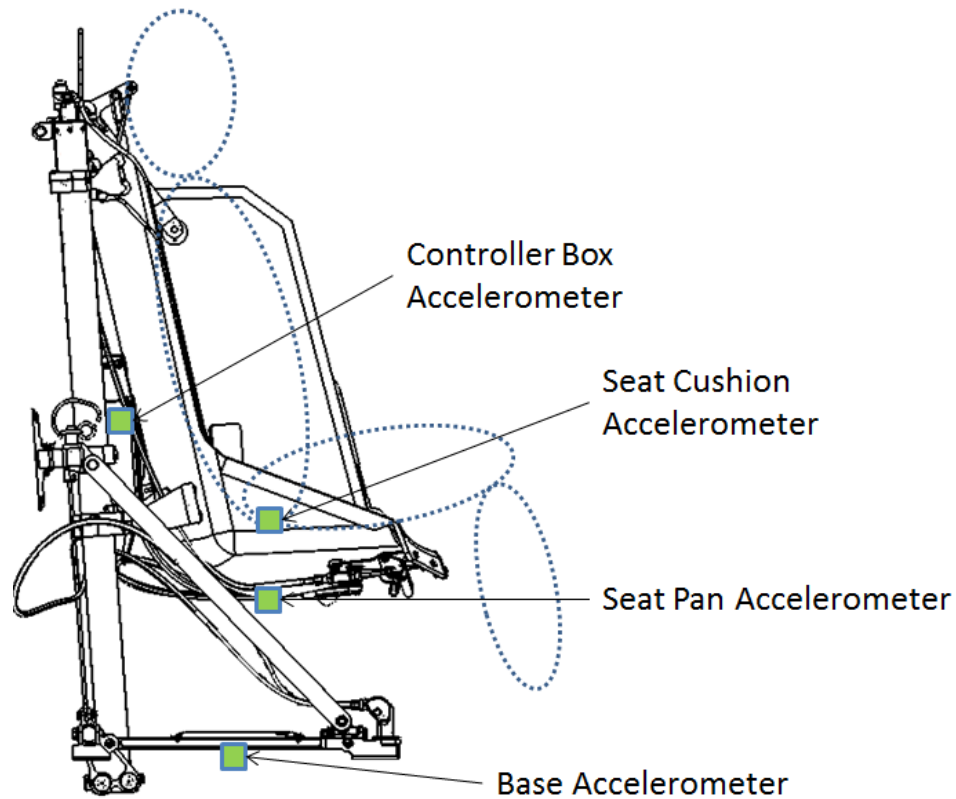


Figure 137: Accelerometer Positions

The effect of the seat cushion can be seen more directly by dividing the seat cushion transmissibility by the seat pan transmissibility. This can be explained mathematically. If the floor is position 1, the seat pan is position 2 and the seat cushion is position 3, the transmissibility of the floor to the seat pan is equivalent to $2/1$ and the transmissibility of the floor to the seat cushion is $3/1$. $3/1$ divided by $2/1$ becomes $3/2$, which is the transmissibility from the seat pan to the seat cushion. A single degree of freedom graph is expected, as the foam has visco-elastomeric properties which could be mimicked as a spring and damper system. Figure 138 shows the results of this test. A resonant peak can be identified right in the middle of the graph. The test was started at 5 Hz to avoid resonance, but it is expected that the results probably would still be higher than 1 at 4.3

Hz, our 1/rev frequency. At the 2/rev, 8.6 Hz there is a factor of 2 multiplying the vibration levels and 3/rev is the closest to the peak at a transmissibility of 4 to 1. These numbers do not bode well for the occupant if the aircraft were to generate even a little noise in this frequency range. Fortunately for the occupant, by the time we are close to the 4/rev the transmissibility is about to cross past 1 and filters vibration quite well after 20 Hz. The point at which the transmissibility of this graph passes 1 is also the point at which the seat cushion and the seat pan intersect in Figure 23. This is important because up to this point the cushion was actually hurting AVASS performance. What AVASS does do well is mitigate a lot of the vibration from the ground to the seat pan, which in turn means that the vibrations to the occupant are reduced. In the final analysis section we will look at this effect again and compare it to the OEM seat performance.

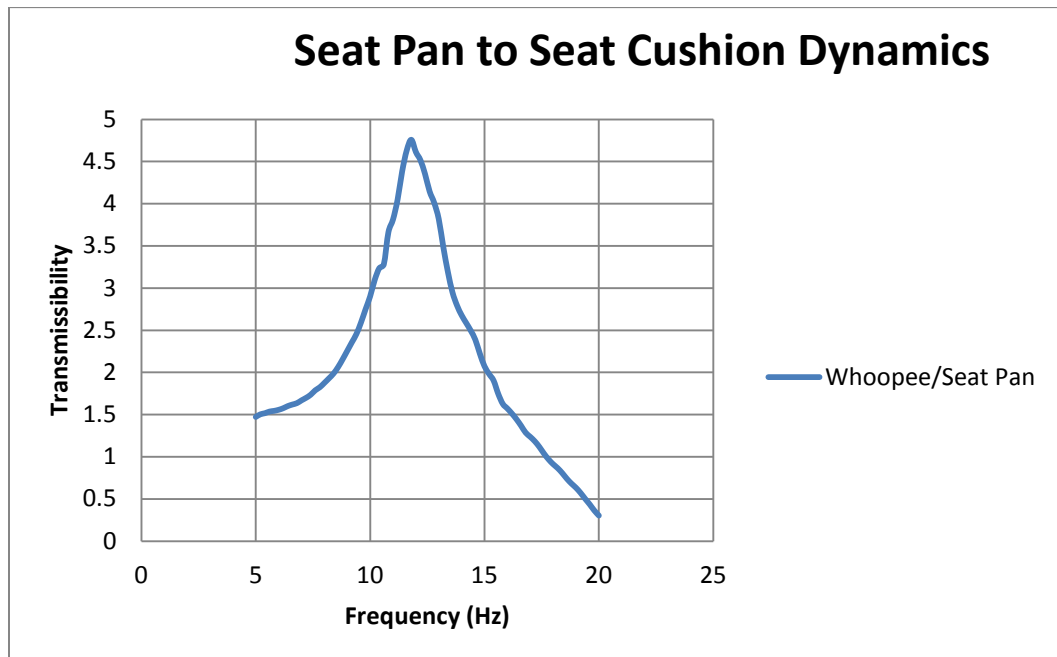


Figure 138: Seat Pan to Seat Cushion Transmissibility

In an effort to test the effect to the occupant of changing the cushion characteristics, alternate seat bottom cushions were applied during testing. The project team had access to an MH-60R (SAMSS) seat cushion and a cushion made from a solid piece of green memory foam. The seat was also tested with no cushion to test the accelerometer and to check to see if this was closer to approaching the single degree of freedom theory plot. Sitting on the seat with the cushion options, little difference could be felt in comfort levels between the AVASS and SAMSS seat cushions and the foam cushion seemed stiff but conforming. Having no cushion was uncomfortable for obvious reasons.

Testing results show that the AVASS cushion has a much higher resonance at a higher frequency than the SAMSS cushion. This leads to higher vibration levels at the seat cushion for the occupant. There is an adjustable air pouch in the seat bottom cushion of the MH-60R (AVASS) cushion which was left deflated. It was found that when the air pouch is inflated, it creates an air spring and a far worse resonance for the leg mass. The foam cushion seems to be almost as stiff as the no cushion case and gives better performance still than both SAMSS and AVASS at the seat pan and at the seat cushion. The no cushion case shows a sharp turn up at 19 Hz which could be an indication of a friction limit in the system. The foam cushion does not seem to suffer from this within the tested range. It is possible that the AVASS or SAMSS cushions may have better attenuation of high frequency ranges, but studies on the effects of whole body vibration weight the frequencies between 2 to 20 Hz as the most important. Unfortunately for the project team, the AVASS cushion ended up being the worst test case of the group. As the discussion of trying to design a better seat cushion has been rejected before, the project

team must move forward into qualification testing with the current MH-60S OEM Seat Cushion. The following plots show the effects of these changes.

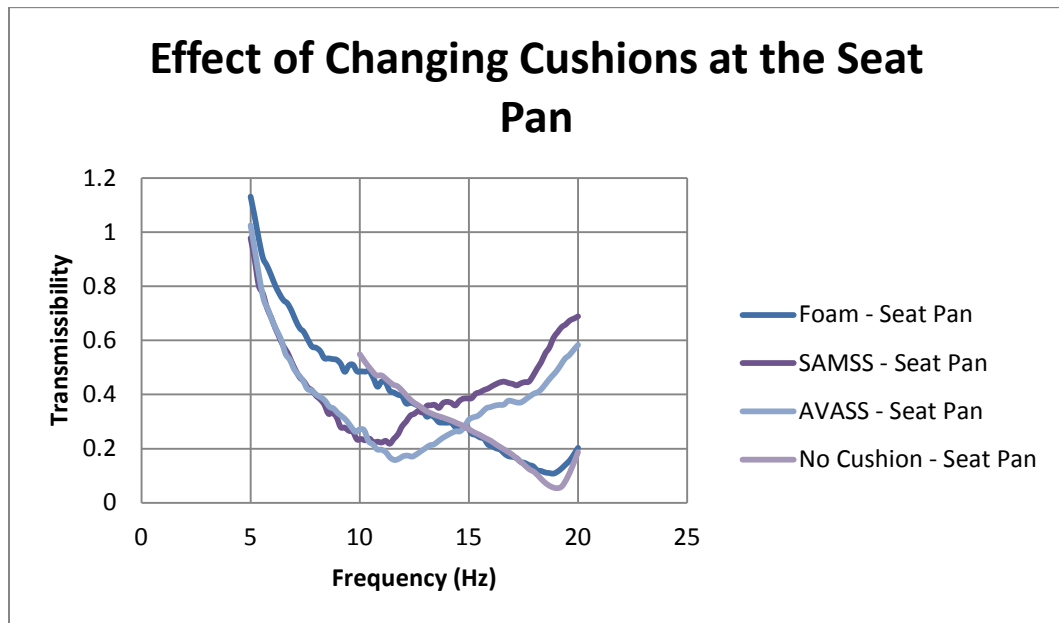


Figure 139: Effect of Changing Cushions at the Seat Pan

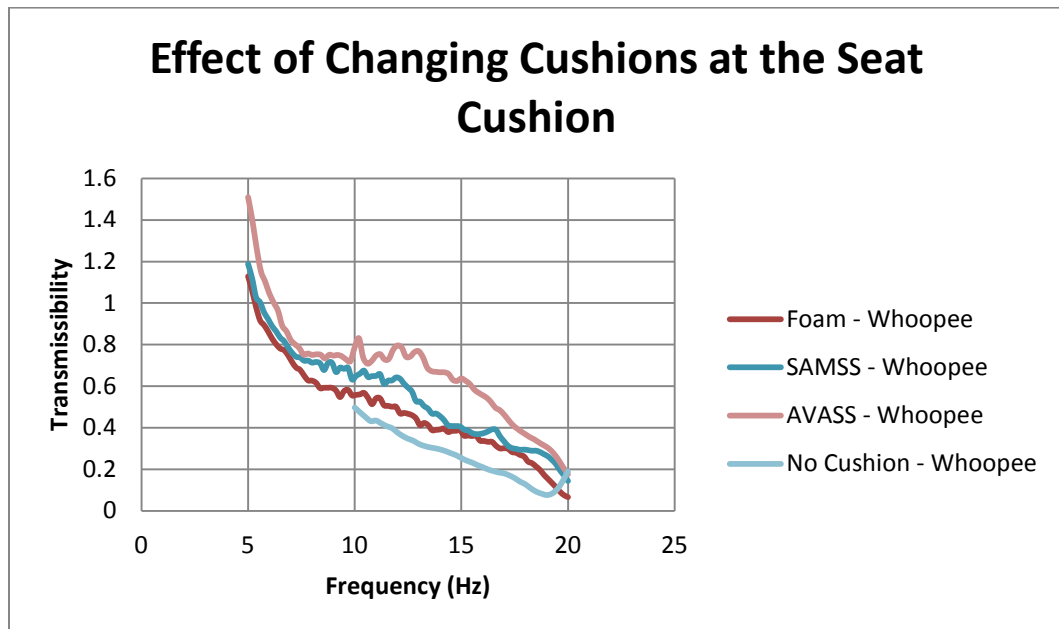


Figure 140: Effect of Changing Cushions at the Seat Cushion

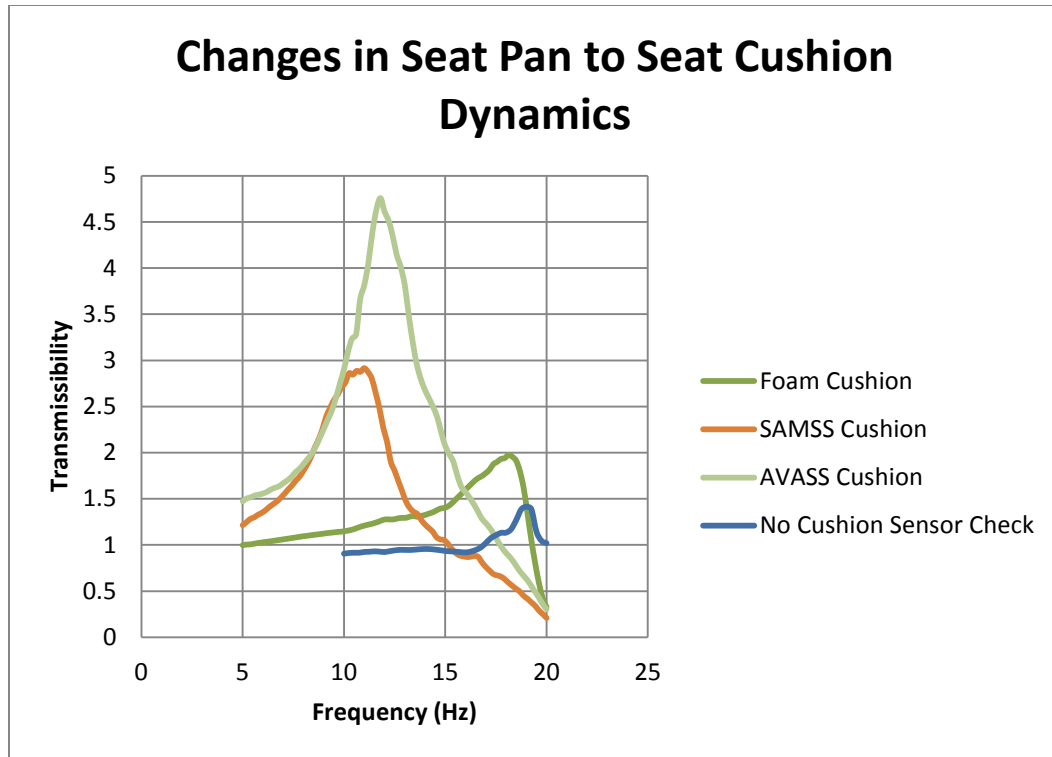


Figure 141: Cushion Dynamics for Tested Seat Cushion Options

The seat cushion is a second degree of freedom in a system which was originally designed by simplifying the system to a single degree of freedom. The expected transmissibility graphs for AVASS were generated using an optimal single degree of freedom equation. Adding the second degree of freedom is like changing the apparent mass of the occupant. The static weight of the occupant is multiplied by the transmissibility to get our new apparent mass. If we take the no cushion performance as a check of the performance of the system, we can compare this to the expected and see the effects of friction on the system. Increased mass to the system should lower the natural frequency, raise the resonant peak amplitude and reduce the transmissibility at the same frequency after the resonant peak. The opposite is true for reducing mass. This is the reason why the lowest transmissibility measured at the seat pan in Figure 140 is seen at

the peak value for all the resonances in Figure 141. The foam cushion seems to be the best case scenario because the peak reduction is almost exactly at the 4/rev. Also, the transmissibility of higher frequencies seems to drop straight down to match the performance of the SAMSS and AVASS cushions. To reiterate, this study was conducted to start the discussion, but no change in seat cushion is planned for the AVASS program. All qualification tests will be performed with OEM MH-60S cushions.

The last experiments which were planned for this test period had the goal of adding a very small amount of spring and degree of freedom to the clevis in an effort to mitigate more high frequency vibration transmission. The seat bucket is suspended from two clevises using the VLEA wires. The AVASS spring and dampers apply forces to the crossbar to which these clevises are attached. There is a possibility, then, of adding a small degree of freedom to the seat bucket, but allowing the system to move free of the dampers inside the clevis area. High frequency vibrations can be filtered out extremely well with just a spring and a freedom of motion.

The SAMSS system takes advantage of this knowledge by using a piece of tubing over an undersized shoulder screw which connects the end of the damper rod to the crossbar through a spherical bearing in a rod end. The fact that the shoulder screw diameter is smaller than the inner diameter of the spherical bearing creates the same freedom of motion which we are hoping to attempt in AVASS. The tubing was initially added to remove metal to metal contact, but it also adds a spring stiffness which helps reduce vibrations.

The first idea was to change the length of the screw used to attach the AVASS clevis to the crossbar. The original design called for a screw which was long enough to secure the VLEA wire vertically. Reducing the length of this screw would allow the seat bucket to stroke vertically. A photo of both configurations can be seen in Figure 142. This didn't seem to change performance too drastically, as can be seen in Figure 143. There is a slight performance gain during the resonance period for the seat cushion, but this is barely registered at the seat cushion. The difference is minimal at the 4/rev.



Figure 142: Photo of Clevis Screw Change

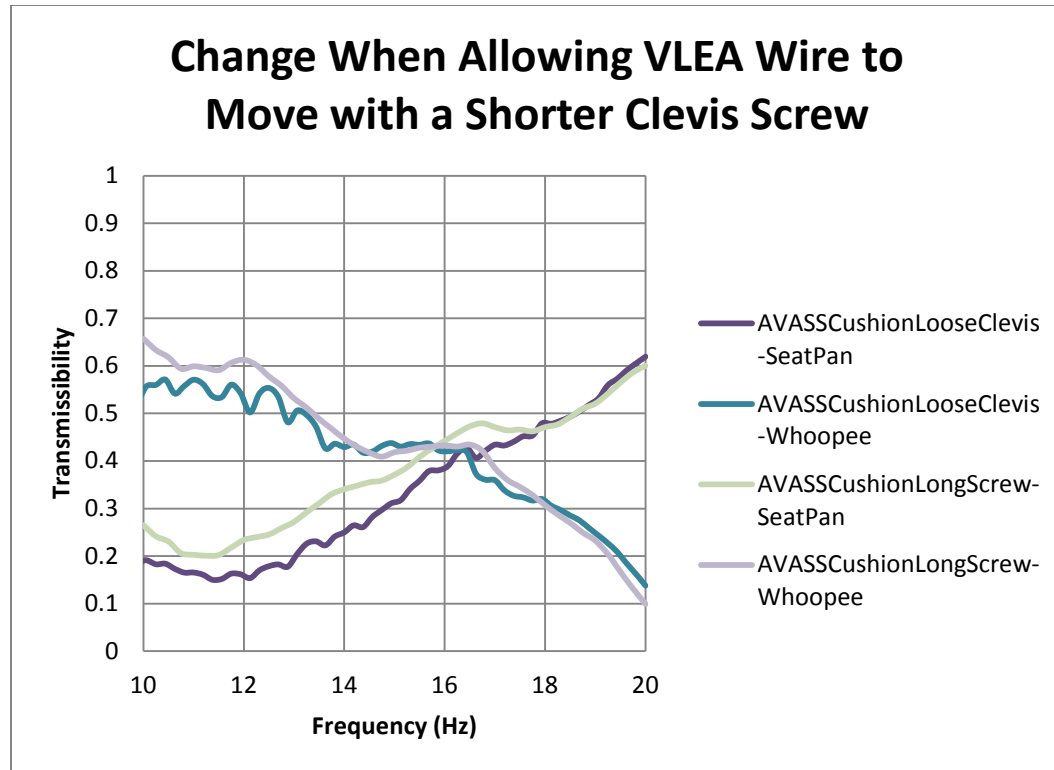


Figure 143: Clevis Screw Length Change Effect

An alternate clevis solution had been prepared for testing. The results above may have been expected because there is some friction between the clevis pin and the wire which is bent around it. For further testing, the project team modified a clevis designed for a 3/8" pin to be used with a 1/4" pin to work with the VLEA wire. This allowed for a freedom of motion as well as the possibility of applying some different tubing options. The team also acquired various types of tubing which would fit over a 1/4" pin and also had an O.D. of less than or close to 3/8". These tubing parts are not characterized but are available on McMaster using these part #'s:

- 1 [5234K981](#) 1 Ft.Super Soft Latex Rubber Tubing, 1/4" Id, 5/16" Od, 1/32" Wall, Semi-clear Amber
- 2 [5119K33](#) 1 Ft.High-temp Viton(r) Fluoroelastomer Tubing, Soft, 1/4" Id, 5/16" Od, 1/32" Wall, Black
- 3 [5119K854](#) 1 Ft.High-temp Viton(r) Fluoroelastomer Tubing, Firm, 1/4" Id, 5/16" Od, 1/32" Wall, Green



Figure 144: Large Clearance Clevis and Samples of Tubing from Testing

The results below show a significant increase in vibration reduction to the seat pan using this freedom of motion method. The difference throughout the spectrum can be seen in Figure 145 and zoomed in to the 4/rev range in Figure 146. This change improved high frequency results, while not changing the low frequency transmissibility. Unfortunately, the gains are lost through the seat cushion. The corresponding graphs of transmissibility at the Seat Cushion are found in Figure 147 and Figure 148. The advantage is negligible in this configuration.

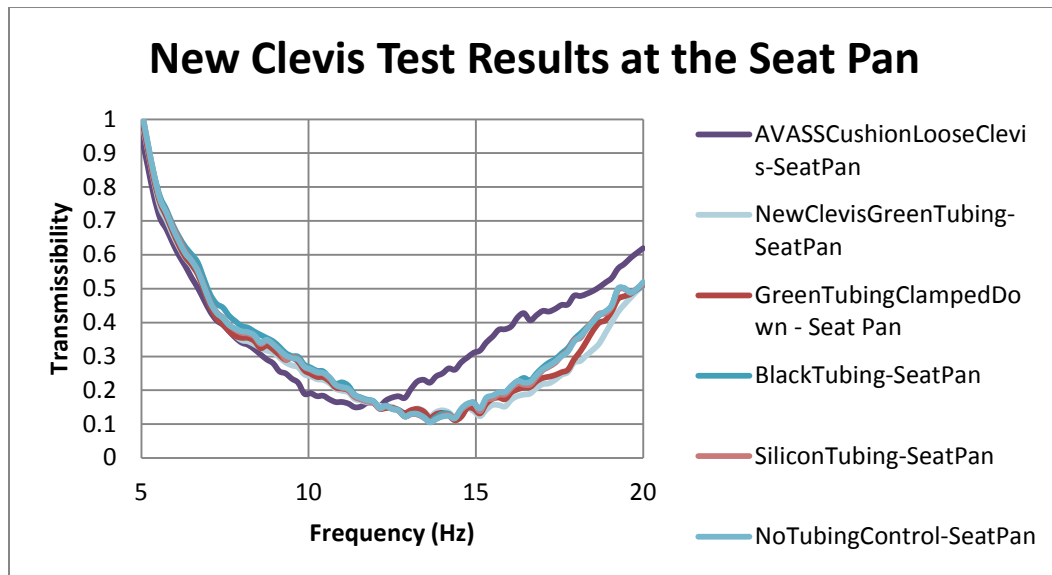


Figure 145: New Clevis with Freedom of Motion Results at the Seat Pan from 5 to 20 Hz

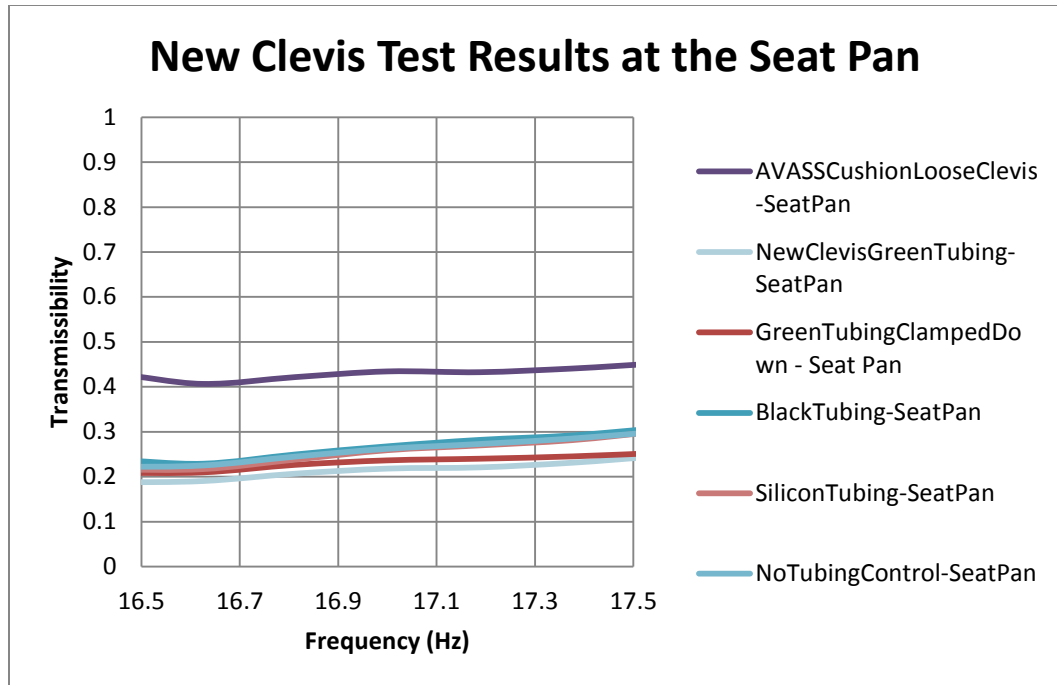


Figure 146: New Clevis with Freedom of Motion Results at the Seat Pan from 16.5 to 17.5 Hz

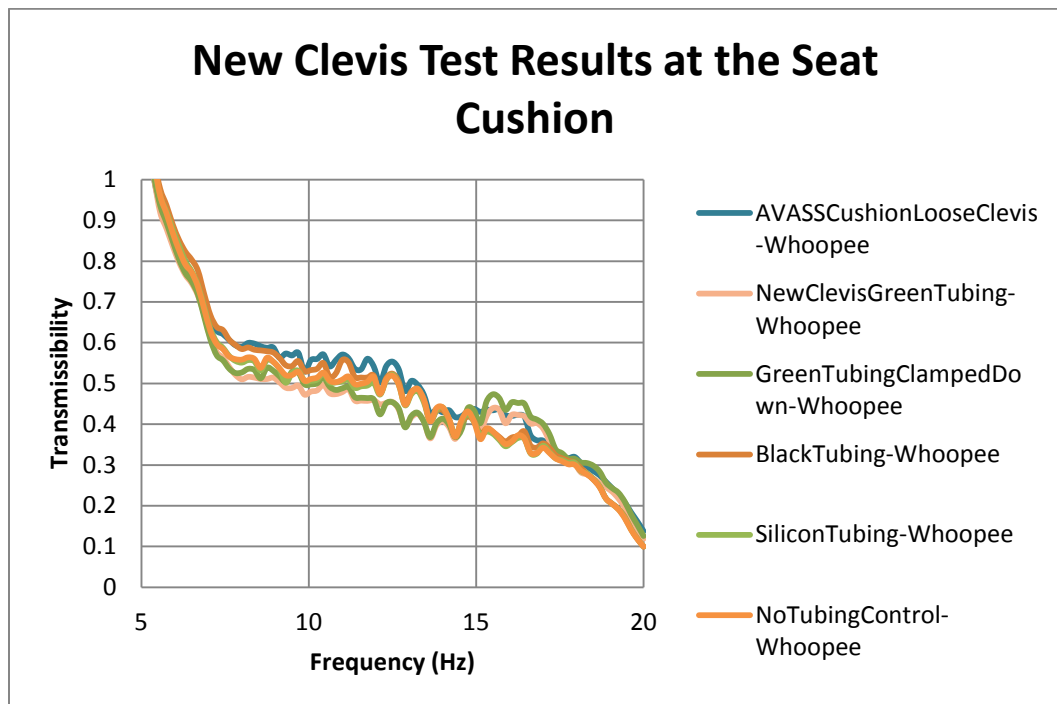


Figure 147: New Clevis with Freedom of Motion Results at the Seat Cushion from 5 to 20 Hz

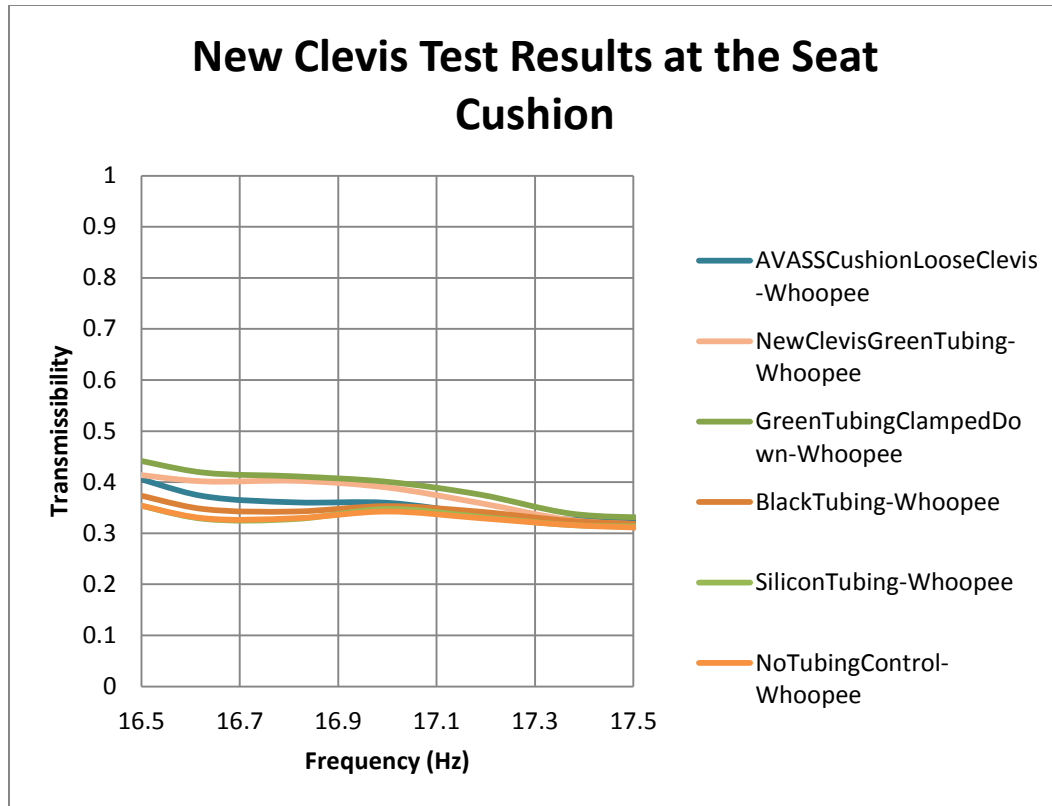


Figure 148: New Clevis with Freedom of Motion Results at the Seat Cushion from 16.5 to 17.5 Hz

It was decided to continue into qualification testing using the original AVASS clevis with the shorter screw. The first reason is that the difference in performance at the seat cushion is not so great to merit changing the clevis at this point. The second reason is that assembly and manufacturing of this first clevis is easier than the new clevis. The original clevis comes with the correct pin and requires a very small modification. The new clevis requires an additional pin and heavy modifications to work with the 1/4" mounting screw. The project team hopes that this possibility for added performance will help in future iterations of MR seat suspension projects.

PAGE LEFT INTENTIONALLY BLANK

CHAPTER 8: FINAL TESTING RESULTS AND CONCLUSIONS

Final Configuration for Testing

After a year and a half of development, the final configuration will consist of v2.0 AVASS Dampers, v2.0 Roller Bearings and a v4.0 MR Controller.



Figure 149: Final Configuration of MH-60S with AVASS

As a reminder, from top to bottom, the AVASS modifications to the OEM MH-60S Helicopter Crew Seat are as follows. The clevises will be replaced in order to lower the seat height 0.5" to offset the effect of the suspension at mid stroke. The riveted aluminum inserts will be removed and replaced by AVASS dampers. The dampers will be fastened through the rivet holes in the guide tube using flat head screws. The 5/16" screw holes at

each end of the crossbar will be opened to 0.38". A machined washer used to fill in the countersink will be applied in order to use a hex head screw to fasten the crossbar to the dampers. The electronics mounting bracket will be attached between the safety belt system and the seat bucket using the same screws and screw holes. The lower attachment points for the electronics mounting bracket will be epoxied to the back of the seat. The electronics enclosure will be fastened to the mounting bracket. Roller bearings will be applied to the four guide bearings holding the seat to the guide posts. The VLEA wires will be cut to 1.5" above the lower cross-member and the VLEA pins will be removed. The Accelerometer enclosure will be fastened to the lower cross-member using the same screw holes as the VLEA pin screws, but with shorter screws. The shorter screws allow for attaching the VLEA wire guide channel using the hole through which the VLEA wires were originally passed. The spring bracket for the Armor return spring will also be changed to reduce the chance of interference during a crash stroke. All other aspects of the seat will remain unchanged.

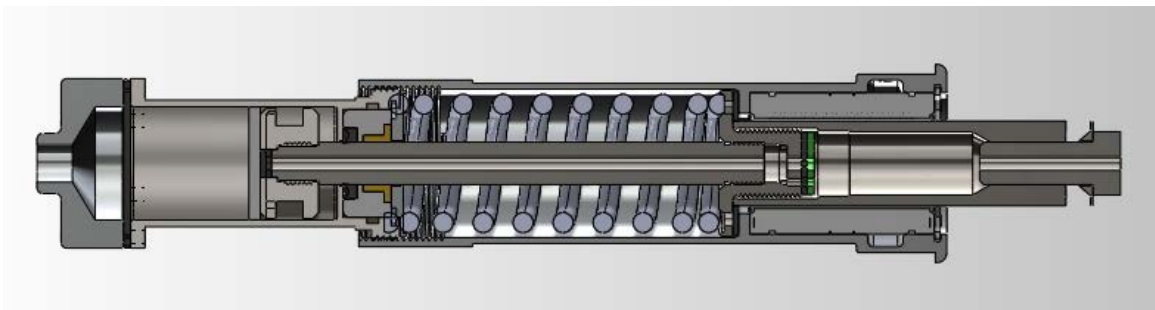


Figure 150: AVASS Damper V2.0

AVASS Damper v2.0 is shown in Figure 150. These dampers are self-contained, spring and damper systems which can be dropped in and fastened to the guide tubes with little effort. The preload is pre-applied and maintained using a set screw. Control wires are

connected to the dampers with a quick disconnect header built into the top portion of the damper shaft.



Figure 151: TSi MR Controller Electronics v4.0 for use with AVASS

MR Controller Electronics v4.0 is shown in Figure 151. The electronics have been reworked to lower cost and complexity of the system. The main electronics are contained on one board. An EMI plastic enclosure with EMI conductive paint covers the electronics which are mounted to a rigid aluminum back plate. Circuitry required for passing MIL-STD-704A and MIL-STD-461E have been integrated into the single board. A single pass-through cable gland removes the cost associated with bayonet style mil-spec connectors. The accelerometers are mounted in a custom made small and light aluminum enclosure. The entire system weighs one third as much as the SAMSS system in flight testing.

Final Vibration Testing Results for Characterization of AVASS

In an effort to have a full set of vibration reduction characteristics for the system which will go into qualification testing, transmissibility plots for the full range of occupant masses are available below. All plots show testing results with the controller on.

Variation between seat pan reduction and seat cushion reductions are discussed and tabulated. Performance differences between masses are also due to the seat height used for each specified seat mass.

All test results for tabulation of vibration reduction characteristics have been performed using the same SigLab system at the University of Maryland. Unless otherwise specified, all tests are performed at a 0.2 g peak to peak amplitude vibration. Instead of using past data, new OEM tests were conducted during this test session to verify continuity of ballast and sensor calibration. Re-running the OEM tests was also a chance to document seat cushion performance for the MH-60S seat. The 5th female test mass was tested with the seat at the 2nd position from the top. The 50th male mass was tested with 6 holes showing above the pin, at the middle position. The 95th male mass was tested at the full down position.

Table 7 shows the percent reduction from the OEM seat system at the frequencies of interest. This improvement was calculated using the data from Table 8 and Table 9, which show direct reduction in vibration from the floor. A negative reduction is representative of an increase in vibration. A positive number is a sign that the system is suppressing more vibration to the occupant than the OEM system. From test data, the

project team concludes that an MH-60S with AVASS provides up to 70.65% more vibration attenuation than the OEM configuration and up to 81.1% reduction in vibration from the floor.

Table 7: AVASS Percent Reduction in Vibration from OEM SH-60S measured at the Seat Pan

	4.3 Hz (1/rev)	8.6 Hz (2/rev)	12.9 Hz (3/rev)	17.2 Hz (4/rev)
5th Female	-9.55%	40.79%	63.71%	70.65%
50th Male	-3.24%	54.97%	58.71%	43.15%
95th Male	-2.64%	47.01%	69.48%	44.57%

Table 8: AVASS Percent Reduction in Vibration from Floor measured at the Seat Pan

	4.3 Hz (1/rev)	8.6 Hz (2/rev)	12.9 Hz (3/rev)	17.2 Hz (4/rev)
5th Female	-20.40%	42.80%	77.10%	81.10%
50th Male	-11.40%	44.70%	80.10%	72.20%
95th Male	-8.90%	60.10%	83.00%	64.30%

Table 9: OEM MH-60S Percent Reduction in Vibration from Floor measured at the Seat Pan

	4.3 Hz (1/rev)	8.6 Hz (2/rev)	12.9 Hz (3/rev)	17.2 Hz (4/rev)
5th Female	-9.90%	3.40%	36.90%	35.60%
50th Male	-7.90%	-22.80%	51.80%	51.10%
95th Male	-6.10%	24.70%	44.30%	35.60%

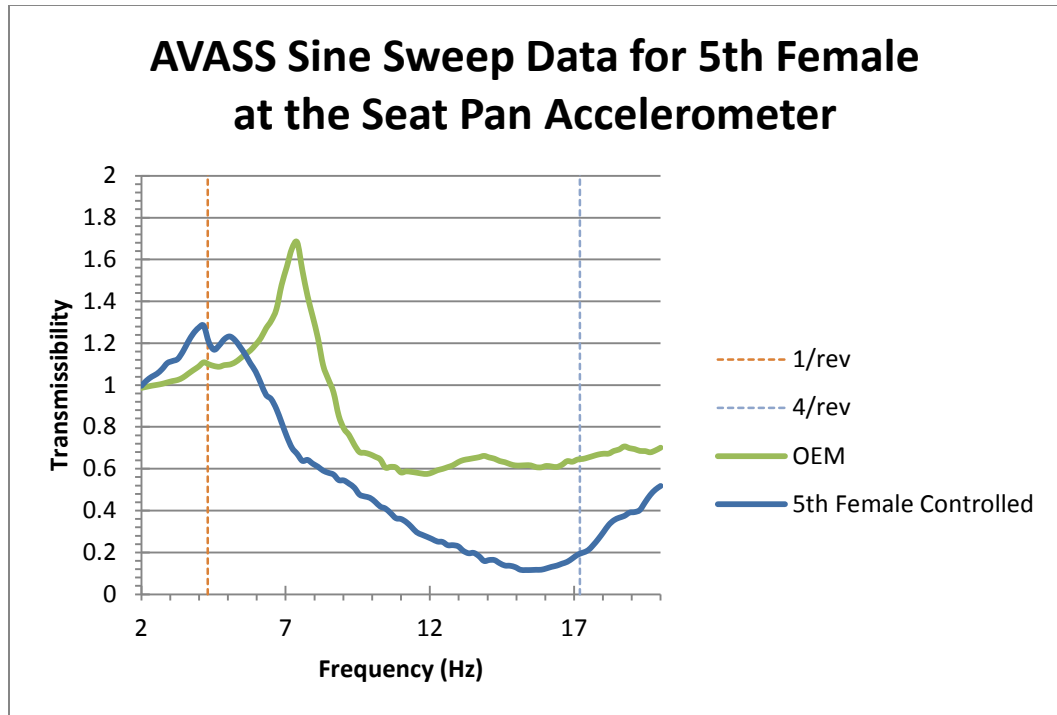


Figure 152: AVASS Sine Sweep Data for 5th Female Mass at the Seat Pan Accelerometer

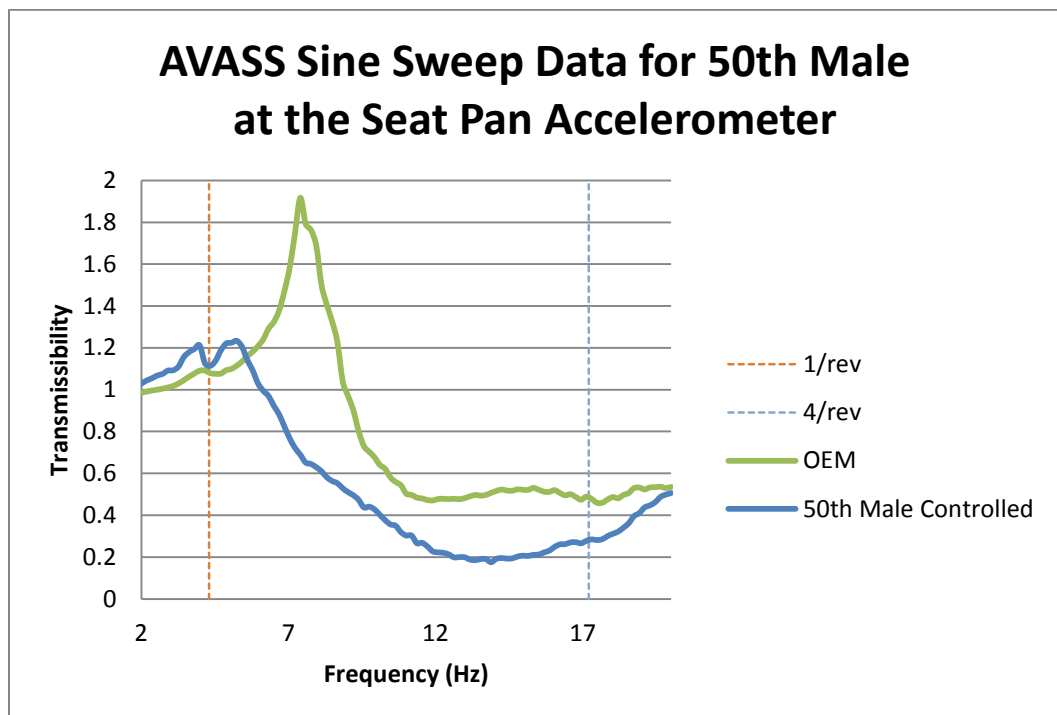


Figure 153: AVASS Sine Sweep Data for 50th Male Mass at the Seat Pan Accelerometer

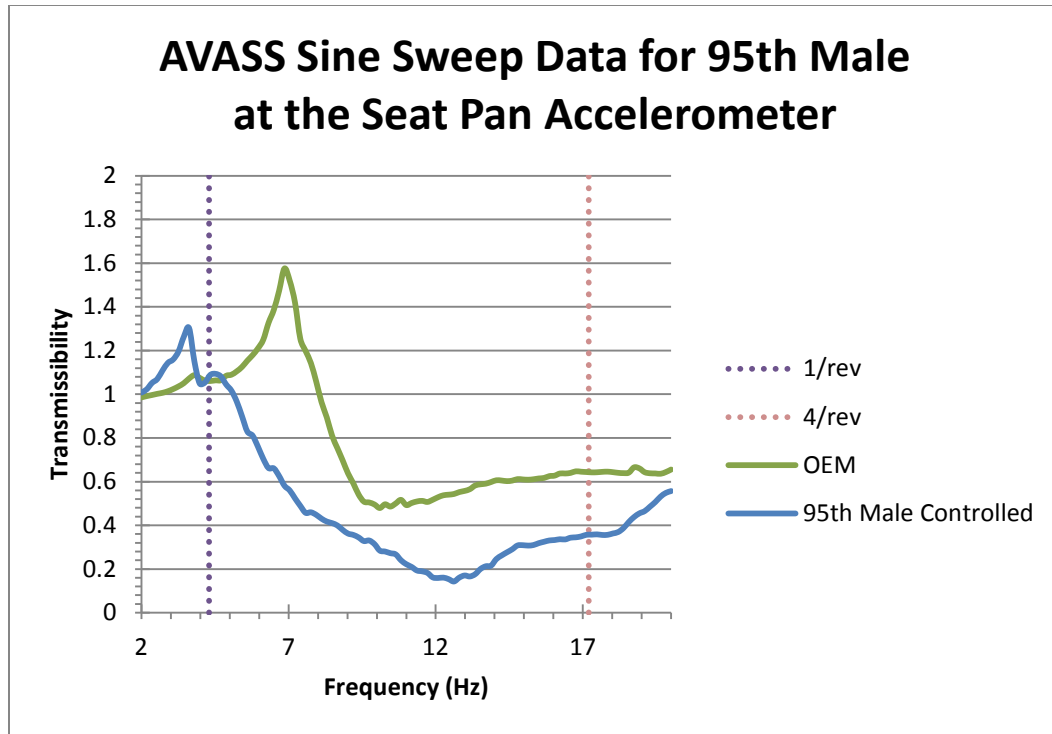


Figure 154: AVASS Sine Sweep Data for 95th Male Mass at the Seat Pan Accelerometer

The plots below are from the same test runs as the plots above, but show the transmissibility measured at the seat cushion for both AVASS and OEM MH-60S seat systems. Table 10 shows the percent reduction in vibration transmissibility from OEM at key frequencies. Table 11 and Table 12 contain AVASS and OEM percent reduction from floor vibrations which were used to create Table 10. There are reductions across the board after AVASS resonance with very slight differences in transmissibility at the 1/rev. The resonance multiplication between the seat rocking mode and the seat cushion is staggering. The data indicates that the amplitude of vibrations at the 2/rev frequency is multiplied 2.67 times through the OEM seat. The gains at the 4/rev frequency for AVASS are slight, but the reduction in vibration for the OEM seat system was already quite good.

Table 10: AVASS Percent Reduction in Vibration from OEM MH-60S measured at the Seat Cushion

	4.3 Hz (1/rev)	8.6 Hz (2/rev)	12.9 Hz (3/rev)	17.2 Hz (4/rev)
5th Female	-5.06%	75.53%	43.28%	8.96%
50th Male	-1.43%	75.23%	39.88%	5.05%
95th Male	0.89%	76.24%	37.62%	39.53%

Table 11: AVASS Percent Reduction in Vibration from Floor measured at the Seat Cushion

	4.3 Hz (1/rev)	8.6 Hz (2/rev)	12.9 Hz (3/rev)	17.2 Hz (4/rev)
5th Female	-41.10%	18.60%	38.40%	63.40%
50th Male	-35.00%	9.00%	31.70%	64.30%
95th Male	-33.80%	31.90%	41.30%	82.10%

Table 12: OEM MH-60S Percent Reduction in Vibration from Floor measured at the Seat Cushion

	4.3 Hz (1/rev)	8.6 Hz (2/rev)	12.9 Hz (3/rev)	17.2 Hz (4/rev)
5th Female	-34.30%	-232.60%	-8.60%	59.80%
50th Male	-33.10%	-267.40%	-13.60%	62.40%
95th Male	-35.00%	-186.60%	5.90%	70.40%

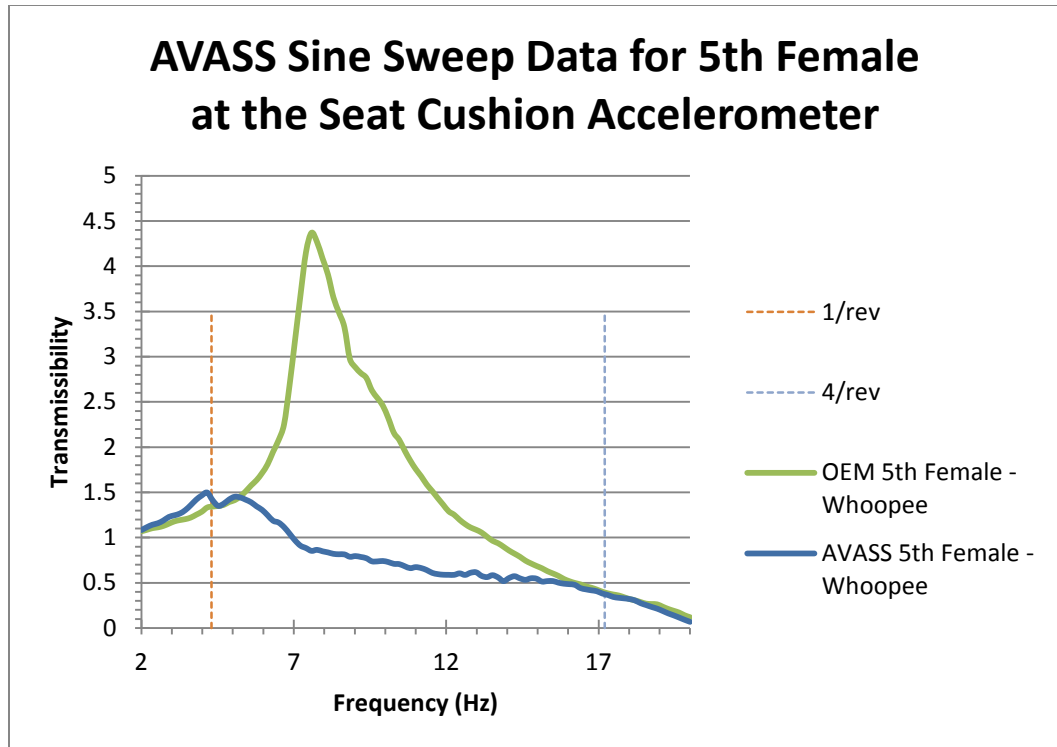


Figure 155: AVASS Sine Sweep Data for 5th Female Mass at the Seat Cushion Accelerometer

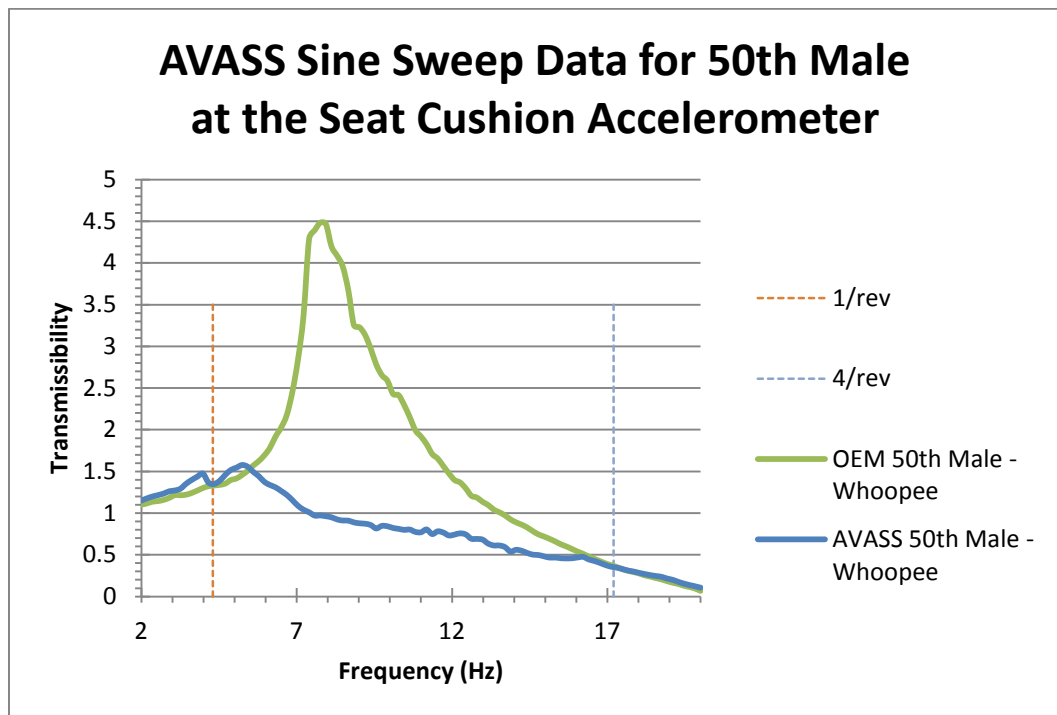


Figure 156: AVASS Sine Sweep Data for 50th Male Mass at the Seat Cushion Accelerometer

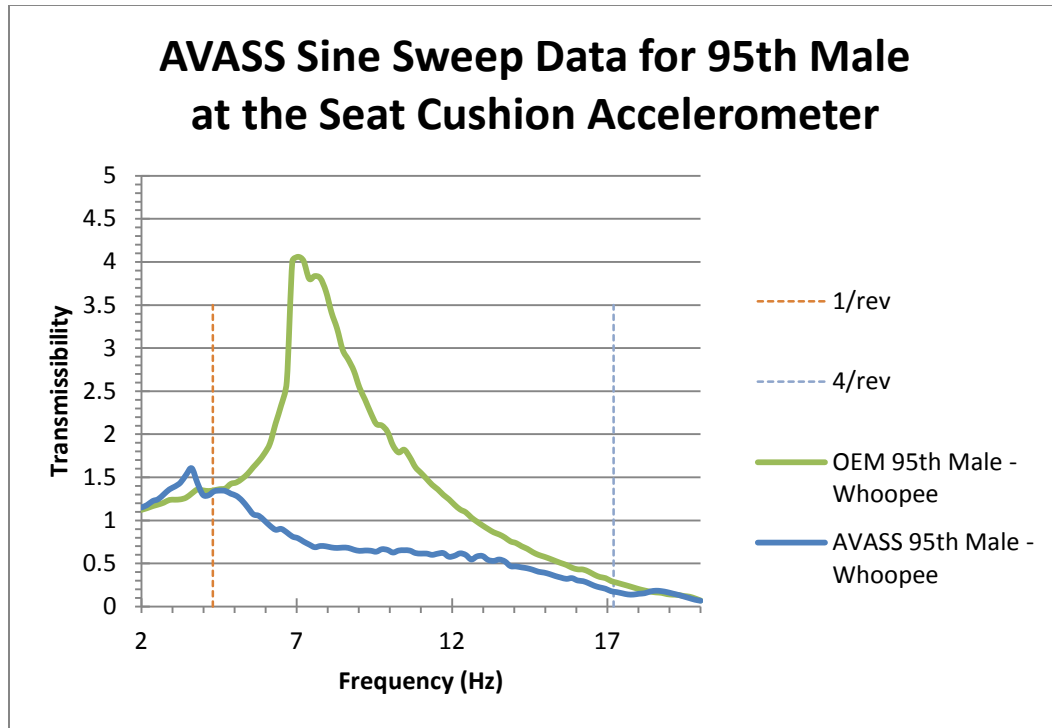


Figure 157: AVASS Sine Sweep Data for 95th Male Mass at the Seat Cushion Accelerometer

At the seat pan, AVASS shows the most improvement from the OEM seat system for the 5th female mass. The project team believes this is mostly due to the position of the seat bucket used for the 5th female test. In theory, a lighter mass should have a lower amount of vibration reduction at the same frequency and amplitude. The cantilever guide tube design of the MH-60S causes a greater amplitude rocking mode when the seat is at its top most position.

In an effort to study the effects of seat height, the project team ran the 50th male mass test at the top most and bottom most position to compare with the middle position result.

What the results show is that indeed, the top most position has the highest resonance, but

that an increasing mass made a large change in the high frequency response. What the AVASS system does is reduce the rocking mode by transferring the energy from a rotating frame to a linear frame. This is apparent on the plot in Figure 158. The largest reductions in transmissibility are measured at the 2/rev and 3/rev, the peak of the rocking mode. At the seat cushion, AVASS is decreasing vibrations in the 2/rev by 82.59% from the OEM MH-60S.

Table 7: AVASS Percent Reduction in Vibration from OEM MH-60S measured at the Seat Pan for 50th Male with Changing Seat Height Positions

	4.3 Hz (1/rev)	8.6 Hz (2/rev)	12.9 Hz (3/rev)	17.2 Hz (4/rev)
TOP	-6.91%	72.03%	48.05%	20.00%
MIDDLE	-3.24%	54.97%	58.71%	43.15%
BOTTOM	-0.91%	62.39%	57.38%	48.16%

Table 8: AVASS Percent Reduction in Vibration from Floor measured at the Seat Pan for 50th Male with Changing Seat Height Positions

	4.3 Hz (1/rev)	8.6 Hz (2/rev)	12.9 Hz (3/rev)	17.2 Hz (4/rev)
TOP	-14.50%	54.30%	82.65%	79.20%
MIDDLE	-11.40%	44.70%	80.10%	72.20%
BOTTOM	-10.80%	46.30%	79.20%	71.80%

Table 9: OEM MH-60S Percent Reduction in Vibration from Floor measured at the Seat Pan for 50th Male with Changing Seat Height Positions

	4.3 Hz (1/rev)	8.6 Hz (2/rev)	12.9 Hz (3/rev)	17.2 Hz (4/rev)
TOP	-7.10%	-63.40%	66.60%	74.00%
MIDDLE	-7.90%	-22.80%	51.80%	51.10%
BOTTOM	-9.80%	-42.80%	51.20%	45.60%

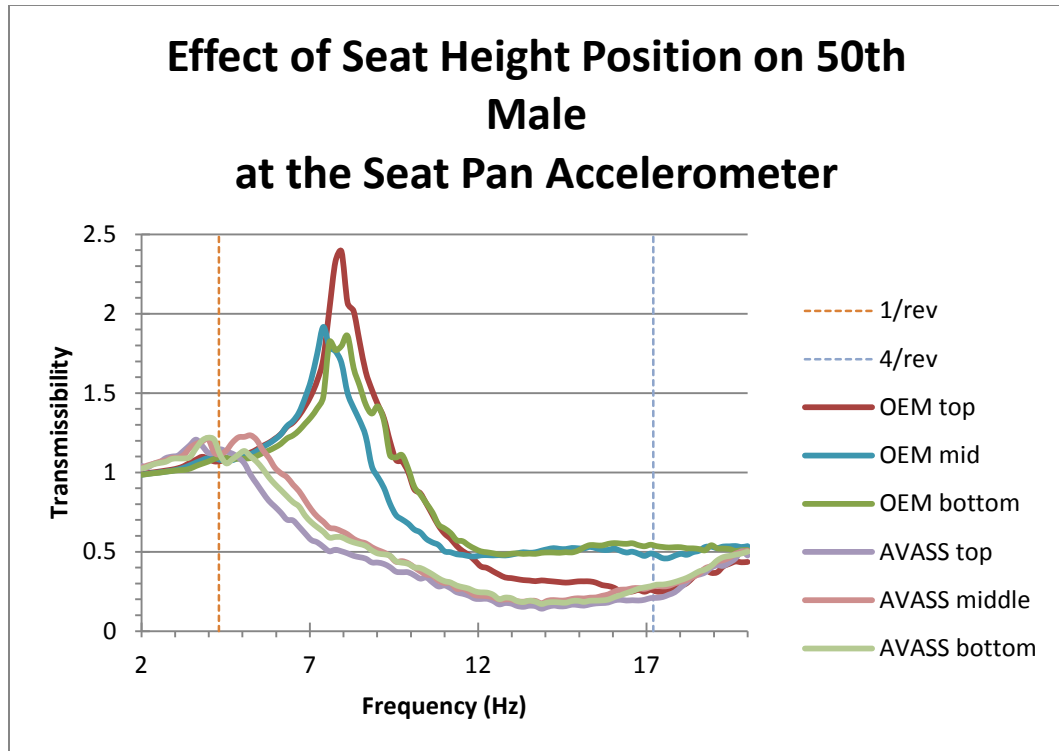


Figure 158: Effect of Seat Height Position on the 50th Male Mass at the Seat Pan Accelerometer

Table 10: AVASS Percent Reduction in Vibration from OEM MH-60S measured at the Seat Cushion
for 50th Male with Changing Seat Height Positions

	4.3 Hz (1/rev)	8.6 Hz (2/rev)	12.9 Hz (3/rev)	17.2 Hz (4/rev)
TOP	-11.48%	82.59%	50.42%	-1.84%
MIDDLE	-1.43%	75.23%	39.88%	5.05%
BOTTOM	-6.48%	73.29%	53.72%	16.50%

Table 11: AVASS Percent Reduction in Vibration from Floor measured at the Seat Cushion for 50th
Male with Changing Seat Height Positions

	4.3 Hz (1/rev)	8.6 Hz (2/rev)	12.9 Hz (3/rev)	17.2 Hz (4/rev)
TOP	-35.90%	30.00%	40.40%	66.80%
MIDDLE	-35.00%	9.00%	31.70%	64.30%
BOTTOM	-34.70%	16.60%	30.90%	57.00%

**Table 12: OEM MH-60S Percent Reduction in Vibration from Floor measured at the Seat Cushion
for 50th Male with Changing Seat Height Positions**

	4.3 Hz (1/rev)	8.6 Hz (2/rev)	12.9 Hz (3/rev)	17.2 Hz (4/rev)
TOP	-21.90%	-302.00%	-20.20%	67.40%
MIDDLE	-33.10%	-267.40%	-13.60%	62.40%
BOTTOM	-26.50%	-212.30%	-49.30%	48.50%

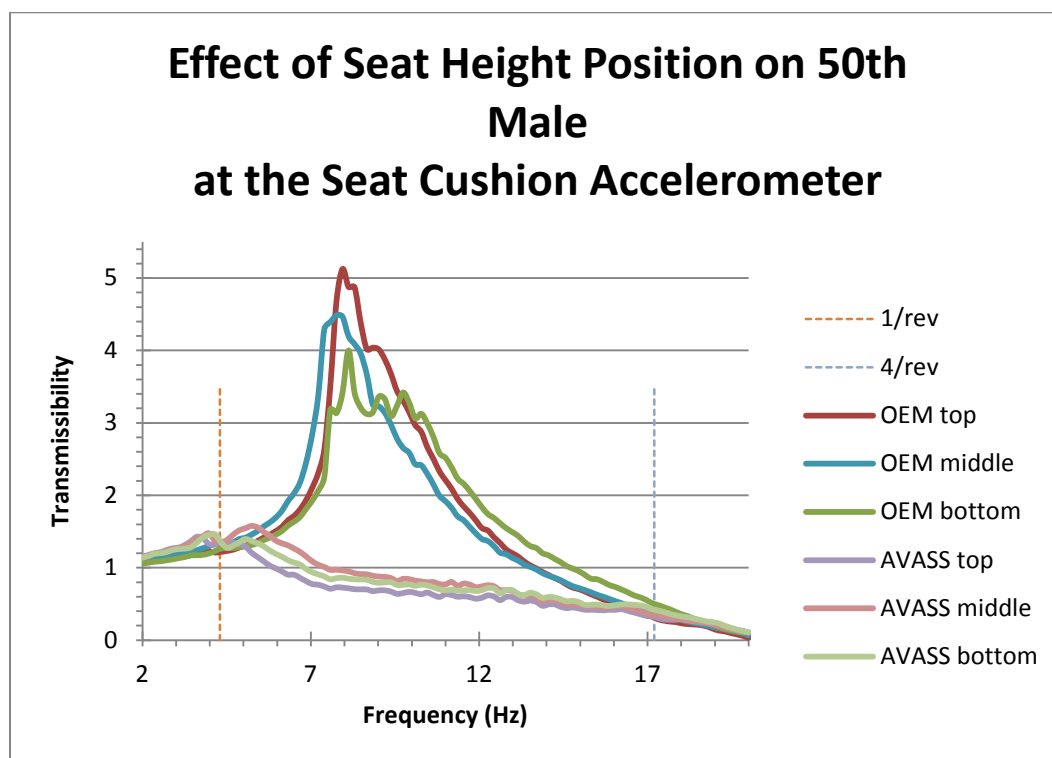


Figure 159: Effect of Seat Height Position on the 50th Male Mass at the Seat Cushion Accelerometer

The project team has often stated in project reports that the performance of AVASS increases with increased vibration amplitude. SAMSS flight data shows stretches of vibration which are upwards of 0.5 g in amplitude. To demonstrate the effect of increased vibration on the frequency response, the two plots below show the performance of

AVASS at 0.2 g and 0.4 g compared to OEM at 0.2 g. The team did not complete a 0.4 g OEM test due to safety problems inherent in the violent nature of the OEM resonance. A 20-50% reduction in transmissibility from the floor to the seat cushion can be seen from 5-17.5 Hz, solely by increasing the vibration amplitude by 0.2 g.

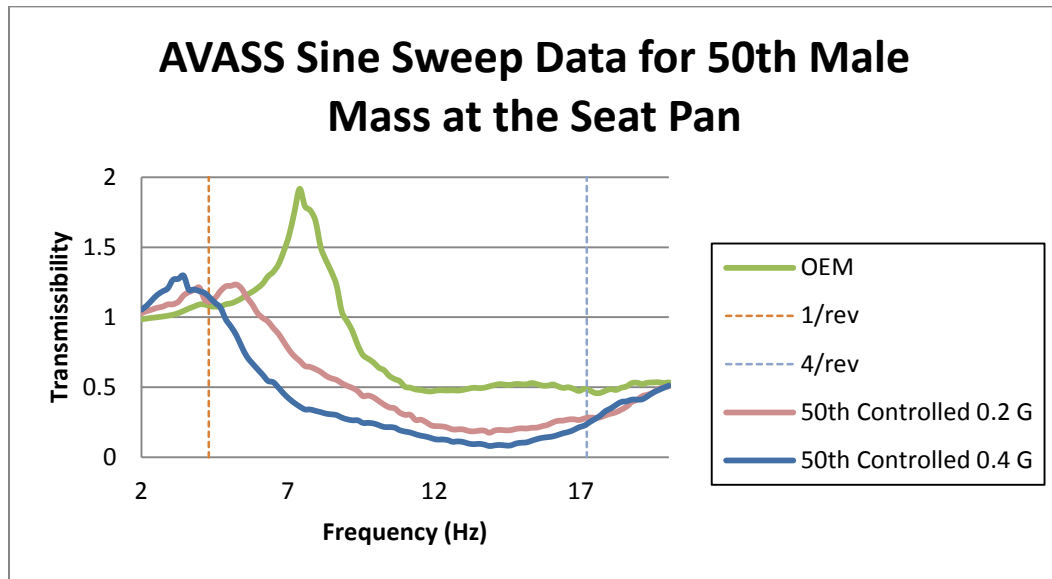


Figure 160: AVASS Sine Sweep Data for 50th Male Mass at the Seat Pan at 0.2 g and 0.4 g

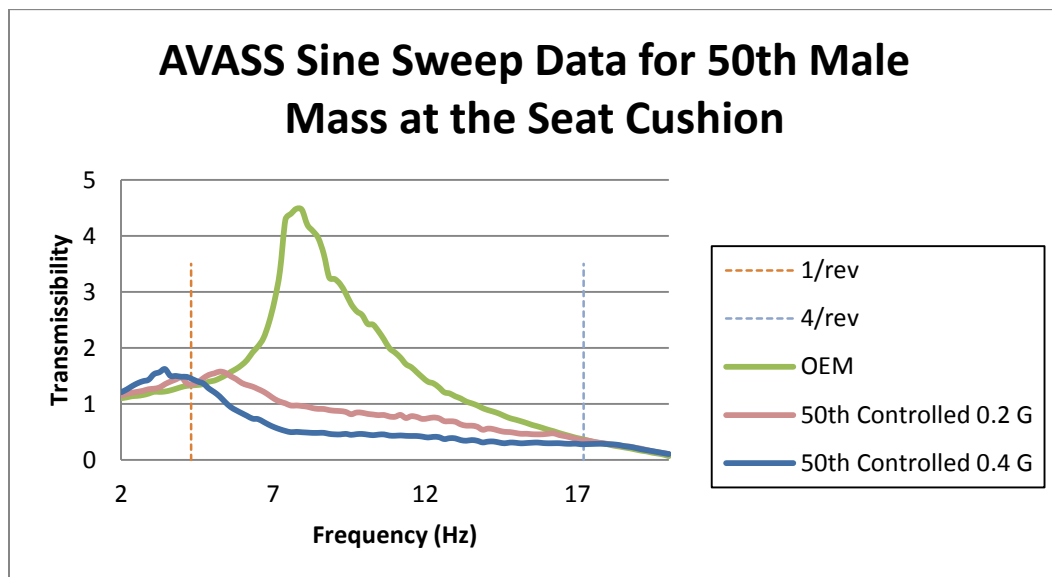


Figure 161: AVASS Sine Sweep Data for 50th Male Mass at the Seat Cushion at 0.2 g and 0.4 g

The plot of OEM seat response shown below has been added to demonstrate why the OEM MH-60S seat system requires AVASS. The OEM system appears to have been tuned, using mostly the seat cushion, to provide good reduction at the 4/rev range. Elsewhere inside the primary harmonics, the response is magnified by the seat cushion. Adding AVASS to the system, as shown above, the project team is able to remove this resonance completely and continue this vibration reduction until the seat cushion is the only thing needed to keep the pilot comfortable.

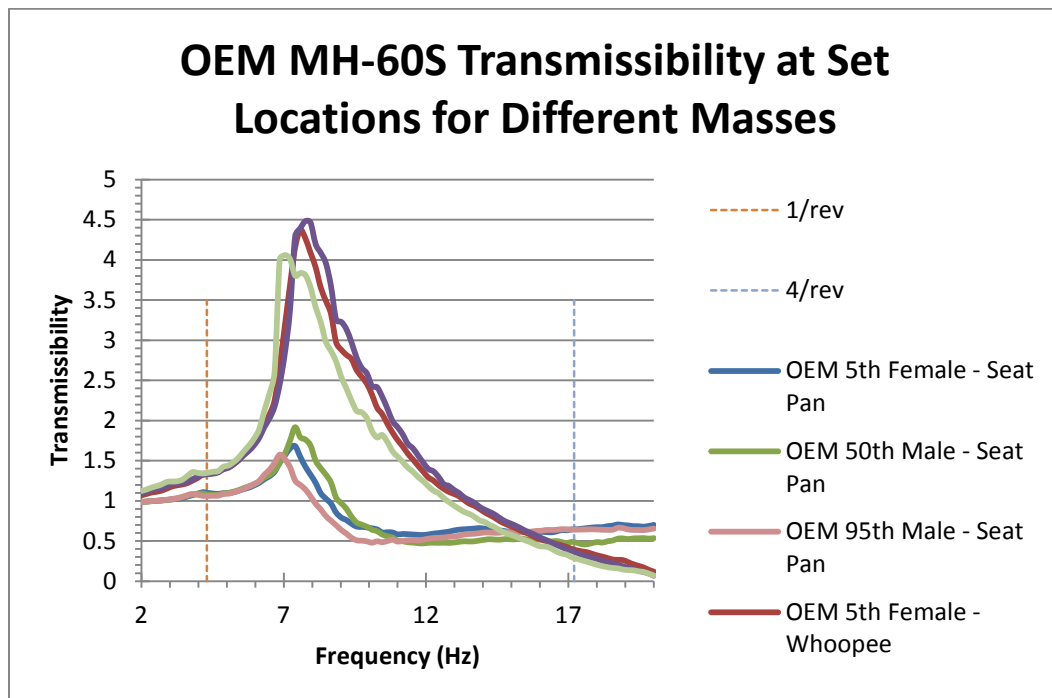


Figure 162: OEM MH-60S Transmissibility for all Occupants at the Seat Pan and at the Seat Cushion

Conclusions and Future Work

The positive results from early testing of the SAMSS system for the MH-60R has spurred increasing attention to the benefits of adding magnetorheological dampers for vibration isolation into other helicopter crew seat models. The SAMSS project is now nearly seven years old and the hurdles that were surmounted have become lessons learned. AVASS is a parallel project which has benefited from the experiences of the SAMSS project.

AVASS is the next generation system for Helicopter Crew Seats and has reached a nearly production ready status.

The AVASS project has been successful in retrofitting an MH-60S helicopter crew seat to reduce vibration to the occupant, compared to the original seat, throughout a large frequency range. The reduction in transmission of floor vibration is noticeable throughout the seat bucket and to the occupant. The testing results clearly show that improvements can be made by tuning the secondary dynamics due to the seat cushion. For this reason, the project team suggests that efforts to design vibration isolation systems for seat suspensions must develop the suspension and seat cushion jointly. Finally, reducing friction further could continue to increase the vibration isolation performance of AVASS installed on an MH-60S crew seat system.

The designs of damper systems in concurrent programs have changed to fit the ever evolving list of requirements from our sponsors, the Navy, as well as the end users, the

pilots. The system has changed to make a more congruent, more mature design. Damper designs have been turned into a single unit with adjustable preload which drop into the guide tubes and fasten to the system using existing mounting holes. Damper shafts have been modified to allow for a low friction, high load linear bearing to be part of each damper. A hidden compartment in a larger diameter damper rod section allows for a PCB with a connector, which is used to connect the magnetic coil wire to the controller harness. The isolator assemblies now weigh just over 1 lb. each including suspension spring and a low friction bearing. The new dampers have been designed to fit in a large variety of seat designs with minimal connection hardware which may need to be refined on a system-by-system basis.

The newest electronics design for the controller has been updated to meet all standards and has seen many evolutionary changes. The electronics currently in flight testing have expanded with modules added to help meet MIL-STD-704A and MIL-STD-1275D. The weight increased due to external enclosures for the new modules and their mounting methods. The designs of both the boards and the packaging have been iterated to reduce weight, complexity and cost. Today, the desired configuration has reduced the number of connectors to a minimum and all the power filtering and control is housed on one board contained within one enclosure. The cost of components and assembly has been reduced significantly, and this savings will be passed on to the customer.

The next cost that can be expected is towards procurement and integration into the fleet. The idea of retrofitting existing, qualified and tested, helicopter crew seats was to quickly

adapt the system for service. This would reduce logistical costs in acquisition and the time frame of the project. The latest design of the system has been changed to reduce the labor and material cost of actually retrofitting the existing seat systems. Minimizing changes to the seat system during the retrofit process will allow for a more efficient transition to the new technology. The hope may be that all installations could be accomplished with minimal downtime for the crew seats in service.

Quoting from *An Introduction to Human Factors in Engineering*: To prove viability “the benefits of the solution must be sufficiently greater than the costs, or the [customer] will not accept the design” [4]. The goal of this program is to improve the human factors experience when flying a helicopter. The cost of developing the technology thus far has been fruitful, and the medical expense of having young pilots with back problems is constantly increasing. This project has a small part to play in helping on both ends of this equation.

Future improvements to the system can be expected to allow the system to be lighter, more user-friendly and cost effective. The AVASS system is only a second generation and there are areas for improvement which the project team would like to note.

Specifically, a study for the design of a cushion for use specifically with AVASS could produce large performance improvements. Also, the MH-60S bearing bracket design can be refined further for weight and friction reduction performance. Finally, as SAMSS continues flight testing, and AVASS hopefully achieves flight clearance itself, the input

from all those who interface with the seat will be imperative for tuning the algorithm and applying changes to the design for future iterations.

APPENDIX I: MRF-132DG Magneto-Rheological Fluid

LORD TECHNICAL DATA

MRF-132DG Magneto-Rheological Fluid

Description

LORD MRF-132DG fluid is a hydrocarbon-based magneto-rheological (MR) fluid formulated for general use in controllable, energy-dissipating applications such as shocks, dampers and brakes.

MRF-132DG fluid is a suspension of micron-sized, magnetizable particles in a carrier fluid. When exposed to a magnetic field, the rheology of MRF-132DG fluid reversibly and instantaneously changes from a free-flowing liquid to a semi-solid with controllable yield strength. Altering the strength of the applied magnetic field precisely and proportionally controls the consistency or yield strength of the fluid.

MRF-132DG fluid can be used in *valve mode* (fluid flowing through an orifice) or in *shear mode* (fluid shearing between two surfaces). In the absence of a magnetic field, MRF-132DG fluid flows freely or allows free movement. Upon application of a magnetic field, the fluid's particles align with the direction of the field in chain-like fashion, thereby restricting the fluid's movement within the gap in proportion to the strength of the magnetic field.

Features and Benefits

Fast Response Time – responds instantly and reversibly to changes in a magnetic field.

Dynamic Yield Strength – provides high yield strength in the presence of a magnetic field and very low yield strength in the absence of a magnetic field; allows for a wide range of controllability.

Temperature Resistant – performs consistently throughout a broad temperature range, meeting the requirements of demanding applications such as automotive shock absorbers.

Hard Settling Resistant – provides high resistance to hard settling; easily redispersed.

Non-Abrasive – formulated to not abrade the devices in which the MR fluid is used.

Application

For more information on MR technology, refer to the MR Design Guides located on www.lord.com/mr.

Mixing – Under common flow conditions, no separation is observed between particles and the carrier fluid. However, a degree of separation may eventually occur under static conditions. If needed, use a paint shaker to redisperse the particles into a homogeneous state prior to use.

Storage

Keep container tightly closed when not in use.

Typical Properties*

Appearance	Dark Gray Liquid
Viscosity, Pa-s @ 40°C (104°F) Calculated as slope 800-1200 sec ⁻¹	0.092 ± 0.015
Density g/cm ³ (lb/gal)	2.98-3.18 (24.7-26.5)
Solids Content by Weight, %	80.98
Flash Point, °C (°F)	>150 (>302)
Operating Temperature, °C (°F)	-40 to +130 (-40 to +266)

*Data is typical and not to be used for specification purposes.

LORD
AskUsHow™

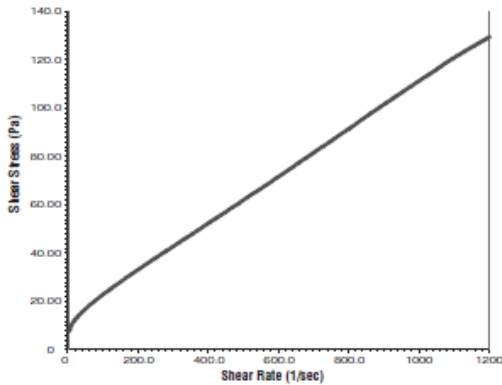
LORD TECHNICAL DATA

Cautionary Information

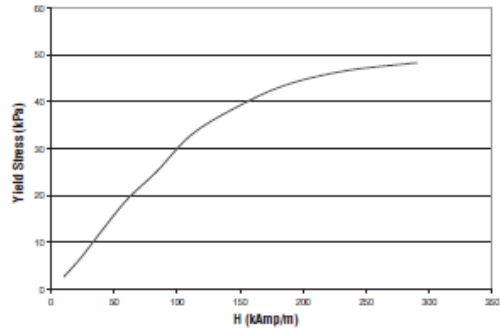
Before using this or any LORD product, refer to the Material Safety Data Sheet (MSDS) and label for safe use and handling instructions.

For industrial/commercial use only. Not to be used in household applications. Not for consumer use.

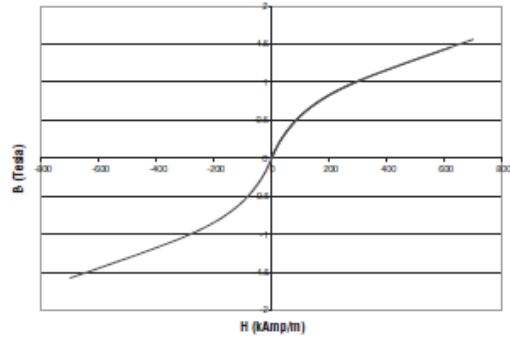
Shear Stress as a function of Shear Rate with no Magnetic Field applied at 40°C (104°F)



Yield Stress vs. Magnetic Field Strength



Typical Magnetic Properties



Values stated in this technical data sheet represent typical values as not all tests are run on each lot of material produced. For formalized product specifications for specific product end uses, contact the Customer Support Center.

Information provided herein is based upon tests believed to be reliable. In as much as LORD Corporation has no control over the manner in which others may use this information, it does not guarantee the results to be obtained. In addition, LORD Corporation does not guarantee the performance of the product or the results obtained from the use of the product or this information where the product has been repackaged by any third party, including but not limited to any product end-user. Nor does the company make any express or implied warranty of merchantability or fitness for a particular purpose concerning the effects or results of such use.

"Ask Us How" is a trademark of LORD Corporation or one of its subsidiaries.

LORD provides valuable expertise in adhesives and coatings, vibration and motion control, and magnetically responsive technologies. Our people work in collaboration with our customers to help them increase the value of their products. Innovative and responsive in an ever-changing marketplace, we are focused on providing solutions for our customers worldwide . . . Ask Us How.

LORD Corporation World Headquarters

111 Lord Drive
Cary, NC 27511-7923
USA

Customer Support Center (in United States & Canada)
+1 877 ASK LORD (275 5673)

www.lord.com

©2008 LORD Corporation CD 087015 (Rev.1 7/08)

LORD
AskUsHow™

Bibliography

- [1] J. Stewart, "DoD asks helicopter pilots about back pain," 8 April 2011. [Online].
Available: <http://www.armytimes.com/news/2011/04/air-force-back-pain-040711w/>.
[Accessed 24 January 2013].
- [2] C. G. de Oliveira, D. M. Simpson and J. Nadal, "Lumbar Back Muscle Activity of Helicopter Pilots and Whole-Body Vibration," vol. 34, no. 10, 2001.
- [3] G. Hiemenz, P. Gupta, W. Hu and N. Wereley, "Semi-Active Magnetorheological Helicopter Crew Seat Suspension for Vibration Isolation," 2008.
- [4] M. Lehto and S. J. Landry, Introduction to Human Factors and Ergonomics for Engineers: Second Edition, Boca Raton, FL: CRC Press, 2013.
- [5] ISO/TC 108/SC4, 2631-1: *Mechanical vibration and shock -- Evaluation of human exposure to whole-body vibration -- Part 1: General requirements*, Geneva, Switzerland: ISO, 1997.
- [6] C. de Oliveira and J. Nadal, "Transmissibility of helicopter vibration in the spines of pilots in flight," vol. 76, no. 6, pp. 576-80, 2005.
- [7] D. F. Shanahan, G. Mastroiane and T. D. Reading, "Back Discomfort in U.S. Army Military Helicopter Aircrew Member," *Backache and Back Discomfort*, vol. Vol. 21, pp. pp. 10-25, 1986.
- [8] Kristin L Harrer; Debra Yniguez; Maria Majar; David Ellenbecker; Nancy Estrada; Mark Geiger; NAVAL MEDICAL CENTER SAN DIEGO CA., "Whole Body

- Vibration Exposure for MH-60S Pilots," *Proceedings of the Forty Third Annual SAFE Association Symposium*, pp. pp. 303-314, 24-26 October 2005.
- [9] S. P. Desjardins, "The Evolution Of Energy Absorption Systems For Crashworthy Helicopter Seats," *J. American Helicopter Society*, vol. 51, no. 2, pp. pp. 150-163, 2006.
- [10] Desjardins, S. P.; Simula Inc., "Aircraft Crash Survival Design Guide," Aviation Applied Technology Directorate USAAVSCOM, 1989.
- [11] Department of Defense, *MIL-STD-58095A*, 1986.
- [12] M. Richards and E. Sieveka, "The Effects of Body-Borne Equipment Weight on ATD Lumbar Loads Measured During Crashworthy Seat Vertical Dynamic Tests," in *Annual Forum Proceedings - Ahs International*, 2011.
- [13] Department of Defense, *MIL-STD-1290A LIGHT FIXED AND ROTARY-WING AIRCRAFT CRASH RESISTANCE*, 1988.
- [14] J. C. Dixon, *The Shock Absorber Handbook Second Edition*, West Sussex, England: John Wiley and Sons, Ltd., 2007.
- [15] D. A. Baz, *Active Vibration Control*, College Park: University of Maryland, 2012.
- [16] D. I. Chopra, *Smart Structures ENAE 651*, College Park: University of Maryland, 2011.
- [17] J. Carlson, D. Catanzarite and K. St. Clair, "Commercial Magneto-Rheological Fluid Devices," in *5th Int. Conf. on Electro-Rheological, Magneto-Rheological Suspensions and Associated Technology*, Sheffield, 1995.

- [18] "LORD Magneto-Rheological (MR)," LORD Corporation, [Online]. Available:
[http://www.lord.com/products-and-solutions/magneto-rheological-\(mr\).xml](http://www.lord.com/products-and-solutions/magneto-rheological-(mr).xml).
[Accessed 19 3 2013].
- [19] N. M. Wereley and L. Pang, "Nondimensional Analysis Of Semi-Active
Electrorheological And Magnetorheological Dampers Using Approximate Parallel
Plate Models," *Smart Materials and Structures*, vol. Vol. 7, no. (5), pp. pp. 732-743,
1998.
- [20] B. Reichert, "Application of Magneto Rheological Dampers for Vehicle Seat
Suspensions," Blacksburg, VA, 1997.
- [21] Y. T. Choi and N. M. Wereley, "Biodynamic Response Mitigation To Shock Loads
Using Magnetorheological Helicopter Crew Seat Suspensions," *AIAA Journal of
Aircraft*, vol. Vol. 42, no. (5), pp. pp. 1288-1295, 2005.
- [22] G. J. Hiemenz, W. Hu and N. M. Wereley, "Investigation of MR Dampers for
Enhanced Crashworthiness and Vibration Isolation of Helicopter Crew Seats,"
Journal of the American Helicopter Society, 2008.
- [23] G. Hiemenz, W. Glass, W. Hu and N. Wereley, "Dynamic Testing of a Semi-Active
Magnetorheological Helicopter Crew Seat Suspension for Vibration Isolation.," in
AHS International, 2009.
- [24] G. Hiemenz, W. Hu and N. Wereley, "Semi-active Magnetorheological Helicopter
Crew Seat Suspension for Vibration Isolation," *Journal of Aircraft*, vol. 3, no. 45,
pp. 945-953, 2008.

- [25] S. Griffin, J. Gussy, S. A. I. H. B. Lane and D. Sciulli, "Virtual Skyhook Vibration Isolation System," vol. 124, no. 1, p. 63, 01 January 2002.
- [26] G. Stix, "Project Skyhook," vol. 284, no. 5, pp. 28-9, 01 January 2001.
- [27] LORD Materials Division, "Engineering Note: Magnetic Circuit Design," LORD Corporation, 1999.
- [28] X. Zhu, X. Jing and L. Cheng, "Magnetorheological fluid dampers: A review on structure design and analysis," vol. 23, no. 839, 2012.
- [29] "Allegheny York Corp.," [Online]. Available: <http://www.alleghenyork.com/>. [Accessed 9 4 2012].
- [30] "Century Spring Corp Compression Springs," [Online]. Available: http://www.centuryspring.com/Store/search_compression.php. [Accessed 9 4 2012].
- [31] "Mid West Spring and Stamping," [Online]. Available: <http://www.mwspring.com/engineering.html>. [Accessed 9 4 2012].
- [32] "Stockwell Elastomerics," [Online]. Available: <http://www.stockwell.com/>. [Accessed 9 4 2012].
- [33] "Roto West Inc.," [Online]. Available: <http://www.test-dummies.com/>. [Accessed 9 4 2012].